A Szilikátipari Tudományos Egyesület lapja

építőanyag

Journal of Silicate Based and Composite Materials

A TARTALOMBÓL:

2022/4

Invitation to CMCEE-14

The 14th International Conference on Ceramic Materials and Components for Energy and Environmental Applications (CMCEE-14) will be held in the beautiful city of Budapest, Hungary. The conference series began in 1980s and has established a strong reputation for state-of-the-art presentations and information exchange on the latest emerging ceramic technologies and their wide ranging applications. CMCEE-14 will contain more than 30 symposia covering wide range of topics, which will facilitate global dialogue and discussion with leading world experts to ceramic technologies for sustainable development of society.

We would like to invite all of you to actively participate in the conference and visit the city of Budapest. We are quite hopeful that this conference will provide excellent forum for interaction and friendship with participants from various continents.

We hope to meet you all in 2024!

About Budapest

Budapest is famous not only for the monuments reflecting its own 1,000-year-old culture, but also for the relics of others who settled here. Remains from both Roman occupation and much later ruled by the Turks can still be seen in the city. After the Ottoman Empire the union with Austria has a particular influence on the city's form and style.

Conference venue

Budapest Congress Center & Novotel Budapest City****Budapest Congress Center is the largest, most convenient, modern event facility in Budapest. It has over 20 meeting rooms in various shapes and sizes, adjustable for every possible need, as well as an exhibition space of over a 4000 m^2, which means it can hold separate events at the same time without them interfering with each other. International congresses, exhibitions, professional conferences, corporate meetings, gala dinners, tradeshows, fairs, concerts, plays or graduation ceremonies – Budapest Congress Center is perfect for them all!

https://akcongress.com/cmcee14

építőanyag

Journal of Silicate Based and Composite Materials

2022/4

TARTALOM

CONTENT

A finomkerámia-, üveg-, cement-, mész-, beton-, tégla- és cserép-, kő- és kavics-, tűzállóanyag-, szigetelőanyag-iparágak szakmai lapja
Scientific journal of ceramics, glass, cement, concrete, clay products, stone and gravel, insulating and fireproof materials and composites

A folyóiratot referálja · The journal is referred by:
ProQuest · Google Scholar · INDEX COPERNICUS INTERNATIONAL · THOMSON REUTERS

A folyóiratban lektorált cikkek jelennek meg.
All published papers are peer-reviewed.
Kiadó · Publisher: Szilikátipari Tudományos Egyesület (SZTE)
Elnök · President: ASZTALOS István
1034 Budapest, Bécsi út 120.
Tel.: +36-1/201-9360 ▪ E-mail: epitoanyag@szte.org.hu
Tördelő szerkesztő · Layout editor: NÉMETH Hajnalka
Címlapfotó · Cover photo: GYURKÓ Zoltán

WWW.EPITOANYAG.ORG.HU
EN.EPITOANYAG.ORG.HU

Online ISSN: 2064-4477
Print ISSN: 0013-970x
INDEX: 2 52 50 ▪ 74 (2022) 119–162

Effect of clay concentration on the mechanical properties and rheological behavior of ceramic slip

Sahra MAHI ▪ Laboratory of Rheology, Transport and Treatment of Complex, University of Science and Technology, Mohamed Boudiaf (USTOMB), Algeria ▪ mahisahra12@gmail.com
Labri HAMMADI ▪ Laboratory of Rheology, Transport and Treatment of Complex, University of Science and Technology, Mohamed Boudiaf (USTOMB), Algeria ▪ larbi.hammadi@univ-usto.dz
Nasr-Eddine BOUDJENANE ▪ Laboratory of Rheology, Transport and Treatment of Complex, University of Science and Technology, Mohamed Boudiaf (USTOMB), Algeria

Érkezett: 2021. 01. 04. ▪ Received:04. 01. 2021. ▪ https://doi.org/10.14382/epitoanyag-jsbcm.2022.19

Abstract
In this paper, we investigate the effect of the clay concentration on the mechanical and rheological properties of the slip used in the fabrication of ceramic. We demonstrate an increase of flexural strength of the slip's with an increase the clay concentration on the composition of the slip's. Concerning the effect of clay concentration on rheological behavior of ceramic slip, the modified Cross model is used to fit the stationary flow curves at different concentration of clay added to ceramic slip and the generalized Kelvin-Voigt's model successfully applied to fit the creep and recovery data and to analyse the viscoelastic properties of ceramic slip modified.
Keywords: clay concentration, slip of ceramic, modified cross model, mechanical properties, rheological behavior
Kulcsszavak: agyagkoncentráció, kerámia massza, módosított keresztmodell, mechanikai tulajdonságok, reológiai viselkedés

Sahra MAHI
He is master in hydraulic, preparing the PHD thesis on Rheological and mechanical characteristics of ceramic slips, at University of Science and Technology of Oran Mohamed Boudiaf (USTO-MB) under the direction of Professor Nasr-Eddine BOUDJENANE and Professor Larbi HAMMADI

Larbi HAMMADI
Larbi Hammadi is professor in Hydraulic (University of Science and Technology of Oran) and Engineer in Mechanical Engineering. Currently is Researcher Professor at the University of Science and Technology of Oran Mohamed Boudiaf (USTO-MB) where he exercised many teaching activities. He is actually the director of Laboratory of Rheology, Transport and Complex Fluids Treatment (LRTTFC) Oran Algeria. Significant results have been obtained in recent years, for example, in emulsions for pharmaceutical use, drilling muds, vases of dams, sewage treatment plant sludge's, ceramic , polymers and cavitation. See https://scholar.google.com/citations?user=LLbBaNAAAAAJ&hl=fr&oi=ao

Nasr-Eddine BOUDJENANE
Nasr-Eddine BOUDJENANE is Professor in Hydraulic and currently works in the Department Hydraulic , University of Science and Technology of Oran Mohamed Boudiaf (USTO-MB) , Algeria. He heads a research group in the Laboratory of Rheology, Transport and Complex Fluids Treatment (LRTTFC) Oran Algeria. His research focuses on subjects in hydraulics, in particular the Rheology and transport of complex fluids, solid transport, and in materials science.

1. Introduction

Ceramic slips consist of raw materials such as clays, feldspars, silicas, calcites, etc., suspended in water in the presence of deflocculates. According to Baccour et al [1] the clay minerals used in the manufacture of ceramic tiles belong to the family of phyllosili. The ceramic product requires clays having particular and appropriate characteristics; they must not contain a swelling phase, and are plasticised to facilitate the shaping of the body [2]. To improve the corrosion resistance of ceramic Shi et al [3] added the $Na_2B_4O_7$ end $EDTA$ in $Na_2SiO_2 - Na_3PO_4$ in order to improve the ceramic coating. The authors indicate that both additives cause an amelioration of corrosions resistance of the ceramic coatings.

The effect of soda ash, liquid glass and sodium tripolyphosphate on rheological properties and stability of ceramic slip have been investigated by Kichkail and Levitskii [4]. It was shown that the introduction of electrolyte on ceramic slip caused stabilization as well as a decrease in the thixotropic behaviour of ceramic slip. Andreola et al [5] demonstrated that adding bentonite to clays used on ceramic improves the plastic components and this causes the amelioration of the mixture's rheological behavior such as the increasing the viscosity and the thixotropy. Moreover, Hammadi [6] has indicated that incorporating a percentage from 0% to 9% of bentonite in the formation of ceramic cases an increase, not only in yield stress, but also in the consistency index of slip of ceramic. Likewise, the author demonstrated that the incorporation of bentonite on slip of ceramic causes an increase of mechanical resistance of slip of ceramic. Contreras et al [7] demonstrated that the incorporation of 7.5% of phosphogypsum in the formation of ceramic cause an increase of the rupture resistance of ceramic tiles. The effect of solid loading on the rheological properties of feedstocks used on fabrication of ceramic has been investigated by Wei et al [8]. The authors have proved the feed stocks viscosity increased with the solid loading increase. Xuand Hilmas [9] studied the rheological behavior of mixtures $BaTiO_3 - Polymer$. It was demonstrated that the rheological behavior of mixtures exhibits shear thinning with a yield stress.The effect of Hyperme KD on rheological properties of ceramic slip has been studied by Xin et al [10]. The authors have demonstrated for lower solids loading (40%) dispersant does not greatly influence the rheological properties of the suspensions but with increasing solids loading to 50%, the rheological properties of the suspensions became more sensitive to the added amount of dispersant. Mohammadi et al [11] investigated the effects of slurry solid concentration on rheological properties of slip ceramics. It was shown that for solid concentration of 76% the rheological behavior of slip ceramics is thixotropic and for solid concentration between 64% and 70% the rheological behavior of slip ceramics is near-Newtonian. In this paper, we investigate the effect of the clay concentration on the mechanical and rheological properties of slip used in the fabrication of ceramic in order to improve the mechanical and rheological properties of ceramic tiles.

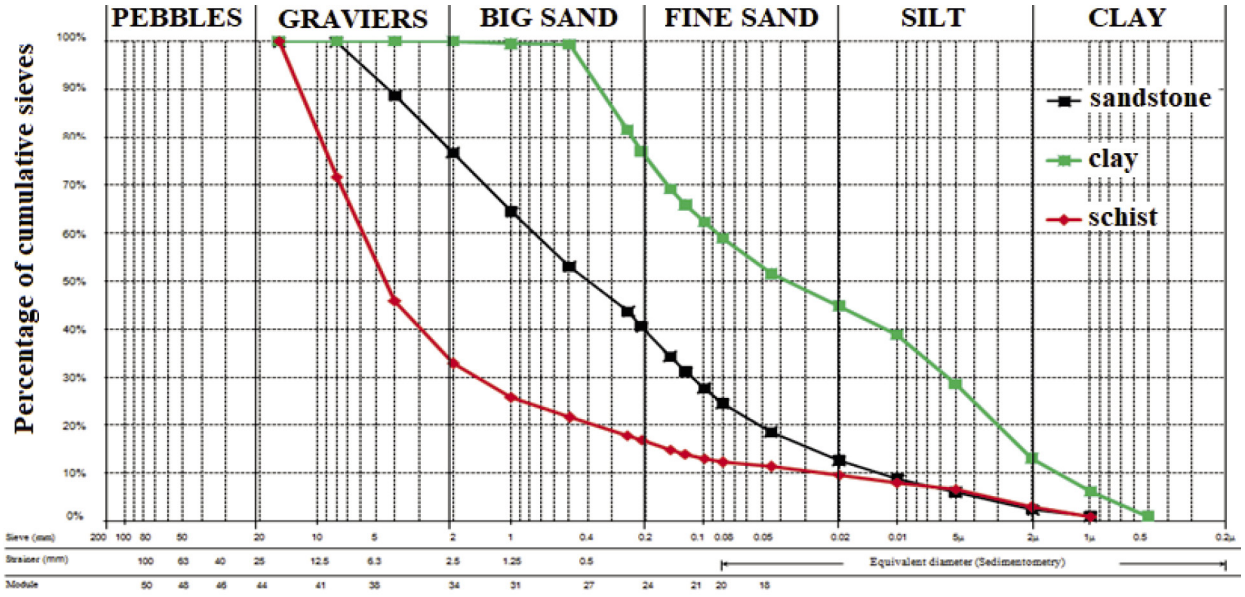

Fig. 1 Particle size of materials used by CERAL Company on fabrication of ceramic
1. ábra A CERAL Company által kerámiagyártáshoz használt anyagok szemcseméret eloszlása

2. Materials and methods

2.1 Materials

The raw materials used in this study are from the "CERAL" Company of Hassi -Amer- Oran Algeria. This company uses clays at fixed percentages by adding deflocculants to facilitate mold release from the plaster molds. *Table 1* presents the various materials used by the company CERAL for the manufacture of ceramics [6, 12].

Materials	Percentage
Schist 1	61%
Schist 2	10%
Sandstone	17%

Table 1 Materials used by the company CERAL for the manufacture of ceramics
1. táblázat A CERAL cég által kerámiagyártáshoz felhasznált anyagok

2.2 Preparation of mixtures

The slips were prepared with 58% dry matter and 42% mixed water and dispersing deflocculant content was fixed at 0.63% (sodium tripolyphosphate of 0.42% and sodium metasilicate of 0.21%) for different quantity of clay. The *Table 2* shows the percentage of mixtures.

Clay (%)	Sandstone (%)	Schist (%)	STPP (%)	MSI (%)	Water (%)
6	23	71	0.42	0.21	42
8	21	71	0.42	0.21	42
10	19	71	0.42	0.21	42
12	17	71	0.42	0.21	42
14	15	71	0.42	0.21	42
16	13	71	0.42	0.21	42
18	11	71	0.42	0.21	42

Table 2 Percentage of mixtures used in this study
2. táblázat A tanulmányban használt keverékek százalékos összetétele

2.3 Preparation of samples

In the first step, each mixture was ground wet in a jet mill long enough until the residue on 63 μm sieves was reduced to require values [6]. In the second step, rectangular samples were carried out using the press (ceramic Instruments Srl) SASSUOLO-ITALY, the maximum pressure of this apparatus is 250 bar and a bending apparatus FLEXI 1000 LX GABTEC, to the company CERAMIR from HASSI AMER Oran. We introduced 100 g of the samples into the press apparatus and a pressure of 80 bars was applied to make tiles with a thickness of 7.8 mm, a length of 100 mm and a width of 45 mm. After 2 hours of drying at 110 °C, the tiles of ceramic were fired at constant temperature of 1140 °C for 45 min in an electric furnace and took 45 min of soaking time [6].

2.4 Steady shear measurements

To study the effect of clay on flow of slip of ceramic the sample was pre-sheared at a frequency of 200 s^{-1} for 60 s in the measuring device in order to avoid any memory effect. After pre-shearing the sample was kept at rest for 600 s prior to measurements in order to permit the material recovering at least its initial structure. After being kept in rest of 600 s, a continuous ramp of shear rate, which is ranging from 0.01 to 200 s^{-1} and has been applied during 600 s.

2.5 Creep-recovery measurements

Creep and recovery tests were carried out as follows: after rest time of 600 s prior to the measurements, a constant shear stress $\tau = 5$ Pa was applied to the samples and the compliance (J) was recorded as a function of creep time; at t = 180 s the stress τ was set to zero and the recoverable part of compliance was measured as a function of the recovery time equal to 180 s.

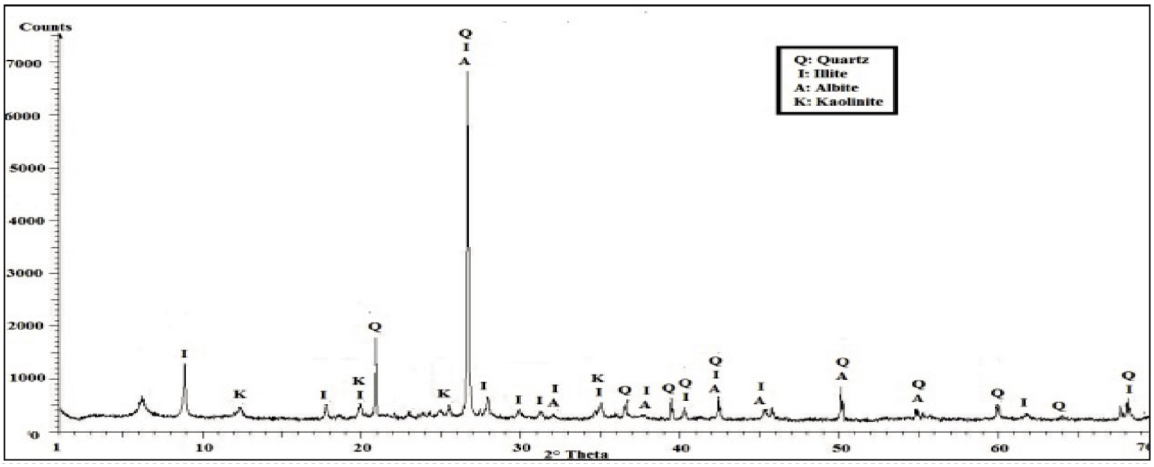

Fig. 2 X-ray diffraction of schist
2. ábra Pala röntgendiffrakciós vizsgálatának eredménye

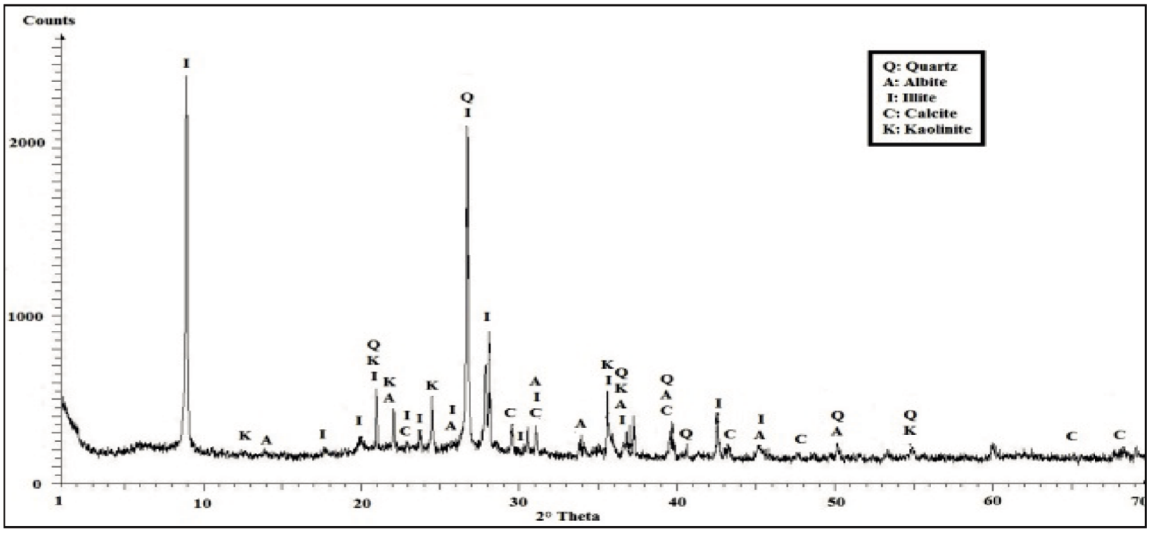

Fig. 3 X-ray diffraction of sandstone
3. ábra Homokkő röntgendiffrakciós vizsgálatának eredménye

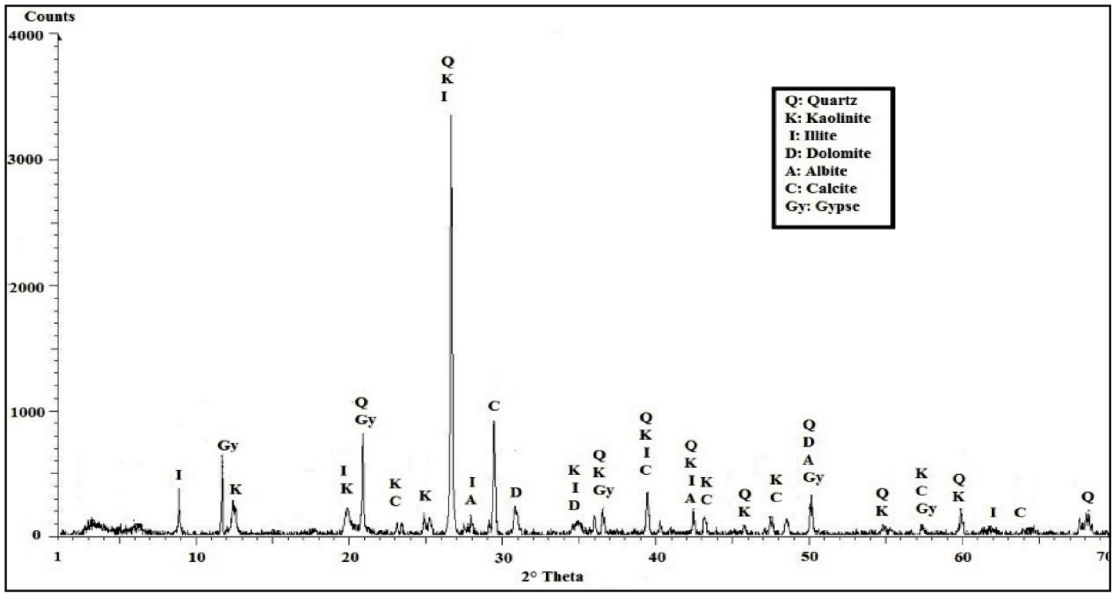

Fig. 4 X-ray diffraction of clay
4. ábra Agyag röntgendiffrakciós vizsgálatának eredménye

3. Results and discussions

3.1 Physical characteristics

The particle size analyses the raw materials are carried out by sieving according to Standard NF P 94-056 and sedimentometry by Standard NF P 94-057.The physical analyses carried out on samples taken from the materials used by CERAL Company gave the following results: the particle size analysis shows that the raw product has a spread out particle size (*Fig. 1*).

The obtained results show that the Schist, Sandstone and clay are aggregates rich in fine elements, composed of an important fraction of silt, sand, gravel and clay. Fractions of clay, silt and sand are listed in *Table 3*. We observe in *Table 3* the Schist indicates a low plasticity the sandstone is medium plasticity and clay is high plasticity.

Physical parameters	Schist	Sandstone	Clay
Clay fraction (<2 μm)	3.70	2.46	13.1
Silt fraction (2-63 μm)	7.70	19.2	42.4
Sand fraction (>63 μm)	88.2	78.3	44.5
Liquidity limits	31.2	39.7	62.0
Limits of plasticity	17.2	21.7	31.9
Plasticity index (%)	14.0	18.0	30.1

Table 3 Physical parameters of schist, sandstone and clay
3. táblázat A pala, homokkő és agyag fizikai paraméterei

3.2 Chemical analysis

Table 4 indicates the chemical analysis of materials used by CERAL (schist, sandstone and clay). The data given in *Table 4* illustrate that the alumina and silica oxide are present in major quantities while other minerals are present in trace amounts.

Elements	Schist (%)	Sandstone (%)	Clay (%)
SiO_2	63.1	61.0	52.9
Al_2O_3	16.6	13.6	14.6
Fe_2O_3	7.62	5.42	7.04
CaO	1.69	6.70	6.22
MgO	1.38	1.47	1.94
SO_3	0.07	0.07	0.51
K_2O	2.56	2.26	1.74
Na_2O	0.33	0.61	0.21
LOI	5.76	6.05	14.3

Table 4 Chemical analysis of schist, sandstone and clay
4. táblázat A pala, homokkő és agyag kémiai összetétele

3.3 Mineralogical RX analysis

The mineralogical RX analysis of the raw materials (Schist, Sandstone and clay) is reported in *Fig. 2*, *3* and *4*. The identified minerals are mainly quartz, calcite and in a smaller amount of clays (kaolinite and illite) on the Schist and Sandstone. In clay, the kaolinite and illite are present on high quantity. According to [13-14] these elements exploitation is favoured in the field of ceramics.

3.4 Effect of quantity of clay on flexural strength of slip

Fig. 5 shows the variation of slip's flexural strength as a function of the clay's concentration on ceramic slip after firings 1140 °C at different pressures. We observe in the *Fig. 5*, an increase in the mechanical resistance with the increase in the amount of quantity of clay in the slip, this rise can be explained by the increase in the kaolinite and illite content as well as the increase in quantity of clay in slip of ceramic. According to Khalfaoui and Hajjaji [15] at 1140 °C the quartz begins to react with the decomposed micaceous phase, contributing to the formation of the glassy phase, this formation of glass cause an increase on flexural strength of slip.

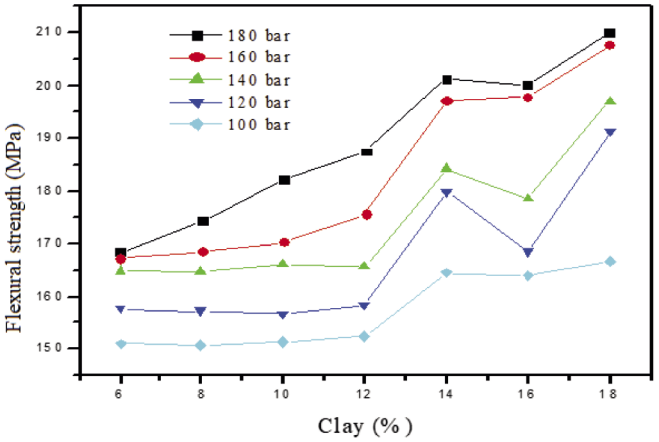

Fig. 5 Flexural strength as a function of clay concentration added to slip of ceramic after firings 1140 °C
5. ábra Hajlítószilárdság az 1140 °C-os kiégetés után a kerámiához adott agyagkoncentráció függvényében

3.5 Effect of clay in flow properties of slip of ceramic

The variation of the shear stress τ as a function of the shear rate $\dot{\gamma}$ at different percentage of clay which vary between 6% and 18% for the studied sample has clearly shown two behaviors separated by a critical shear rate: a Non-Newtonian behavior after a yield stress followed by a plastic behavior (*Fig. 6*). Experimental data were fitted to modified Cross model (Eq. (1)) developed by Grassi et al [16] which has been successfully employed for weak gel systems.

$$\tau = \tau_0 + \eta_\infty \dot{\gamma} + \frac{(\eta_0 - \eta_\infty)\dot{\gamma}}{1+(\lambda_c \dot{\gamma})^m} \quad (1)$$

where τ_0 is the yield stress, η_0 is the zero shear rate viscosity (lower Newtonian plateau), η_∞ is the infinite shear rate viscosity (upper Newtonian plateau), λ_c is a characteristic time and is a dimensionless exponent. It should be noted here that, in the case of plastic systems, the zero shear viscosity η_0 represents the estimated value for the viscosity in which this system is maintained a typical solution behavior for low values of shear rates.

As it can be observed from *Fig. 7* the increase of clay in slip of ceramic causes an increase in the yield stress τ_0 and in the infinite shear rate viscosity η_∞. According to Reeds [17] and Blanc and Van Damme [18] the increase in the yield stress and the viscosity of slip ceramic can be explained by the Van der Walls attracting forces, which are responsible for the formation

of flocks and aggregates and for the resistance to flow. When the clay percentage increases, so do the number of particles and the double layer repulsions, thus leading to higher interaction forces and finally to a rigid continuous network [19].

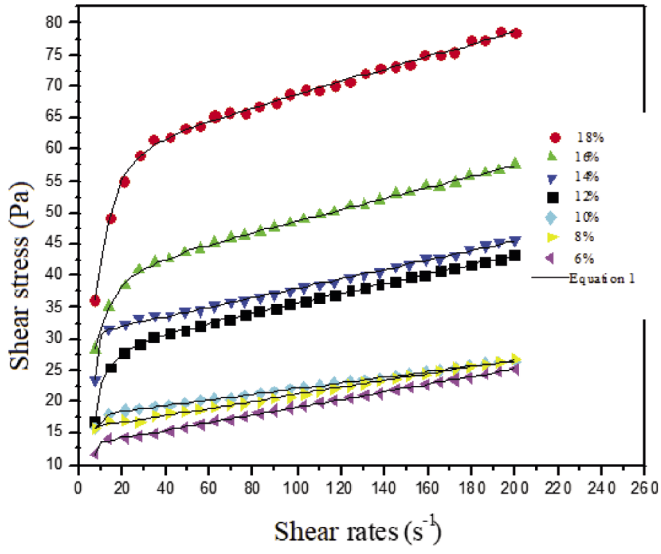

Fig. 6 *Flow curves for slip ceramic at different quantity of clay*
6. ábra *A kerámia massza folyási görbéi különböző mennyiségű agyag adagolása esetén*

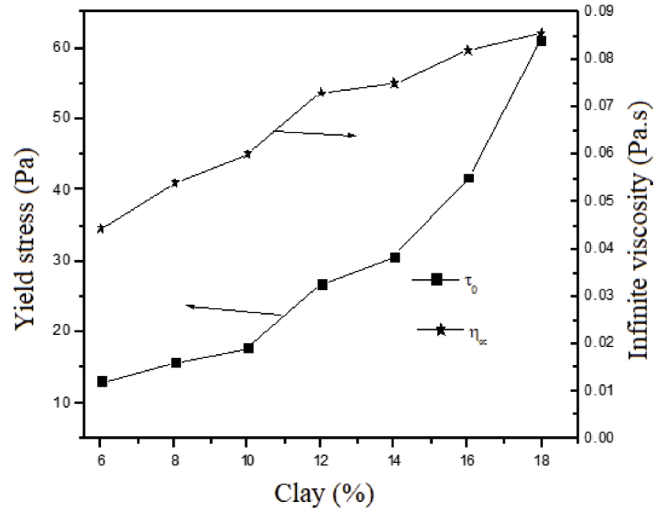

Fig. 7 *Variation of the yield stress τ_0 and the infinite shear rate viscosity η_∞ of slip ceramic as a function of quantity of clay*
7. ábra *A kerámia massza τ_0 folyáshatárának és végtelen nyírási viszkozitásának η_∞ változása az agyag mennyiségének függvényében*

3.6 Effect of quantity of clay on creep and recovery of slip of ceramic

Fig. 8 shows the values of compliance $J(t) = \frac{\gamma}{\tau}$, as a function of time, for the creep tests corresponding to the ceramic slip studied for mass concentration of clay range between 6% and 18% added in slip of ceramic , in a period of time intervals between 0 and 180 $s \leq 360$ s. For the interval time, we have represented the corresponding recovery. We observe on this figure a decrease of the elastic compliance with the increase of quantity of clay added to the slip of ceramic, i.e. the increase of the elastic modulus $\frac{1}{J}$, indicating an increase of the viscoelastic properties of the slip of ceramic. In other words, the creep deformation decreases with increasing the clay in slip and the time necessary to reach a constant deformation during recovery decreases, after removal of the shear stress.

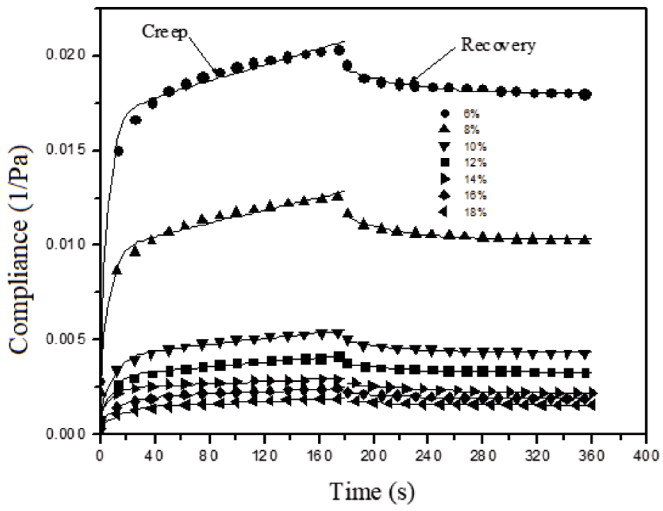

Fig. 8 *Compliance versus time in creep and recovery test for quantity different of clay added to slip of ceramic*
8. ábra *Megfelelőség az idő összefüggése a kúszási és visszanyerési teszt során a kerámia masszához adott különböző mennyiségű agyag esetében*

The elastic properties were defined by correlating the results with the well-known viscoelastic models of Burger model or Generalized Kelvin-Voigt [20-22], comprising the association in series of the Maxwell model and the Kelvin-Voigt.

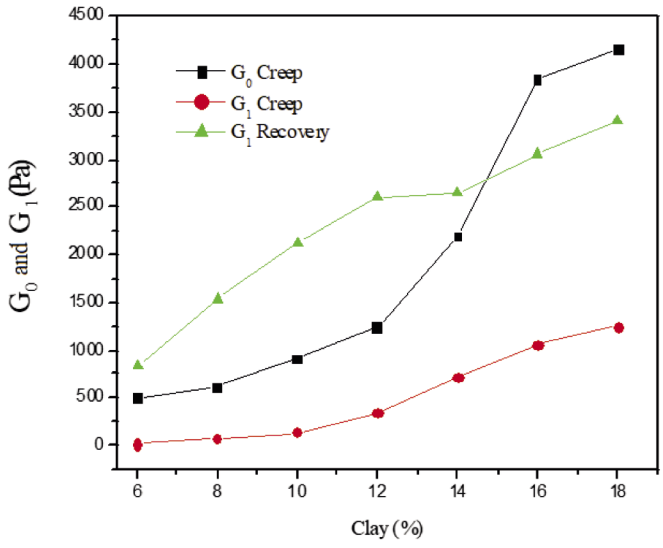

Fig. 9 *Instantaneous elastic modulus of the Maxwell G_0 and elastic modulus of Kelvin–Voigt G_1 as a function of quantity of clay in slip of ceramic*
9. ábra *A Maxwell G_0 pillanatnyi rugalmassági modulus és a Kelvin–Voigt G_1 rugalmassági modulus a kerámiában lévő agyag mennyiségének függvényében*

The creep curves are described by:

$$J_F = J_0 + \frac{t}{\eta_0} + \sum_{i=1}^{N} J_i \left[1 - \exp\left(-\frac{t}{\theta_i}\right)\right] \quad (2)$$

$$\theta_i = \frac{J_i}{\eta_i} \quad (3)$$

Whereas the recovery strain is given by:

$$J_R = \frac{t_1}{\eta_0} + \sum_{i=1}^{N} J_i \left[\exp\left(\frac{t_1}{\theta_i}\right) - 1\right] \exp\left(-\frac{t}{\theta_i}\right) \quad (4)$$

Where J_0 is the purely elastic contribution (or the instantaneous elastic compliance), η_0 is the purely viscous contribution, represented by the dashpot of the Maxwell model, i.e., the uncoupled or residual steady-state viscosity obtained from the creep curve at long times when the compliance curve is linear, J_i is the contribution to retarded elastic compliance, θ_i is the retarded time, η_i is the retarded viscosity and t_1 is the time where the stress is applied for $t \leq t_1$ and removed at $t = t_1$.

The fittings in *Fig. 8* were performed with just one Kelvin–Voigt solid (N=1) and the fitting parameters are shown in *Fig. 9* and *10*. The $G_0 = \frac{1}{J_0}$ represents the instantaneous elastic modulus of the Maxwell unit at t = 0; that is, the instantaneous elastic response of the system and the $G_1 = \frac{1}{J_1}$ is the elastic modulus of Kelvin–Voigt. The latter represents the contributions of the retarded elastic region to the total compliance. The strong increase is observed in G_0 and G_1 when the quantity of clay is added, the slip of ceramic is varied between 6% and 18% and it is a manifestation of the shift from viscous to elastic behaviour and an increase of the viscoelastic properties in that range of clay.

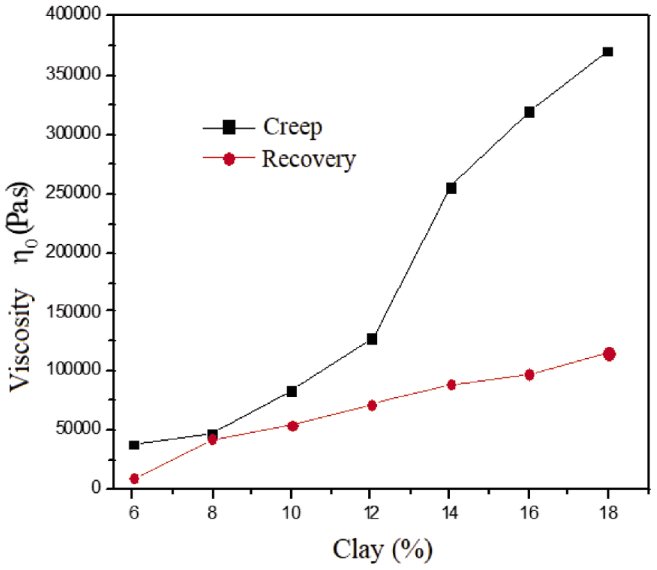

Fig. 10 Viscosity of slip ceramic as function of quantity of clay
10. ábra Kerámia massza viszkozitása az agyag mennyiségének függvényében

Fig. 10 shows the variation of viscosity η_0 of slip ceramic as function of quantity of clay; it is important to mention that it has the meaning of viscosity of the system in the Newtonian regime, whereas it shows a clearly increasing trend as the quantity of clays is increased in slip of ceramic. This increasing of viscosity could be explained by the effect of Brownian motion on the strong network structure formed in the dispersion with the increasing of clay concentration in slip of ceramic [6, 23]. According to Hammadi [6] at high quantity of clay (18%) added to slip of ceramic, the applied stress is not sufficient to break weak particle-to-particle bonds, and the suspensions do not flow.

4. Conclusions

In this work, the effect of the clay concentration on the mechanical properties and rheological behavior of slip used in fabrication of ceramic was studied. The study shows that an increase of flexural strength with increase of quantity of clay in slip of ceramic.

The non-Newtonian stationary flow behavior of slip of ceramic was successfully modeled by using the coupled Cross and Bingham models over the studied range of clay concentration. The increase of clay concentration ranging between 6% and 18% in ceramic slip, caused the augmentation in the yield stress τ_0 and the infinite shear rate viscosity η_∞ with adding dose of clays. The increase of these parameters was mainly related to the interaction between the solid particles and viscous effects. Then, the increase of the parameters of modified Cross model causes an increase, not only in the friction, but also in the viscosity of the ceramic slip. The study also shows that the increase of quantity of clay in the slip of ceramic causes an increase on the viscoelastic behavior of slip of ceramic and structure of particle-to-particle bonds. The structure of particle-to-particle bonds of slip of ceramic facilitates the operation of demolding the tiles of ceramic. Finally in order to ameliorate mechanical properties and rheological behavior of slip of ceramic we suggest the use of 18% of clay, 11% of Sandstone and 71% of Schist for the preparation of the tiles of ceramic.

References

[1] Baccour, H. - Medhioub, M. - Jamoussi, F. *et al. (2009):* Influence of firing temperature on the ceramic properties of Triassic clays from Tunisia. Journal of materials processing technology.Vol. 209, No. 6, pp. 2812-2817, https://doi.org/10.1016/j.jmatprotec.2008.06.055.

[2] Arsenović, M. - Stanković, S. - Radojević, Z. - & Pezo, L. (2013): Prediction and fuzzy synthetic optimization of process parameters in heavy clay brick production. Ceramics International. Vol. 39, pp. 2013-2022, https://doi.org/10.1016/j.ceramint.2012.08.053.

[3] Shi, L. - Xu, Y. - Li, K. - Yao, Z. - Wu, S. (2010): Effect of additives on structure and corrosion resistance of ceramic coatings on Mg–Li alloy by micro-arc oxidation. Current Applied Physics. Vol. 10, pp. 719-723, https://doi.org/10.1016/j.cap.2009.10.011.

[4] Kichkailoand, O. V. - Levitskii, A. (2017): Rheological characteristics of slips in making heat-resistant lithium-aluminum-silicate ceramic. Glass and Ceramics.Vol. 74, pp. 257-263, https://doi.org/10.1007/s10717-017-9975-3.

[5] Andreola, F. - Siligardi, C. - Manfredini, T. - Carbonchi, C. (2009): Rheological behaviour and mechanical properties of porcelain stoneware bodies containing Italian clay added with bentonites. Ceramics International. Vol. 35 pp. 1159-1164, https://doi.org/10.1016/j.ceramint.2008.05.017.

[6] Hammadi, L. (2018): Improving of the mechanical and rheological properties of slip of ceramic. Construction and Building Materials.Vol. 173, pp. 118-123, https://doi.org/10.1016/j.conbuildmat.2018.04.035.

[7] Contreras, M. - Teixeira, S. R. - Santos, G. T. A. - Gázquez, M. J. - Romero, M. - Bolívar, J. P. (2018): Influence of the addition of phosphogypsum on some properties of ceramic tiles. Construction and Building Materials. Vol. 175, pp. 588-600, https://doi.org/10.1016/j.conbuildmat.2018.04.131.

[8] Wei, J. - Li, J. - Song, X. - Feng, Y. - Qiu, T. (2018): Effects of solid loading on the rheological behaviors and mechanical properties of injection-molded alumina ceramics. Journal of Alloys and Compounds. Vol. 768, pp. 503-509, https://doi.org/10.1016/j.jallcom.2018.07.036.

[9] Xu, X.-Hilmas, G. E. (2007): The rheological behavior of ceramic/polymer mixtures for coextrusion processing.Journal of materials science.Vol. 42, pp. 1381-1387, https://doi.org/10.1007/s10853-006-1221-2.

[10] Xu, X. - Oliveira, M. I. - Fu, R. -& Ferreira, J. M. (2003): Effect of dispersant on the rheological properties and slip casting of concentrated sialon precursor suspensions. Journal of the European Ceramic Society. Vol. 23, pp. 1525-1530, https://doi.org/10.1016/S0955-2219(02)00349-7.

[11] Mohammadi, F. - Mirzaee, O. - Tajally, M. (2018): Influence of solid loading on the rheological, porosity distribution, optical and the microstructural properties of YAG transparent ceramic. CeramicsInternational.Vol. 44, pp. 12098-12105, https://doi.org/10.1016/j.ceramint.2018.03.230.

[12] Kreirzti, L. K. - Benamara, L. - Boudjenane, N. E. (2019):Valorization of dredging sediments of dam BOUHNIFIA in ceramic. Journal of the Australian Ceramic Society. Vol. 55, pp. 1081-1089, https://doi.org/10.1007/s41779-019-00321-x.

[13] Oikonomopoulos, I. K. - Perraki, M. - Tougiannidis, N. - Perraki, T. - Kasper, H. U. - Gurk, M. (2015): Clays from NeogeneAchlada lignite deposits in Florina basin (Western Macedonia, N. Greece): A prospective resource for the ceramics industry. Applied Clay Science. Vol. 103, pp. 1-9, https://doi.org/10.1016/j.clay.2014.11.002.

[14] Ngayakamo, B. - Park, S. E. (2018): Effect of firing temperature on triaxial electrical porcelain properties made from Tanzania locally sourced ceramic raw materials. Journal of Silicate Based and Composite Materials. Vol. 4, pp. 106-109, https://doi.org/10.14382/epitoanyag-jsbcm.2018.19.

[15] Khalfaoui, A. - Hajjaji, M. (2009) : A Chloritic-illitic clay from Morocco: Temperature–time–transformation and neoformation. Applied Clay Science. Vol. *45*, pp. 83-89, https://doi.org/10.1016/j.clay.2009.03.006.

[16] Grassi, M. - Lapasin, R. - Pricl, S. (1996): A study of the rheological behavior of scleroglucan weak gel systems.Carbohydrate Polymers.Vol. 29, pp. 169-181, https://doi.org/10.1016/0144-8617(95)00120-4.

[17] Reed, W. F. (1995): Data evaluation for unified multi-detector size exclusion chromatography-molar mass, viscosity and radius of gyration distributions.Macromolecular Chemistry and Physics.Vol. 196 pp. 1539-1575, https://doi.org/10.1002/macp.1995.021960515.

[18] Blanc, R. - Van Damme, H. (1995): Rheology of pastes.In Mobile Particulate Systems. Vol. 87, pp. 129-160, https://doi.org/10.1007/978-94-015-8518-7_10.

[19] Van Olphen, H. (1955): Forces between suspended bentonite particles. Clays and clay minerals. Vol. 4, pp. 204-224, https://doi.org/10.1346/CCMN.1955.0040128.

[20] Mainardi, F. - Spada, G. (2011): Creep, relaxation and viscosity properties for basic fractional models in rheology. The European Physical Journal Special Topics. Vol. 193, pp. 133-160, https://doi.org/10.1140/epjst/e2011-01387-1.

[21] Hammadi, L. - Boudjenane, N. - Belhadri, M. (2014): Effect of polyethylene oxide (PEO) and shear rate on rheological properties of bentonite clay. Applied Clay Science. Vol. 99, pp. 306-311, https://doi.org/10.1016/j.clay.2014.07.016.

[22] Hammadi, L. -Ponton, A. (2017): Rheological investigation of vase of dam: effects of aging time, shear rate, and temperature. Applied Rheology. Vol. 27, pp. 21-29, https://doi.org/10.3933/applrheol-27-14667.

[23] Durán, J. D. G. - Ramos-Tejada, M. M. - Arroyo, F. J. - Gonzalez-Caballero, F. (2000): Rheological and electrokinetic properties of sodium montmorillonite suspensions: I. Rheological properties and interparticle energy of interaction. Journal of Colloid and Interface Science. Vol. 229, pp. 107-117, https://doi.org/10.1006/jcis.2000.6956.

Ref.:
Mahi, Sahra – **Hammadi**, Labri – **Boudjenane**, Nasr-Eddine: *Effect of clay concentration on the mechanical properties and rheological behavior of ceramic slip*
Építőanyag – Journal of Silicate Based and Composite Materials, Vol. 74, No. 4 (2022), 122–128. p.
https://doi.org/10.14382/epitoanyag-jsbcm.2022.19

Compressive strength optimisation of rice husk ash concrete using Scheffe's mathematical model

Godwin A. AKEKE ▪ Department of Civil Engineering, University of Cross River, Nigeria ▪ greatakeke@yahoo.com
Chidozie C. NNAJI ▪ Department of Civil Engineering, University of Nigeria, Nigeria ▪ chidozie.nnaji@unn.edu.ng
Udeme U. UDOKPOH ▪ Department of Civil Engineering, Akwa Ibom State University, Nigeria ▪ udemeudokpoh@aksu.edu.ng

Érkezett: 2021. 10. 31. ▪ Received: 31. 10. 2021. ▪ https://doi.org/10.14382/epitoanyag-jsbcm.2022.20

Abstract
The high cost of cement as a significant component of concrete has led to the high cost of concrete production in most developing countries. Because of its longevity and good benefit-to-cost ratio, blended cement has grown in popularity in developed countries. Rice husk ash (RHA) is a residue produced by the burning of rice husk that is abundant in rice mills. RHA has been proven as a good supplementary cementitious material for concrete production due to its low energy requirements, minimal greenhouse gas emissions during processing and service life, and strong pozzolanic reaction. Using Scheffe's (4, 2) simplex-lattice design, a mathematical model was developed to optimise the compressive strength of RHA reinforced concrete in this research. RHA was used as the second component in concrete, along with water, cement, fine and coarse aggregates, at a partial replacement ratio of 20% in cement. The compressive strength of RHA concrete was determined using Scheffe's Simplex technique for the various componential ratios as well as the control points that would be used to validate the Scheffe's model. The model's adequacy was assessed using the f-statistics test, the student's t-test, and ANOVA at a 5% significance level. The statistical result shows a satisfactory correlation between the values produced from the developed Scheffe's model and the control laboratory data. The maximum compressive strength of RHA concrete obtained was 40.75 N/mm^2 corresponding to a mix ratio of 0.475: 1.0: 2.75: 3.50 and the minimum compressive strength obtained was 7.41 N/mm^2 corresponding to a mix ratio of 0.47: 1.0: 2.5: 4.5 for water, binder (80% cement and 20% RHA), fine aggregate, and coarse aggregate, respectively. The ratio of the mix elements to a particular required compressive strength value may be calculated with a high degree of precision using the established Scheffe's simplex model, while also giving the answer in less time by resolving trial mix challenges.

Keywords: compressive strength, concrete, optimisation, Scheffe's model, rice husk ash
Kulcsszavak: nyomószilárdság, beton, optimalizálás, Scheffe-modell, rizshéj pernye

Godwin A. AKEKE
Senior Lecturer: Department of Civil Engineering, University of Cross River, Calabar, Nigeria. Registered Engineer at Council for the Regulation of Engineering in Nigeria (COREN). Member, Nigerian Society of Engineers (NSE). Research Interests: concrete technology; supplementary cementitious materials (SCM); concrete recycling; mathematical modelling.

Chidozie C. NNAJI
Professor; Former Head, Department of Civil Engineering, University of Nigeria, Nsukka, 410001 Enugu State, Nigeria. Senior Research Associate: Faculty of Engineering and Built Environment, University of Johannesburg, South Africa. Registered Engineer at Council for the Regulation of Engineering in Nigeria (COREN). Member, Nigerian Society of Engineers (NSE). Research Interests: water resources, environmental engineering..

Udeme U. UDOKPOH
M. Eng student at Department of Civil Engineering, Nigerian Defence Academy, Kaduna, Nigeria. Assistant Lecturer: Akwa Ibom State University, Ikot Akpaden, Akwa Ibom State, Nigeria. Member, International Association of Engineers (IAENG) Graduate member, Nigerian Society of Engineers (NSE). Research Interests: solid waste management; agro-based cementitious materials; environmental pollution.

1. Introduction

Concrete compressive strength is one of the most significant material properties utilised in structural design and quality control [1]. Concrete is mainly utilised in civil engineering under compression loading situations because its compressive strength is significantly greater than its tensile and/or flexural strengths. Furthermore, because it is directly connected to the structure of the hydrated cement paste, compressive strength is frequently regarded as a diagnostic of concrete quality [2]. For these reasons, compressive strength is commonly used to make choices about the strength and serviceability of concrete components and structures [3]. The compressive strength of concrete is one of its major engineering features, and it has become a standard in industrial practice to classify concrete based on its compressive strength (i.e. grades) [4]. The compressive strength of concrete is defined by its capacity to withstand cracking and fissure failure. The ultimate compressive strength of a material is equal to the value of uniaxial compression stress attained at the complete failure point and is affected by factors such as constituent compressive strength, water-cement ratio, material quality, curing methods, air entrainment, temperature effects, and mixture constituent proportion. Concrete compressive strength is proportional to its density. Additionally, it is dependent on the mix proportion, aggregates, cement properties, water-cement ratio, curing duration, and SCMs replacement level [5-6]. The experimental technique of concrete mix design consists of a series of lengthy experiments that are mostly based on trial and error and entail approximate estimations based on practical experience without the use of a mathematical or statistical scientific approach [7]. To reduce the number of experimentation tests required before determining the ideal combination ratio for concrete mixed with RHA, an analytical approach that tries to justify the initial trial mix into a logical and systematic procedure is being developed. Based on established knowledge of certain empirical connections, particular weights of mixture ingredients, and findings from previous literatures, this will aid in determining the optimal combination for the mixture ingredients in spending less resources [8].

Scheffe's approach is a mixed model strategy for adjusting statistical significance levels in a linear regression study to account for multiple comparisons. When performing evaluation of simultaneous confidence levels for regression analysis using objective functions [9], it is critical for a particular kind of regression analysis known as analysis of variance. Scheffe's simplex second order regression model is created statistically to maximise the compressive strength attribute of RHA concrete. The statistical method used for recycling, use, and re-use of agricultural solid waste material such as RHA has been proven to be a beneficial strategy in engineering practice [4-10]. The application of Scheffe's simplex lattice design to accomplish mixture design has been used in various civil engineering applications to provide solutions in fields such as material science, pavement material changes, soil stabilisation, geotechnical and concrete technology [11-13]. Ambrose et al. [14]; in their work on Compressive strength and Scheffe's optimisation of mechanical properties of recycled ceramics tile aggregate concrete. Laboratory tests were performed in relation to the calculated Scheffe's design point. To validate the established mathematical model, statistical analysis was performed. In their results, the maximum predictable response from the compressive strength model was 42.13 N/mm^2 existing at vertex X_5 of the simplex and corresponding to mix ratio of 0.45:1:0:1:2 for water, cement, sand, recycled-ceramic tiles (CRT) and coarse aggregates (CA). Conversely, the lowest predictable compressive strength was found to be 20.34 N/mm^2 existing very close to Vertex X_3 and corresponding to mix ratio of 0.64:1:2.35:0.06:4.35. Their investigation also revealed that CRT, which is widely available and inexpensive, has been effectively employed to produce concrete. Also, Alaneme and Mbadike [15]; in their research study on compressive strength modelling of palm nut fiber concrete using Scheffe's theory. The concrete mixture consists of five components: cement, water, coarse aggregates, fine aggregates, and palm-nut fiber, an agricultural waste. At a strength value of 31.53 N/mm^2, the best combination ratio of 0.525:1.0:1.45:1.75:0.6 was found, while the lowest combination ratio of 0.6:1.0:1.8:2.5:1.2 for water, cement, fine and coarse aggregate, and palm nut fiber was reached at a strength value of 17.235 N/mm^2. Furthermore, Chiemela et al. [45] used Scheffe's theory to model the compressive strength property of concrete when given componential ratios, as well as predict the corresponding portions of the mixture ingredients with prescribed values of compressive strength vale of concrete obtained by substituting quarry dust for river sand in their work. The formulated model was then put to the test with the response value of the control point. F-statistics and a student's t-test with a 95% confidence level were employed in this statistical investigation. The results demonstrate that the anticipated and measured values are not significantly different.

There are currently no mathematical models for RHA concrete, but the demand for such models is essential. Therefore, this research seeks to investigate the use of RHA, a residual agricultural waste, as a partial replacement in the second component (binder) in concrete mixtures. The goal of this study is to partially integrate ash material at 20% replacement level into concrete mixtures rather than using it as a separate component, and to use statistical methods to determine the best mixture combination of the concrete mixture's ingredients, which include water, cement, RHA, fine aggregate, and coarse aggregate. RHA is being employed in this study to improve ecological infrastructure development by recycling solid wastes originating from agricultural or industrial operations, which is accomplished by substituting traditional concrete materials. The compressive strength of concrete is typically influenced by the mix proportions of its constituents. The optimal combination ratio for the mix elements of water, binder (cement and RHA) fine aggregate, and coarse aggregate was determined using Scheffe's optimisation approach to predict the concrete compressive strength behaviour. This study will add to the body of information regarding the optimisation of concrete mixtures including solid waste materials as an additive. The findings of this study will allow for improved choice in terms of determining concrete grade and batching of its constituents for structural application. Additionally, this will simplify mix designs by resolving trial mix issues, reducing experimental blunders.

1.1 The Scheffe's Simplex-lattice Design

Simplex lattice design is a type of mixed experiment that is used to study response and component correlations. Simplex lattice designs are simply referred to as Scheffe's simplex lattice designs in Scheffe's theory. Mixture experiment approaches are generally used in instances when the response is determined by the mass or volume proportions of individual components rather than their overall mass or volume, as is common of concrete properties [9, 17]. According to [4], if q indicates the number of mixture components, X_1, X_2, X_3, X_4,...,Xq, however, y signifies the intended response. No component has a negative value in a mixing experiment, and the sum of the component ratios must be one.

The simplex-lattice is an orderly arrangement of lines that connects the expected experimental points of the mixed constituent ratio design. The factor space in a q-component mixing experiment is a regular {q-1} simplex [18]. If q = 2, the lattice simplex is a straight line; if q = 3, it is an equilateral triangle; and if q = 4, it is a regular tetrahedron with each vertex representing one of the components. However, Scheffe proposed that in a mixture design, each component of the mixture resides on a vertex of a simplex lattice with {q-1} factor space, such that if the degree of the polynomial to be fitted to the design is denoted by n, then a {q, n} simplex lattice for q-components consists of uniformly spaced points defined by all the possible combinations of {n+1} levels of each component [19]. Concrete's properties are determined by the appropriate mass or volume mix proportion of its ingredients, not by its overall mass or volume. Scheffe's optimisation theory, as a result, may be employed to model and optimise concrete properties. According to [14], for a 4-compomponent mixture adopted in this work, the reduced second-degree polynomial can be obtained as follows:

$$\sum X_i = 1 \; or \; X_1 + X_2 + X_3 + X_4 = 1 \quad (1)$$

Where; X_1= Water/Cement Ratio; X_2 = Binder (80% OPC and 20% RHA); X_3 = Fine Aggregates (Sand); X_4 = Coarse Aggregates (Granite).

$$Y = \propto_i X_1 + \propto_2 X_2 + \propto_3 X_3 + \propto_4 X_4 + \propto_{12} X_1X_2 + \propto_{13} X_1X_3 + \propto_{14} X_1X_4 + \propto_{23} X_2X_3 + \propto_{24} X_2X_4 + \propto_{34} X_3X_4 \quad (2)$$

The number of terms in the simplified polynomial is also related to the design points on Scheffe's lattice simplex. As a result, the equations' coefficients can be expressed as functions of expected responses (y_i) at the simplex's design and control points. The general relationship between the two is as follows:

$$a_i = y_i \quad (3)$$

And for a (4,2) polynomial

$$a_{ij} = y_i = 4_{ij} - 2y_i - 2y_j \quad (4)$$

Obam [20] also considered experiments with mixtures in which the property he studied was determined by the proportions of the components but not by their quantities in the mixture. The relationship between the compressive strength of concrete and the proportion of w/c (water/cement), cement, fine and coarse aggregates is an obvious example of such a study. If a mixture has q components in total, and Xi is the proportion of the components (ingredients) of the ith component in the mixture such that

$$Xi \geq 0 \ (i = 1\text{-}4) \ (2) \quad (5)$$

Then, assuming the mixture to be a unit quantity, he calculated that the sum of all the proportions of the components must equal unity. That is to say

$$\sum_{i=1}^{4} X_i = 1 \quad (6)$$

where in this case,
X_1 is proportion of water/cement (w/c) ratio
X_2 is proportion of cement
X_3 is proportion of sand
X_4 is proportion of crushed stone.
Thus, the factor space is a regular (q-l) dimensional simplex.

1.1.1 Components relationship in Scheffe's factor space

For a quaternary system, q = 4, the regular simplex is a tetrahedron where each vertex represents a straight component, an edge represents a binary system and a face a tertiary one. Points inside the tetrahedron correspond to quaternary systems as shown below. Each point in the tetrahedron therefore represents a certain composition of the quaternary system. The component X_1 is therefore absent in the face X_2, X_3, X_4 but as tetrahedron sections parallel to the face approach vertex X_1, component X_1 in them grows concentration.

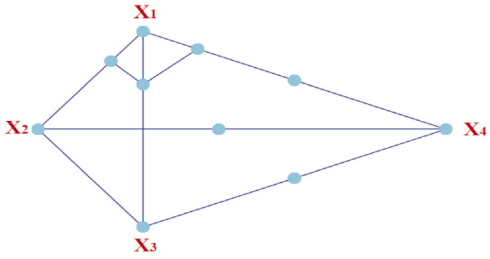

Fig. 1 A {4.2} Scheffe's simplex lattice with the tetrahedron and corresponding points
1. ábra A {4.2} Scheffe tetraéder szimplex rács a hozzátartozó csomópontokkal

The mixed components are uniformly dispersed in Scheffe's simplex design, and the proportions assumed by each component are n+1 equally spaced levels from 0 to 1 according to Eq. (7).

$$X_i = 0, \frac{1}{n}, \frac{2}{n}, \ldots . 1 \quad (7)$$

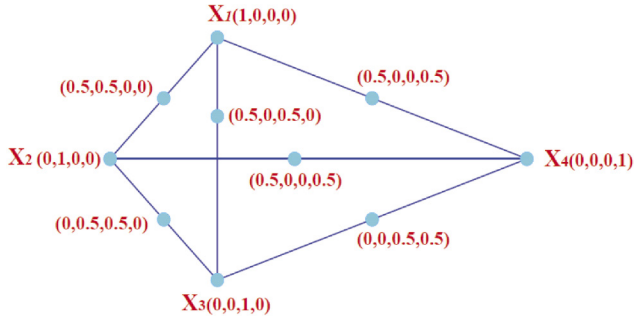

Fig. 2 A {4.2} Scheffe's simplex lattice with pseudo ratios at design points
2. ábra A {4.2} Scheffe szimplex rács pszeudoarányokkal a tervezési pontokban

The factor space for a 4,2 Scheffe's simplex lattice, as illustrated in *Fig. 2* above, is a tetrahedron, and each component has the proportions 0, and 1. There are 10 points at the tetrahedron's borders and vertices, which correspond to the number of terms in the simplified second-degree polynomial in Eq. (4). The four points indicated by (1,0,0,0); (0,1,0,0); (0,0,1,0); and (0,0,0,1) at the vertices represent single component mixes, whereas the remaining six points in the middle of each edge represent binary blends of two component mixtures [14].

2. Methodology

The investigation in this work was divided into two stages. The compressive strength of concrete with varied degrees of RHA substitution with Portland limestone cement (PLC) was investigated in the first stage (part A). Polynomial models were developed in the second stage (part B) for optimisation and prediction of compressive strength of RHA concrete using Scheffe's simplex lattice model.

2.1 Laboratory experiment

Water, cement, RHA, fine aggregates (river sand), and coarse aggregates (granite chippings) were used in laboratory tests in both stages of this study. The cement utilised in this study, Unicem brand of Portland Limestone cement of grade 32.5R was used and it met the requirements of the CEM II class of cements as described in NIS 444-1 [21]. The river sand was collected from a river sand mining location in Nsukka, Enugu State, while the granite chippings were sourced from a quarry in Abakaliki, Ebonyi State, all in Nigeria. The rice husks were obtained from Ogoja in Cross River State. They were burned in the open air, and the ash was collected and stored in a dry place in the laboratory. Physical examination revealed that RHA obtained was greyish in colour after being burned. The ashes were chemically analysed to identify the elemental content of each ash.

The main elemental oxide composition of rice husk ash (RHA) was determined using X-Ray Fluorescence at the Standard Organisation of Nigeria (SON) Engineering laboratory, Enugu State Office, Emene Industrial Layout, Enugu State, Nigeria. The compressive strength test is used

to determine the behavior of materials under compression. Compressive strength is widely regarded as the most significant feature of concrete. Three duplicate concrete samples were produced in 150 mm × 150 mm × 150 mm moulds for each mix ratio. Following the mixing and casting of the concrete, the specimens were removed from the mould and cured for 28 days in a curing tank before being tested for compressive strength in accordance with BS EN 12390 [22]. The compressive strength of concrete was calculated using the formula:

$$\sigma = \frac{P}{A} \quad (8)$$

where P is the failure load; A is the cross sectional area of the concrete cube.

2.2 Mathematical modelling

The number of design components in the second phase of this study, which required modelling, was four, and the data would be fitted into Scheffe's second-degree polynomial. As a result, the mixed experiment was planned with a 4, 2 simplex lattice using a commercial statistical software and the design matrix is shown in *Tables 1* and *2*. The simplex condition that $X_1+X_2+X_3+X_4 = 1$ makes it impossible to use standard mix ratios such as 1:3:6 at a given water-cement ratio. As a result, a modification of the real components (normal mix ratios) is required to fulfill this criterion. The design matrix for the Xi experimental points given in *Table 1* is referred to as "Peudo-components," whereas Zi are the actual experimental components.

$$X=AZ \quad (9)$$

Where A is the inverse of Z matrix and

$$Z=AX^T \quad (10)$$

Where A is the inverse of Z matrix, X^T is the transpose of matrix X.

Table 1 presents the values of the computed real components (Z_1, Z_2, Z_3, Z_4), whereas *Table 2* shows the values for the control locations.

S/N	X1	X2	X3	X4	Response	Z1 Water	Z2 Binder	Z3 FA	Z4 CA
1.	1	0	0	0	Y_1	0.45	0.50	0.46	0.44
2.	0	1	0	0	Y_2	1	1	1	1
3.	0	0	1	0	Y_3	1.5	2.0	2.5	3.0
4.	0	0	0	1	Y_4	3	4.0	5.0	6.0
5.	½	½	0	0	Y_{12}	0.475	1	2.75	3.5
6.	½	0	½	0	Y_{13}	0.455	1	2.0	5.0
7.	½	0	0	½	Y_{14}	0.445	1	2.25	4.5
8.	0	½	½	0	Y_{23}	0.48	1	2.25	4.5
9.	0	½	0	½	Y_{24}	0.47	1	2.5	4.5
10.	0	0	½	½	Y_{34}	0.45	1	2.75	5.5

Binder (PLC-80%, RHA-20%); FA-fine aggregate; CA-coarse aggregate

Table 1 Actual and pseudo components for Scheffe's {4, 2} simplex lattice
1. táblázat Scheffe {4, 2} szimplex rácsának aktuális és pszeudo komponensei

S/N	X1	X2	X3	X4	Response	Z1 Water	Z2 Binder	Z3 FA	Z4 CA
11.	½	¼	1/4	0	C_1	0.465	1	1.88	3.75
12.	¼	¼	1/4	1/4	C_2	0.463	1	2.25	4.5
13.	0	¼	0	3/4	C_3	0.46	1	2.63	5.5
14.	½	0	1/4	1/4	C_4	0.48	1	2.13	4.25
15.	½	¼	0	1/4	C_5	0.46	1	2.0	4.0
16.	0	¼	3/4	0	C_6	0.47	1	2.38	4.75
17.	0	½	1/4	1/4	C_7	0.475	1	2.13	4.75
18.	¼	1/8	1/2	1/8	C_8	0.46	1	2.25	4.50
19.	¼	¼	0	½	C_9	0.458	1	2.38	4.75
20.	1/8	1/8	1/4	½	C_{10}	0.454	1	2.56	5.13

Table 2 Control points for Scheffe's {4, 2} simplex lattice
2. táblázat Scheffe {4, 2} szimplex rácsának kontrolpontjai

S/N	Z_1	Z_2	Z_3	Z_4	Z_1Z_2	Z_1Z_3	Z_1Z_4	Z_2Z_3	Z_2Z_4	Z_3Z_4
1	0.08	0.23	0.23	0.46	0.018	0.018496	0.036993	0.052847	0.105694	0.105694
2	0.07	0.168	0.253	0.51	0.012	0.018706	0.037411	0.042513	0.085025	0.127538
3	0.07	0.155	0.31	0.47	0.011	0.021633	0.03245	0.048074	0.072111	0.144222
4	0.05	0.095	0.286	0.57	0.005	0.013605	0.027211	0.027211	0.054422	0.163265
5	0.06	0.135	0.269	0.54	0.008	0.015578	0.031157	0.036229	0.072457	0.144915
6	0.05	0.111	0.278	0.56	0.006	0.014881	0.029762	0.031002	0.062004	0.155009
7	0.04	0.087	0.348	0.52	0.004	0.015399	0.023098	0.030193	0.04529	0.181159
8	0.04	0.107	0.322	0.54	0.004	0.011373	0.018955	0.034463	0.057439	0.172317
9	0.06	0.117	0.234	0.58	0.008	0.015047	0.037618	0.027359	0.068397	0.136794
10	0.06	0.099	0.248	0.59	0.006	0.014704	0.035291	0.024507	0.058818	0.147044

Table 3 Z^T Matrix based on Eq. (14)
3. táblázat A Z^T matrix a 14-es egyenlet alapján

$\alpha_1 = 35.72$, $\alpha_2 = 27.99$, $\alpha_3 = 23.1$, $\alpha_4 = 18.23$

From *Eq. (4)*

$$\alpha_{12} = 4(40.75) - 2(35.72) - 2(27.99) = 35.58$$

$$\alpha_{13} = 4(34.6) - 2(35.72) - 2(23.1) = 20.76$$

$$\alpha_{14} = 4(17.35) - 2(35) - 2(24) = -48.6$$

$$\alpha_{23} = 4(30.6) - 2(27.99) - 2(23.1) = 20.22$$

$$\alpha_{24} = 4(7.42) - 2(27.99) - 2(18.23) = -62.76$$

$$\alpha_{34} = 4(24.63) - 2(23.1) - 2(18.23) = 15.86$$

Thus, from *Eq (2)*, we have;

$$\sigma_c = 35.7X_1 + 27.99X_2 + 23.1X_3 + 18.23X_4 + 35.42X_1X_2 + 20.56X_1X_3 - 47.60X_1X_4 + 20.22X_2X_3 - 62.76X_2X_4 + 15.86X_3X_4 \quad (11)$$

Eq. (11) is the mathematical model for the optimization of the compressive strength of RHA concrete based on Sheffe's (4,2) polynomial.

3. Results and discussion

3.1 Material characterisation

Fig. 3 shows the results of the particle size distribution study performed on cement and non-ground RHA. The results reveal that the percentage passage of non-ground RHA is equivalent to cement and, as such, should be expected to play a pozzolanic role as well as a microfiller effect in order to increase the particle packing density of concrete. The chemical composition of the ash used for the experiment is shown in *Table 4* below; the findings shows that RHA is a highly reactive pozzolana due to a combined SiO_2, and Fe_2O_3 content of 85.60 percent, which is greater than the minimum value of 70 percent prescribed in ASTM C 618 [23].

Fig. 4 depicts the compressive strength of concrete at various levels of RHA replacement. As a consequence, it is clear that incorporating RHA enhances the compressive strength of the resultant concrete substantially.

S/N	Samples	Chemical composition (%)							
		ZnO	SiO_2	CaO	Fe_2O_3	K_2O	MnO	MgO	Na_2O
1	Cement (PLC)	0.12	23.5	65.2	3.40	0.40	0.18	1.35	0.30
2	RHA	0.75	84.6	0.30	0.25	0.69	0.43	0.45	0.51

Table 4 Chemical composition of PLC and RHA
4. táblázat A PLC és az RHA kémiai összetétele

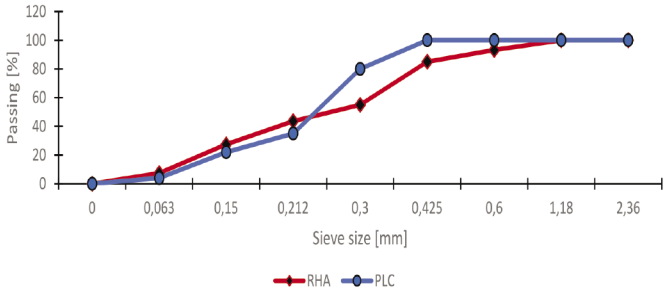

Fig. 3 Particle size distribution for RHA and PLC
3. ábra RHA és PLC szemcseméret-eloszlása

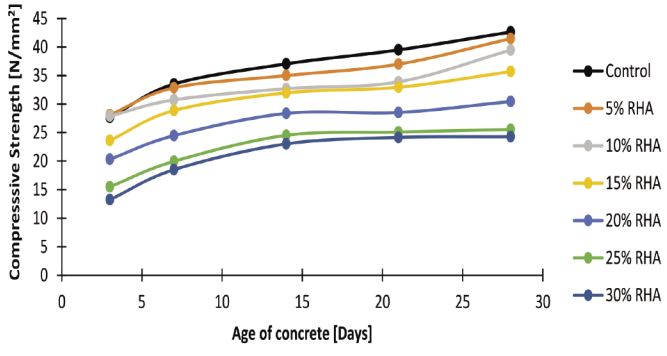

Fig. 4 Compressive strength result at different RHA replacement levels
4. ábra Nyomószilárdság eredménye különböző RHA helyettesítési szinteken

3.2 Mathematical modelling results

S/N	X_1	X_2	X_3	X_4	Lab. response	Z_1 Water	Z_2 Binder	Z_3 FA	Z_4 CA
1.	1	0	0	0	35.72	0.45	0.50	0.46	0.44
2.	0	1	0	0	27.99	1	1	1	1
3.	0	0	1	0	23.10	1.5	2.0	2.5	3.0
4.	0	0	0	1	18.23	3	4.0	5.0	6.0
5.	½	½	0	0	40.75	0.475	1	2.75	3.5
6.	½	0	½	0	34.64	0.455	1	2.0	5.0
7.	½	0	0	½	17.50	0.445	1	2.25	4.5
8.	0	½	½	0	30.67	0.48	1	2.25	4.5
9.	0	½	0	½	7.41	0.47	1	2.5	4.5
10.	0	0	½	½	24.63	0.45	1	2.75	5.5

Table 5 Compressive strength test results and replication based on Scheffe's (4,2) simplex lattice
5. táblázat Nyomószilárdság-vizsgálati eredmények és azok visszabontása a Scheffe-féle (4,2) szimplex rács alapján

S/N	X_1	X_2	X_3	X_4	Response	Z_1 Water	Z_2 Binder	Z_3 FA	Z_4 CA
11.	½	¼	1/4	0	31.09	0.465	1	1.88	3.75
12.	¼	¼	1/4	1/4	37.72	0.463	1	2.25	4.5
13.	0	¼	0	3/4	19.37	0.46	1	2.63	5.5
14.	½	0	1/4	1/4	31.22	0.48	1	2.13	4.25
15.	½	¼	0	1/4	20.25	0.46	1	2.0	4.0
16.	0	¼	3/4	0	24.23	0.47	1	2.38	4.75
17.	0	½	1/4	1/4	26.09	0.475	1	2.13	4.75
18.	¼	1/8	1/2	1/8	37.33	0.46	1	2.25	4.50
19.	¼	¼	0	½	31.67	0.458	1	2.38	4.75
20.	1/8	1/8	1/4	½	36.67	0.454	1	2.56	5.13

Table 6 Control points
6. táblázat Kontrol pontok

Res ponse Symbol	Lab. Response (Y_K)	Model Response (Y_E)	$Y_K - \overline{Y_K}$	$Y_E - \overline{Y_E}$	$(Y_K - \overline{Y_K})^2$	$(Y_E - \overline{Y_E})^2$
C1	31.09	29.57	1.525	-0.654	2.325625	0.427716
C2	37.72	37.72	8.155	7.496	66.50402	56.19002
C3	19.37	19.57	-10.195	-10.654	103.938	113.5077
C4	31.22	30.41	1.655	0.186	2.739025	0.034596
C5	20.25	23.52	-9.315	-6.704	86.76923	44.94362
C6	24.23	24.26	-5.335	-5.964	28.46223	35.5693
C7	26.1	26.10	-3.465	-4.124	12.00623	17.00738
C8	37.33	39.24	7.765	9.016	60.29522	81.28826
C9	31.67	33.20	2.105	2.976	4.431025	8.856576
C10	36.67	38.65	7.105	8.426	50.48103	70.99748
∑	295.7	302.24			417.9517	428.8226
Mean	29.57	30.224			46.43907	47.64696
	F Critical one-tail=	3.178893	F =	1.02601		

Table 7 F-statistics test on experimental and model results for the control points
7. táblázat A kontrollpontok kísérleti és modelleredményeinek F-statisztikai vizsgálata

	Laboratory Response	Model Response
Mean	29.565	30.224
Variance	46.43907222	47.64696
Observations	10	10
Pearson Correlation	0.977327267	
Hypothesized Mean Difference	0	
Df	9	
t Stat	-1.424297987	
P(T<=t) one-tail	0.0940481	
t Critical one-tail	1.833112933	
P(T<=t) two-tail	0.188096201	
t Critical two-tail	2.262157163	

Table 8 T-Statistical tests on experimental and model results
8. táblázat A kísérleti és modelleredmények T-statisztikai vizsgálata

Group	Count	Sum	Average	Variance
Laboratory response	10	295.65	29.565	46.43907
Model response	10	302.24	30.224	47.64696

Table 9 ANOVA: Single Factor
9. táblázat Egyfaktoros ANOVA

3.3 Model validation and test for adequacy

To ascertain whether the formulated model in Eq. (11) is acceptable to be used in predicting compressive strength, it is essential to carry out statistical test. The test for adequacy of the model was carried out with the aid of f-statistics test, student's t test and analysis of variance. Fifteen extra points were used to test the model's validity and adequacy of the model was tested by comparing the experimental results of the control points with the predicted results. In this test, the two hypotheses tested are that: There is no significant difference between the obtained laboratory results of the compressive strength and the model predicted values at 0.05 critical value (α), this is the null hypothesis. There is a significant difference between the obtained laboratory results of the compressive strength and the model predicted values at 0.05 critical value (α), this is the alternate hypothesis. The F-test two-sample for variance was used to compare the two laboratory and model results. If $F > F_{crit}$, we reject the null hypothesis. *Table 7* shows the analytical results: F = 1.02601 and F_{crit} = 3.178893, indicating that $F_{crit} > F$. As a result, we do not reject the null hypothesis. This, however, implies that there was no substantial difference between the experiment and model results. As a result, the model is now suitable for predicting the compressive strength of rice husk ash mixed cement concrete. A two-tailed student t test with a critical value of 0.05 (α) was also employed to compare the two groups. If $t_{stat} > t_{critical}$ two-tail, we reject the null hypothesis. *Table 7* shows the experimental and model results of compressive strength for the control points. For the t test, t_{stat} = -1.424297987 and t critical two-tail = 2.262157163, therefore $t_{critical} > t_{stat}$. As a result, we reject the null hypothesis. *Table 8* shows the results.

If $F > F_{crit}$, the null hypothesis of the analysis of variance is rejected. *Table 9* shows the analytical results: F = 0.046158 and F_{crit} = 4.413873, indicating that $F_{crit} > F$. As a result, we do not reject the null hypothesis. This, however, implies that there was no substantial difference between the experiment and model results. As a result, the model is now suitable for predicting the compressive strength of rice husk ash mixed cement concrete.

Source of Variation	SS	df	MS	F	P-value	F_{crit}
Between Groups	2.171405	1	2.171405	0.046158	0.832304	4.413873
Within Groups	846.7743	18	47.04302			
Total	848.9457	19				

Table 10 Statistical analysis of the results
10. táblázat Az eredmények statisztikai analízise

3.4 Discussion of results

In general, the simplex technique of Scheffe was used in this research, and the outcomes of 28 days compressive strength were achieved. *Tables 5* and *6* show the compressive strength findings derived from both the laboratory response and the model response. Based on the developed model, a peak compressive strength of 40.75 N/mm^2 was obtained with a corresponding mix ratio of 0.475: 1.00: 2.75: 3.50 for the fractions of water, binder (80% cement, 20% RHA), fine aggregate, and coarse aggregate. It is worth noting that the addition of approximately 2.598 percent by weight of rice husk ash to the concrete mix with a water cement ratio of 0.475 resulted in maximum compressive strength value. The lowest compressive strength response was 7.41 N/mm^2 as a result of adding approximately 2.36 percent by weight of rice husk ash to the concrete mix with water cement ratios of 0.47: 1.00: 2.50: 4.5 for binder, fine aggregate, and coarse aggregate, respectively. The maximum 28 days compressive strength value was higher than the minimum requirements of 20 and 25 N/mm^2 cube strength of concrete for structural application NCP 1 [24] and reinforced concrete according to BS 8110: Part 1 [25]. This indicates, however, that the compressive strength model may be used to predict concrete grades C8/10 to C32/40 according to BS EN 206 [26]. Furthermore, this finding shows that RHA, although being an excellent SCM, may still be used as a building material in concrete structures in order to promote environmental protection, eliminate waste management issues, and promote sustainable development.

4. Conclusions and recommendations

Scheffe's second degree polynomial was used in this study to develop a model for optimising the compressive strength of rice husk ash blended cement concrete. The results showed that the response predicted by the formulated model corresponds well with the practically observed results. The maximum compressive strength of 40.75 N/mm^2 was obtained with a mix ratio of 0.475: 1.00: 2.75: 3.50 for the fractions of water, binder (80% cement and 20% RHA), fine aggregate, and coarse aggregate, respectively. In contrast, the minimum compressive

strength response was 7.41 N/mm^2 with a matching mix ratio of 0.47: 1.00: 2.50: 4.5. Based on the test of adequacy, F-statistical tests, student t test, and analysis of variance (ANOVA) test at 95 percent confidence level were used to check the adequacy of the models, and the results show that there is a strong relationship between the control laboratory values and computed model results, with a p-value of 0.832 obtained from the ANOVA statistical results. ANOVA, on the other hand, proved to be the most appropriate approach for this objective. Furthermore, using the model equations, equivalent optimisation for any desired response within the simplex may be performed.

Notations

k	=	degree of dimensional space
q	=	number of components
n	=	order of polynomial regression
m	=	order of the Scheffe's polynomial
X_i	=	proportion of ith components of mixtures
X_1	=	proportion of water cement ratio
X_2	=	proportion of binder (cement and RHA)
X_3	=	proportion of fine aggregate
X_4	=	proportion of coarse aggregate
Z	=	actual components
X	=	pseudo components

Y_1, Y_2, Y_3, Y_4, Y_{12}, Y_{13}, Y_{14}, Y_{23}, Y_{24}, Y_{34} = responses from treatment mixture proportions

C_1, C_2, C_3, C_4, C_5, C_6, C_7, C_8, C_9, C_{10} = responses from control mixture proportions

α_1, α_2, α_3, α_4, α_{12}, α_{13}, α_{14}, α_{23}, α_{24}, α_{34}, = model coefficients

Y = optimised compressive strength of RHA concrete

References

[1] Vu, C.-C., Plé, O., Weiss, J. and Amitrano, D., 2020. Revisiting the concept of characteristic compressive strength of concrete. Construction and Building Materials,263, 120126. https://doi.org/10.1016/j.conbuildmat.2020.120126.

[2] Neville, A.M. and Brooks, J.J., 2010. Properties of concrete, 4th ed., Pearson Education Limited. https://doi.org/10.4135/9781412975704.n88.

[3] Mehta, P.K. and Monteiro, P.J.M., 2006. Concrete: microstructure, properties, and materials, 3rd ed., McGraw-Hill. https://doi.org/10.1036/0071462899.

[4] Attah, I.C., Etim, R.K., Alaneme, G.U. and Bassey, O.B., 2020. Optimization of mechanical properties of rice husk ash concrete using Scheffe's theory. SN Applied Sciences 2, 928. https://doi.org/10.1007/s42452-020-2727-y

[5] Wille, K., Naaman, A.E., El-Tawil, S. and Parra-Montesinos, G.J., 2012. Ultra-high performance concrete and fiber reinforced concrete: achieving strength and ductility without heat curing. Mater. Struct. 45, 309-324. https://doi.org/10.1617/s11527-011-9767-0.

[6] Yang, I.H., Joh, C. and Kim, B.-S., 2010. Structural behavior of ultra-high performance concrete beams subjected to bending. Eng. Struct. 32, 3478–3487. https://doi.org/10.1016/ j.engstruct.2010.07.017.

[7] Orie, O.U., Osadebe, N.N., 2009. Optimization of the compressive strength of five component concrete mix using scheffe's theory - a case of mound soil concrete. Journal of the Nigerian Association of Mathematical Physics 14, 81-92.

[8] Okere, C.E., Onwuka, D.O., Onwuka, S.U., Arimanwa, J.I., 2013. Simplex-based concrete mix design. International Organisation of Scientific Research Journal of Mechanical and Civil Engineering 5, 46-55.

[9] Okafor, F.O., Oguaghamba, O., 2010. Procedures for optimizationusing scheffe's model, Journal of Engineering Science and Application 7(1), 36-46.

[10] Onuamah, P.N., 2014. Modeling and optimization of compressive strength of hollow sandcrete block with rice husk ash admixture. Journal of Experimental Research 2(1).

[11] Attaha, I.C., Okafor, F.O. and Ugwu, O.O., 2020. Optimization of California bearing ratio of tropical black clay soil treated with cement kiln dust and metakaolin blend. International Journal of Pavement Research and Technology. https://doi.org/10.1007/s42947-020-0003-6.

[12] Ezeh, J.C., Ibearuegbulem, O.M. and Anyaogu, L., 2010. Optimization of compressive strength of cement-sawdust ash sandcrete block using scheffe's mathematical model. Int J Eng 2010, 487-94.

[13] Attaha, I.C., Okafor, F.O. and Ugwu, O.O., 2021. Experimental and optimization study of unconfined compressive strength of ameliorated tropical black clay. Engineering and Applied Science Research 48(3), 238-248. https://doi:10.14456/easr.2021.26.

[14] Ambrose, E.E., Okafor, F.O. and Onyia, M.E., 2021. Compressive strength and Scheffe's optimization of mechanical properties of recycled ceramics tile aggregate concrete. Epitőanyag-Journal of Silicate Based and Composite Materials 73(3), 91-102. https://doi.org/10.14382/epitoanyag-jsbcm.2021.14.

[15] Alaneme, G.U. and Mbadike, E.M., 2020. Compressive strength modelling of palm nut fiber concrete using Scheffe's theory. J Mater Sci Nanotechnol 8(1), 102.

[16] Chiemela, C., Okoye, P.C., Nwosu, P.C., Oke, O.M. and Ohakwe, C.N, 2014. Optimization of concrete made with Abakaliki quarry dust as fine aggregate using Scheffe's optimization model. Int Lett Nat Sci 15, 115-28.

[17] Akhnazarova, S., Kafarov, V., 1982. Experiment optimization in chemistry and chemical engineering, MIR Publishers, Moscow.

[18] Osadebe, N.N., Mbajiorgu, C.C. and Nwakonobi, T. U., 2007. An optimization model development for laterized concrete mix proportioning in building constructions. Nigerian Journal of Technology 26(1), 37-45.

[19] Scheffe, H., 1958. Experiment with mixtures, Journal of Royal Statistics Society 20(2), 344-360. https://doi.org/10.1111/j.2517-6161.1958.tb00299.x.

[20] Obam, S.O., 2006. The accuracy of scheffe's third degree over second-degree, optimization regression polynomials nigerian journal of technology, vol. 25(2).

[21] NIS 444-1, 2008. Composition, specification and conformity criteria for common cements, Standard Organization of Nigeria, Abuja.

[22] B Standard (BS) EN 12390 part 3, 2009. Methods for determination of compressive strength. British Standard Institution, London.

[23] ASTM C 618, 2008. Specification for coal fly ash and raw or calcined natural pozzolanas for use as mineral admixtures in Ordinary Portland Cement Concrete. Annual book of ASTM standards, West Conshecken, USA.

[24] Nigerian code of practice part 1 (NCP 1), 1973. The structural use of concrete in building. Nigeria Standards Organization. Federal Ministry of Industries, Lagos.

[25] British standard (BS) 8110 part 1, 1997. Structural use of concrete, code of practice for design and construction. British Standard Institution, London.

[26] BS EN 206, 2013. Concrete-specification, performance, production and conformity. British Standard Institute, London.

Ref.:
Akeke, Godwin A. – **Nnaji**, Chidozie C. – **Udokpoh**, Udeme U: *Compressive strength optimisation of rice husk ash concrete using Scheffe's mathematical model*
Építőanyag – Journal of Silicate Based and Composite Materials, Vol. 74, No. 4 (2022), 129–135. p.
https://doi.org/10.14382/epitoanyag-jsbcm.2022.20

Rheological properties of clay-polymer systems: application on water-based drilling mud

Safaa HATHOUT ▪ Laboratory of Rheology, Transport and Treatment of the Complex Fluids, University of Science and Technology, Algeria

Larbi HAMMADI ▪ Laboratory of Rheology, Transport and Treatment of the Complex Fluids, University of Science and Technology, Algeria ▪ larbi.hammadi@univ-usto.dz

Nasr-Eddine BOUDJENANE ▪ Laboratory of Rheology, Transport and Treatment of the Complex Fluids, University of Science and Technology, Algeria

Érkezett: 2022. 02. 20. ▪ Received: 20. 02. 2022. ▪ https://doi.org/10.14382/epitoanyag-jsbcm.2022.21

Abstract

The objective of this work is the study of the effect of the addition of anionic polymers on the rheological characteristics of a water-based drilling mud (WBM). The modified Cross model is successfully applied to fit the flow curves of WBM at different quantity of poly-salt. The incorporation of poly-salt in a concentration range between 0 and 1 wt% induces an increase in the yield stress τ_0 in the zero shear rate viscosity η_0 and in the infinite shear rate viscosity η_∞ of the WBM. It is also shown the addition of poly-salt between 0 and 1 wt% to WBM that may cause an increase of their degree of thixotropy. Finally the thixotropic behavior studied at different concentration of poly-salt added in WBM at 20 °C is analyzed by using a structural kinetic model (SKM) in order to investigate time dependent effect.

Keywords: bentonite, poly-salt, structural parameter, thixotropic, kinetic model
Kulcsszavak: bentonit, polimer só, szerkezeti paraméter, tixotróp, kinetikai modell

Safaa HATHOUT
He is engineer in hydraulic, preparing the PHD thesis on Rheological properties water-based drilling mud, at University of Science and Technology of Oran Mohamed Boudiaf (USTO-MB) under the direction of Professor Larbi HAMMADI and Professor Nasr-Eddine BOUDJENANE.

Larbi HAMMADI
Larbi Hammadi is professor in Hydraulic (University of Science and Technology of Oran) and Engineer in Mechanical Engineering. Currently is Researcher Professor at the University of Science and Technology of Oran Mohamed Boudiaf (USTO-MB) where he exercised many teaching activities. He is actually the director of Laboratory of Rheology, Transport and Complex Fluids Treatment (LRTTFC) Oran Algeria. Significant results have been obtained in recent years, for example, in emulsions for pharmaceutical use, drilling muds, vases of dams, sewage treatment plant sludge's, ceramic, polymers and cavitation. See https://scholar.google.com/citations?user=LLbBaNAAAAAJ&hl=fr&oi=ao

Nasr-Eddine BOUDJENANE
Nasr-Eddine BOUDJENANE is Professor in Hydraulic and currently works in the Department Hydraulic, University of Science and Technology of Oran Mohamed Boudiaf (USTO-MB), Algeria. He heads a research group in the Laboratory of Rheology, Transport and Complex Fluids Treatment (LRTTFC) Oran Algeria. His research focuses on subjects in hydraulics, in particular the Rheology and transport of complex fluids, solid transport, and in materials science.

1. Introduction

Clay-polymer systems are commonly used as basic constituents of water-based drilling fluids to meet such requirements as fluid which facilitates the smooth running of operations [1-3]. First of all, the drilling fluids have an ability to create a hydrostatic pressure making it possible to ensure the stability of bored walls and to prevent the coming of fluids underground aquifers crossed [4-6]. Drilling muds have also a great importance to ride up the cuttings from the bottom of the well to the surface. The consistency of the drilling muds must therefore be sufficient to prevent sedimentation of these cuttings in the updraft. During stops circulation of drilling muds for manoeuvres, dispersed cuttings and solid particles must remain perfectly in suspension. This also has certain rheological properties which, however, must not hinder recirculation or hamper manoeuvres or have harmful influences during them. A prior knowledge of the rheological properties of the drilling fluid, as well as the success of modelling the pressure losses and the transport of cuttings which may occur there, are very essential to adapt the composition of the fluid and the flow parameters to the drilling conditions. For this reason, several studies have been carried out on the rheological properties of drilling mud and different additives to drilling mud for the most effective formulation which meets the requirements of drilling techniques. Thus, the effects of pH and electrolyte concentration on the rheological properties of water-based drilling have been studied by Kelessidis et al [7]. It was observed a maximum of the yield stress, flow consistency index and apparent viscosity at the natural pH of the drilling muds, while there is monotonous decrease of these parameters with increasing of salt concentration. Moreover, the effects of sodium carboxymethyl cellulose, xanthan gum and sodium dodecyl sulfate on rheological properties of water-based drilling were studied by Benchabane and Bekkour [8]. It has been shown that for these additives make the apparent viscosities of the solutions increase with increasing concentrations. Hammadi et al [1] have investigated the effect of polyethylene Oxide (PEO) and the shear rate on rheological properties of water-based drilling mud. The authors demonstrated that addition of polyethylene oxide (PEO) to water-based drilling muds lead to the increase of yield stress and fluid consistency index of the mixture. Likewise, the authors explained that this trend was due to the interactions between clay particles and the viscous effect of the polymer solution. Recently, Ben Azouz et al [9] studied the effect of the temperature on the rheological properties of a complex bentonite-sodium carboxymethylcellulose. They observed that in the liquid like regime, the viscosity of the fluids decreased as the temperature increased and at low shear stresses, the solid-like regime have been observed. According to these authors the increase of temperature generates an increase of the Brownian motion. Salehnezhad et al [10] investigated the effect of ZnO nanoparticles and starch on rheological properties of drilling mud. The authors used the power law and Bingham-plastic models in order to modelling the effect of both additives on flow behaviour of the drilling mud. It was demonstrated that

the parameters of power law (consistency index and flow index) and Bingham-plastic models (plastic viscosity and yield point) are improved, when nanoparticles and starch were added to water-based drilling muds. Another study by Bayat and Shams [11] who demonstrated that the incorporation the quantity of titanium dioxide, silicon dioxide and zinc oxide between 0.01 and 0.5 wt% in drilling mud caused the increase on their plastic viscosity and yield stress so the adding of nanoparticles improved the rheological proprieties of drilling mud. Du et al [12] have shown the incorporation the concentration of $P_2O_7^{4-}$ between 0 and 8 wt% in 7 wt% bentonite-*0.1 M KCl* caused the decrease in yield stress. In fact, up to a quantity of transferred form 2 wt%, the yield stress stayed almost constant. Also the authors demonstrated that adding a quantity of $P_3O_{10}^{5-}$ between 0 and 8 wt% in 7 wt% bentonite- $0.01M\ MgCl_2$ caused the decrease in yield stress. From their part, Mudaser Ahmad et al [13] investigated the impact of copolymer of acrylamide and 2-acrylamido-2-methylpropane sulfonic acid and terpolymer of acrylamide, 2-acrylamido-2-methylpropane sulfonic acid on rheological proprieties of system deionised and salt water-bentonite. It was proved that the incorporation of the polymer in system deionised and salt water-bentonite at 25 °C and 85 °C caused a good improvement of their rheological properties compared to the copolymer. In order to minimize the fluid loss, Ahmed et al [14] incorporated the iron oxide or Hematite in KCl–Glycol–PHPA polymer to water based drilling mud system. It has been shown that the incorporation of the 3 wt% nanoparticles in KCl–Glycol–PHPA polymer to this system caused an increase of yield point by 3%. Likewise, the authors demonstrated that when 0.5 wt% of nanoparticles is added to the KCl–Glycol–PHPA polymer to this mud also, their API fluid filter reduce by 13.6% and their plastic viscosity increase by 10%. According to Kuma et al [15] the addition of carboxymethyl cellulose, sodium salt, PHPA polymer and polyacrylamide in water-based drilling mud improving their rheological properties (plastic viscosity and yield stress) and reducing the fluid loss. The same authors also proved that the NaCl is good additive for minimizing swelling phenomena. From the literature, different rheological properties of bentonite and the mixtures bentonite-sodium carboxymethylcellulose, bentonite-xanthan and bentonite-polyethylene. Oxide have been investigated and analyzed by various models [16-21]. Although many researchers have studied the rheological behavior of water-based drilling muds and polymer-water clays, the obtained results from this present article is quite different since we are proposing using new economical polymer as additive for the purpose of improving the rheological properties of water-based drilling mud.

2. Materials and methods

2.1 Materials and sample preparation

2.1.1 Materials

The poly-salt, as polymer chosen to this work, it can reduce the fluid loss and increase the viscosity of all WBM. It is especially applicable and economical in saturated salt and brine systems rather than others products which are not effective. The poly-salt as function in $NaCl$, KCl, $MgCl_2$, $CaCl_2$ and complex brines. The poly-salt used in this work was supplied from Sonatrach society (Algeria). *Table 1* presents the physical properties of the poly-salt used in this study.

Physical properties	Granular powder
Specific gravity	1.5
pH	7.0
Solubility in water	Soluble
Bulk density	561 kg/m^3

Table 1 Typical physical properties of the poly-salt used in this study
1. táblázat A tanulmányban használt polimer só tipikus fizikai tulajdonságai

The clay used is bentonite of Maghnia (Algeria) which is marketed by Bental Company. The main components of this sample are: SiO_2 (61.78%), Al_2O_3(17.15%), Fl_2O_3 (3.82%), MgO (3.56%), CaO (0.26%).

2.1.2 Preparation of samples

Given that the way of preparation has a great influence on the final state of suspensions, and thus on the rheological behavior, all tests were carefully carried out under equal conditions to allow for comparison of the results.

For each mixture, the bentonite suspension has the same mass concentration (4 wt%). The bentonite powder was dispersed in the required amount of distilled water without any chemical addition. The homogenization was performed under continuous magnetic agitation for 24 h. The additives at different concentrations (0; 0.2; 0.4; 0.6; 0.8 and 1 wt%) were then added to the base suspension, afterwards, the system poly-salt-water-bentonite obtained were subjected to a continuous agitation for 24 h.

2.2 Experimental setup

The rheological measurements were performed by using a torque controlled rheometer (Discovery Hybrid Rheometer DHR2 from TA instrument), equipped with a cone-plate geometry (diameter: 60 mm; angle: 2°; gap: 54 µm). It has a Peltier temperature control system that allows having a very quick response to any change in temperature range to -40 at 150 °C. In order to prevent changes in composition during measurements due to water evaporation, a solvent trap was placed around the measuring device.

2.3 Experimental methods

2.3.1 Hysteresis loop

The hysteresis loop test consisted of four stages:

- The stress history was minimised by pre-shearing the sample at 4 Pa for 120 s,
- The shear stress was linearly increased for 0 to the maximum shear stress in 600 s,
- The sample was sheared at the maximum shear stress for 120 s,
- The shear stress was linearly decreased for maximum to 0 Pa in 600 s.

The maximum shear stress range depends on the mass concentration of poly-salt added to based bentonite. In this case, the concentration of poly-salt less than 1% of the maximum shear stress is 4 Pa, however, the concentrations greater or equal to 1% the maximum shear stress is 6 Pa.

2.3.2 Apparent viscosity evolution under constant shear rate

After a rest time (time during which the sample is left at rest time of 600 s under geometry, the samples were sheared during 180 s at different constant shear rates (25 and 50 s^{-1}) at constant temperature (20 ± 0.2 °C). A new fresh sample was used for each applied shear rate in order to avoid any irreversible evolution of the samples.

3. Results and discussion

3.1. Particles size distribution

Fig. 1 shows the particle size distribution of bentonite and poly-salt polymer measured by the light scattering technique with a Malvern Instruments Mastersizer 2000 system. In order to avoid the formation of aggregates during the measurements, the sample was submitted to ultrasound excitation. We observed in *Fig. 1* the particle sizes of bentonite ranging between 0.12 and 138 μm were found with a symmetric distribution centered at about 46 μm, and particle sizes of poly-salt polymer ranging between 17 and 830 μm were found with a symmetric distribution centered at about 455 μm. We also observed the maximum volume distribution of poly-salt is greater than of maximum volume distribution of bentonite which means that this poly-salt is more flocculated compared to bentonite [21-23].

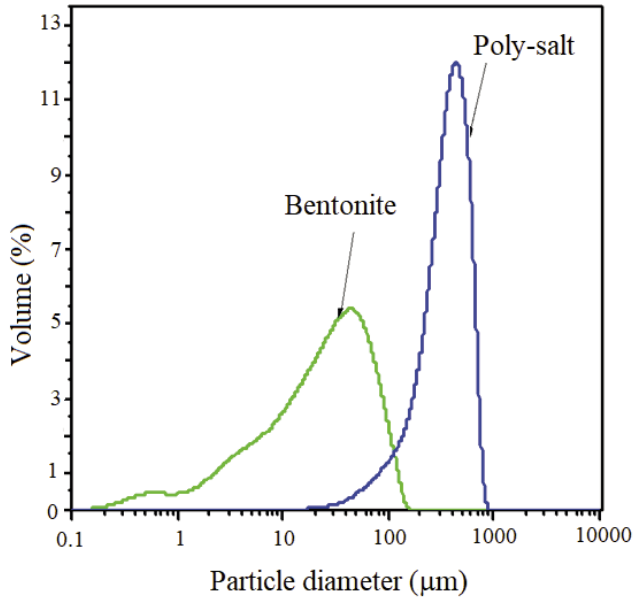

Fig.1 Particle size distribution of bentonite and poly-salt
1. ábra A bentonit és a polimer só szemcseméret-eloszlása

3.2 Hysteresis loop

The thixotropic loops of bentonite suspension-poly-salt with different concentration of poly-salt (0%, 0.4%, 0.6%, 0.8% and 1%) in bentonite suspension are shown in *Fig. 2*. It can be seen in this figure that with concentration of poly-salt between 0% to 1% added to system poly-salt-water-bentonite, the downward curves are under the upward curves which represents positive thixotropy. For concentration of poly-salt equal 1% added in system poly-salt-water-bentonite, it is clearly found a crossover point that divide the loops into three sections: for the shear stress between 0 to 3.5 Pa, the downward curves are under the upward curves which represents positive thixotropy. However, for the shear stress between 3.5 Pa to 4.20 Pa, the upward curve is under the downward curve which indicates the negative thixotropic character; and finally, for shear stress between 4.20 Pa to 6 Pa the lower shear rate section, the downward curve is under the upward curve, which indicates positive thixotropic character.

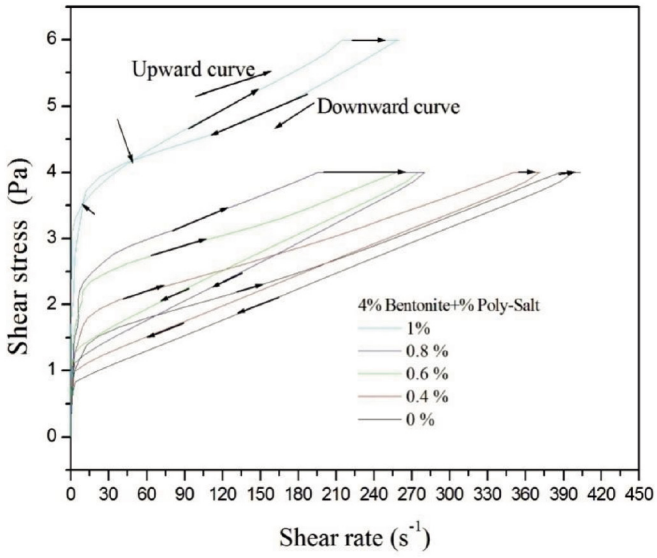

Fig. 2 Hysteresis loop of system poly-salt-water-bentonite at different concentration of poly-salt
2. ábra A polimer só-víz-bentonit rendszer hiszterézise különböző polimer só koncentrációknál

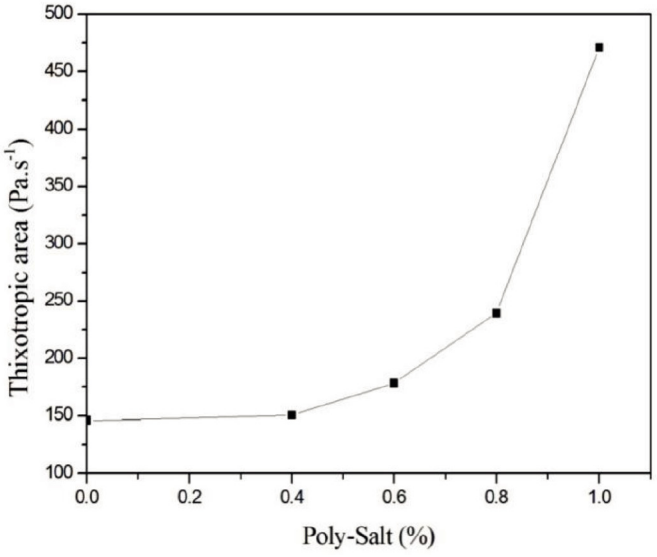

Fig. 3 Thixotropic area of system poly-salt - water - bentonite as a function of poly-salt additive
3. ábra Polimer só-víz-bentonit rendszer tixotróp területe a polimer só adalék függvényében

In this work, it is found that there is a great effect of poly-salt polymer on thixotropy of system poly-salt-water-bentonite, so the area between the upward and downward curves was calculated using the data analysis option of Trios V4.2.1. 36612 of TA instrument. *Fig. 3* presented the area of hysteresis loops of bentonite suspension as a function of poly-salt concentration. It is clear that the degree of thixotropy increasing with increasing of poly-salt concentration in based water drilling mud, this behavior could be explained by increase the degree of flocculation caused by the poly-salt [24]. According to Shaikh et al [18] the increase of the flocculation degree (thixotropy) improves the stability of system poly-salt - water - bentonite.

3.3 Flow curve

The variation of the shear stress τ as a function of the shear rate $\dot{\gamma}$ at different concentration of poly-salt from 0 to 1% added in bentonite suspension clearly indicates two behaviors separated by a critical shear rate: a Non-Newtonian behavior after a yield stress followed by a plastic behavior (*Fig. 4*). Experimental data were fitted to modified Cross model (*Eq. 1*) developed by Grassi et al [25], which has been successfully employed for weak gel systems.

$$\tau = \tau_0 + \eta_\infty \dot{\gamma} + \frac{(\eta_0 - \eta_\infty)\dot{\gamma}}{1+(\lambda_c \dot{\gamma})^m} \quad (1)$$

where τ_0 is the yield stress, η_0 is the zero shear rate viscosity (lower Newtonian plateau), η_∞ is the infinite shear rate viscosity (upper Newtonian plateau), λ_c is a characteristic time and m is a dimensionless exponent. It should be noted here that, in the case of plastic systems, the zero shear viscosity η_0 represents the estimated value for the viscosity and the system would have if it maintained a typical solution behavior for low values of shear rate.

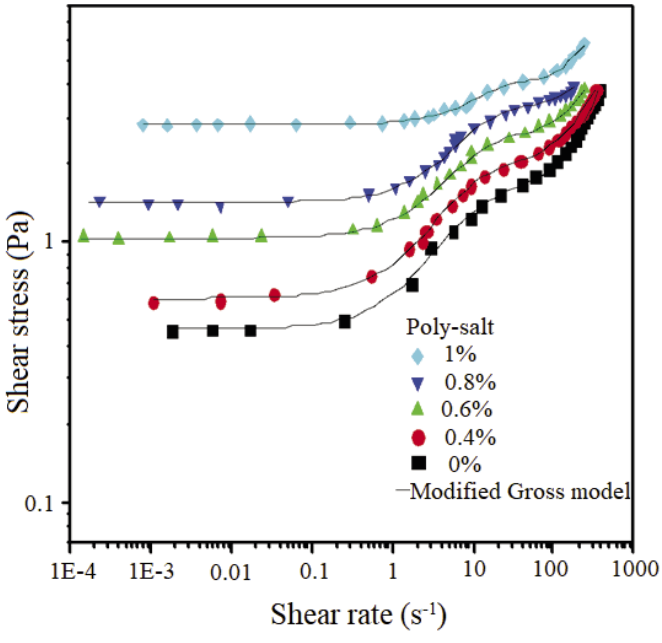

Fig. 4 Shear stress as a function of shear rate at different mass concentrations of poly-salt add (0, 0.4, 0.6, 0.8 and 1%) in bentonite suspension
4. ábra Nyírófeszültség a nyírási sebesség függvényében különböző tömegkoncentrációjú (0; 0,4; 0,6; 0,8 és 1%-os) polimer só adalékok esetén a bentonit szuszpenzióban

Fig. 5 and *6* show the variation of the parameters of the modified Cross model for bentonite–poly-salt mixtures system as a function of different concentration of poly-salt added to based bentonite suspension. We observe on *Figs. 5* and *6*, a rapid increase in the yield stress τ_0, zero shear rate viscosity η_0 and the infinite shear rate viscosity η_∞ with dose of poly-salt. The increase of yield stress τ_0 , zero shear rate viscosity η_0 and the infinite shear rate viscosity η_∞ is occurred due to the adsorption of poly-salt by bentonite. This adsorption makes the specific surface highly rigid bentonite and causes an increase of interaction between the bentonite particles.The high particles size of ploy-salt provoke the increase of hydrodynamic particle interactions, this hydrodynamic interactions caused the increase of the yield stress and viscosity's on the system poly-salt - water - bentonite. According to Guler et al [26] and Hammadi et al [1] the polymer chains formed network of aggregate and particles of the gel-like structures that made interactions between the bentonite particles and polymer which reinforce of the rigidity and the consistency of the mixture and also caused an increase of the yield stress and viscosity's. Moreover, Abu-Jdayil [27] explained that the increase in the yield stress they have observed is a direct consequence of an interconnected three dimensional network of flocs.

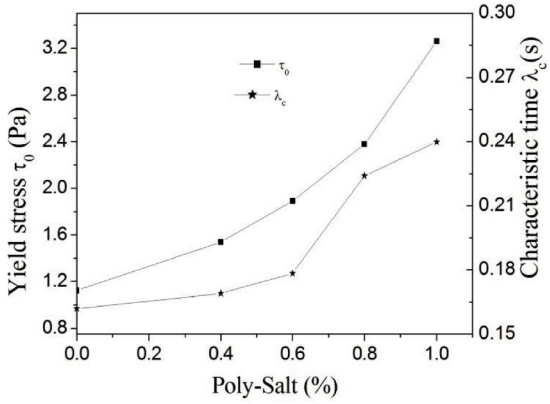

Fig. 5 Variation of yield stress and characteristic time of system poly-salt- water-bentonite at different concentration of poly-salt (0, 0.4, 0.6 , 0.8 and 1%)
5. ábra A polimer só-víz-bentonit rendszer folyáshatárának és jellemző idejének változása a polimer só különböző koncentrációinál (0; 0,4; 0,6; 0,8 és 1%)

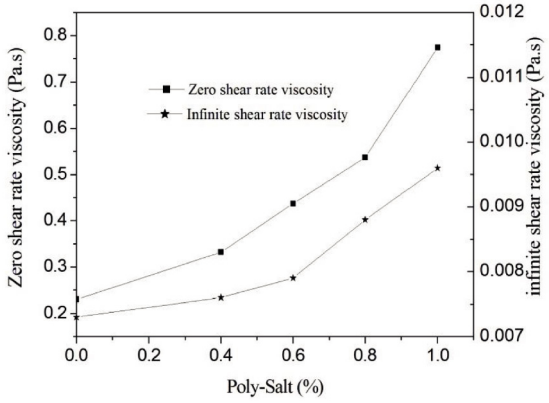

Fig. 6 Variation of zero shear rate viscosity η_0 and the infinite shear rate viscosity η_∞ of system poly-salt- water- bentonite at different concentration of poly-salt (0, 0.4, 0.6, 0.8 and 1%)
6. ábra A nulla η_0 és a végtelen nyírási sebességű η_∞ viszkozitás változása a polimer só-víz- bentonit rendszerben különböző polimer só koncentrációknál (0; 0,4; 0,6; 0,8 és 1%)

3.4 Apparent viscosity evolution under constant shear rate and determination of the structural parameter of system poly-salt - water- bentonite

Figs. 7 and *8* show time dependence of apparent viscosity for constant shear rates (25 s^{-1} and 50 s^{-1}) at different concentration of poly-salt (0, 0.2, 0.4, 0.6 and 0.8%) added to system water-bentonite. For all studied, quantities of poly-salt add in system poly-salt-water-bentonite and both shear rate, the viscosity decreases significantly with shearing time, particularly in the initial stages of shear. After approximately 100 s shearing period for shear rate of 25 s^{-1} applied on the mixtures and after approximately 120 s of shearing period for shear rate of 50 s^{-1} applied on the mixtures, the viscosity tends to an equilibrium value. Therefore the equilibrium state of system poly-salt-water-bentonite depends on the shear rate applied to the system. In order to determine the structural evaluation of the bentonite suspension-poly-salt, we applied the structural kinetic model (SKM) developed by Nguyen et al [28] (Eq. (2)), which has been successfully employed for starch pastes and concentrated suspensions of minerals.

$$\left(\frac{\eta-\eta_e}{\eta_0-\eta_e}\right)^{1-n} = (n-1)kt + 1 \qquad (2)$$

where η_0 is the initial apparent viscosity at t=0 (structured state), η_e is the equilibrium apparent viscosity as t → ∞ (non-structured state). Note that, both η_0 and η_e are functions of the applied shear rate only [29] and $\lambda(t,\dot{\gamma}) = \frac{\eta-\eta_e}{\eta_0-\eta_e}$ is the structural parameter ranged between the initial value of unity for zero shear time and the equilibrium structural $\lambda_e = \frac{\eta_e}{\eta_0}$ lower than unity. The initial apparent viscosity and the equilibrium apparent viscosity were found by fitting the time dependence of the viscosity (*Figs. 7* and *8*) by the second-order model SKM (Eq. (2) with n = 2). A good concordance was found between the model fitted results (solid line) and the experimental transient apparent viscosity data for all quantity of poly-salt add in system poly-salt-water-bentonite for the both shear rates applied.

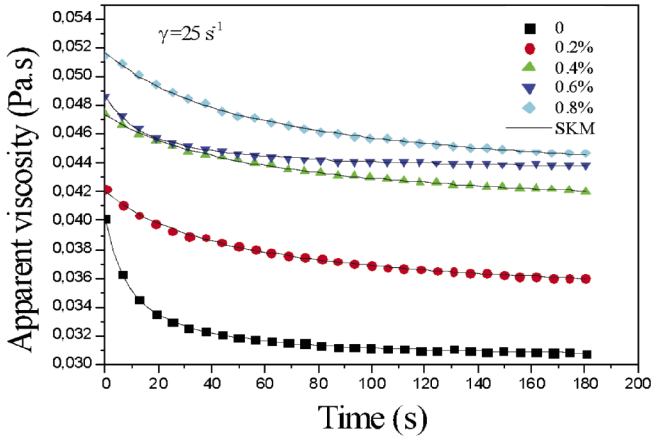

Fig. 7 Apparent viscosity data of poly-salt-water-bentonite mixtures as a function of shearing time at 20°C for different concentration of poly-salt added to system poly-salt - water- bentonite and for constant shear 25 s^{-1}

7. ábra Polimer só-víz-bentonit keverékek látszólagos viszkozitási adatai a nyírási idő függvényében 20°C-on, a polimer só - víz - bentonit rendszerhez hozzáadott különböző koncentrációjú polimer só esetén és 25 s^{-1} állandó nyírás esetén

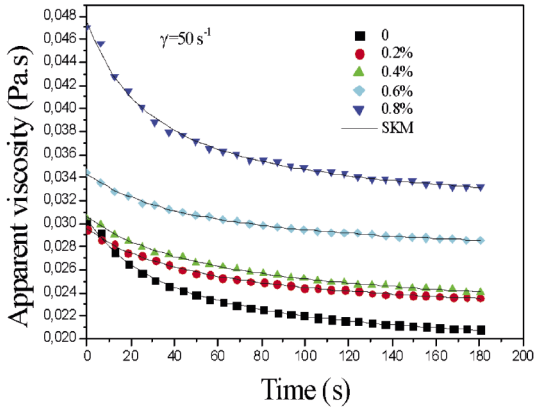

Fig. 8 Apparent viscosity data of poly-salt-water-bentonite mixtures as a function of shearing time at 20°C for different concentration of poly-salt added to system poly-salt-water-bentonite and for constant shear 50 s^{-1}

8. ábra Polimer só-víz-bentonit keverékek látszólagos viszkozitási adatai a nyírási idő függvényében 20°C-on a polimer só-víz-bentonit rendszerhez hozzáadott különböző koncentrációjú polimer só és 50 s^{-1} állandó nyírás esetén

Fig. 9 shows the variation of the rate constant k and equilibrium structural parameter λ_e as a function of the quantity of poly-salt added in system poly-salt-water-bentonite and for both shear rates applied. The rate constant, k can be considered as a measure of the rate of the structure breakdown, i.e. the degree of thixotropy. On other hand, the ratio of equilibrium to initial viscosity can be considered as an equilibrium structural parameter. We observed in *Fig. 10* an increase of the degree of thixotropy with increase the quantity of poly-salt in system poly-salt-water-bentonite.This increase in the degree of thixotropy leads to an increase in the yield stress and the apparent viscosity of the system poly-salt-water-bentonite at rest [30]. For the same system, we also find that equilibrium structural parameter with increasing of the quantity of polymer added to the system. This behavior could be explained by the flocculation of mixtures particles in the water at high quantity of poly-salt add the mixture. As a result, there is a development of network or structure and also enhance organization of the particles of the mixtures concerning its microstructural level as it is investigated before by Wang et al [31].

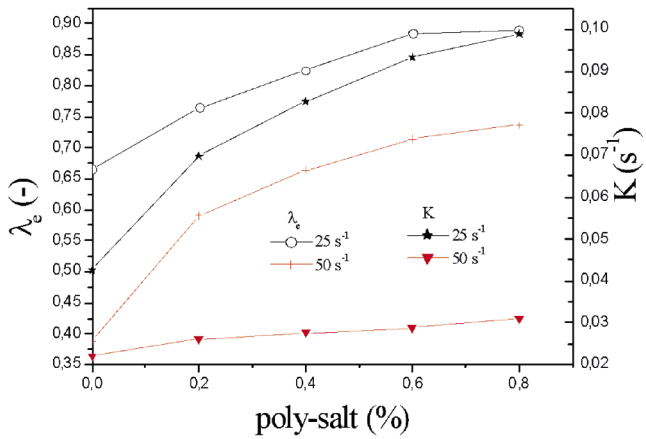

Fig. 9 Variation of the rate constant k and equilibrium structural parameter λ_e as a function of the quantity of poly-salt added to system poly-salt –water-bentonite for both shear rate applied

9. ábra A k sebességi állandó és a λ_e egyensúlyi szerkezeti paraméter változása a polimer só-víz-bentonit rendszerhez hozzáadott polimer só mennyiségének függvényében mindkét alkalmazott nyírási sebesség esetén

3.5 Comparison between poly-salt and others additives

Fig. 10 shows the evolution of apparent viscosity as a function of time of 4% bentonite suspension and 4% bentonite suspension-0.4% additives (poly-salt, CMC and HEC) under constant shear stress of 4Pa.

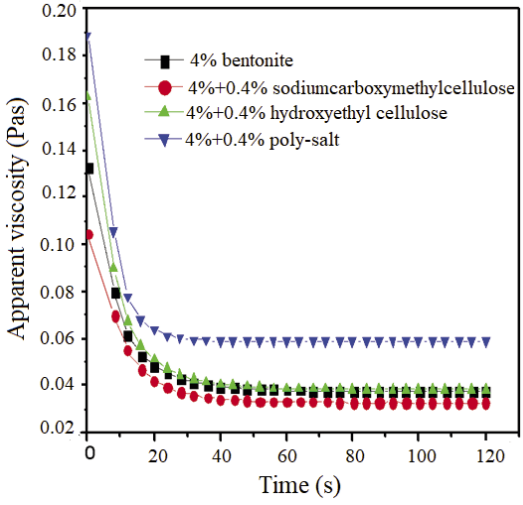

Fig. 10 Apparent viscosity as a function of time of 4% bentonite suspension and 4% bentonite suspension-0.4% additives (poly-salt, CMC and HEC) under constant shear stress of 4Pa
10. ábra A 4%-os bentonit szuszpenzió látszólagos viszkozitása az idő függvényében 4 Pa állandó nyírófeszültség és különböző adalékanyagok (polimer só, CMC és HEC) adalékolása mellett

The viscosity decreases significantly with shearing time, particularly in the initial stages of shear and tends to an equilibrium value after 60 s of shearing under shear stress of 4Pa. From the *Fig. 10,* adding the CMC caused decreasing in zero viscosity and infinite shear rate viscosity by 21% and 13% respectively, the incorporation of HEC in drilling mud improved their viscosity zero by 22% and infinity viscosity by 1.9% and finally the addition of the new poly-salt polymer in water-based drilling mud improve their zero viscosity by 42% and infinity viscosity by 54%. On one hand the decreasing of the zero viscosity and infinite shear rate viscosity of drilling muds caused by the CMC due to the high negative charge of CMC who favors the deflocculation of the mixture bentonite-CMC [16]. On the other hand the increase of the zero viscosity and infinite shear rate viscosity of drilling muds caused by HEC and poly-salt and this is due to the number of entanglement caused by long polymer chains [32].

3.6 FTIR spectra of bentonite and system poly-salt-water-bentonite

The infrared spectroscopic measurement of bentonite and bentonite-poly-salt were obtained using a PerkinElmer Spectrum Two FT-IR spectrophotometer at room temperature. The spectrum was collected over the spectral range of 4000–400 cm^{-1}. The IR spectrum of the bentonite and system poly-salt-water-bentonite is shown in *Fig. 11*. For bentonite the band at 3610.77 characterizes montmorillonite this is attributed to bending vibrations of the OH coordinated octahedral layer $Al + Mg$. The addition of poly-salt caused the shifting of this band to the band of 3313.60 which is correspondent to the stretching vibrations of $Al - OH$ [33]. The absorption peaks of 3398.41 cm^{-1} and 1629.87 cm^{-1} are attributed to the stretching and bending vibrations of H–OH groups of water molecules adsorbed on the surface of bentonite, the addition of poly-salt in system water-bentonite shifted this absorption peaks to 1635.53 cm^{-1} and 1106.76 cm^{-1} respectively. The absorption peaks at 981.22 of system poly-salt-water-bentonite was attributed to $Al - OH - Al$ band corresponds to pure montmorillonite [34, 35]. The band at 507.35 of system poly-salt-water-bentonite is correspondent to absorption of the characteristic bond of Si-O-Al [34].

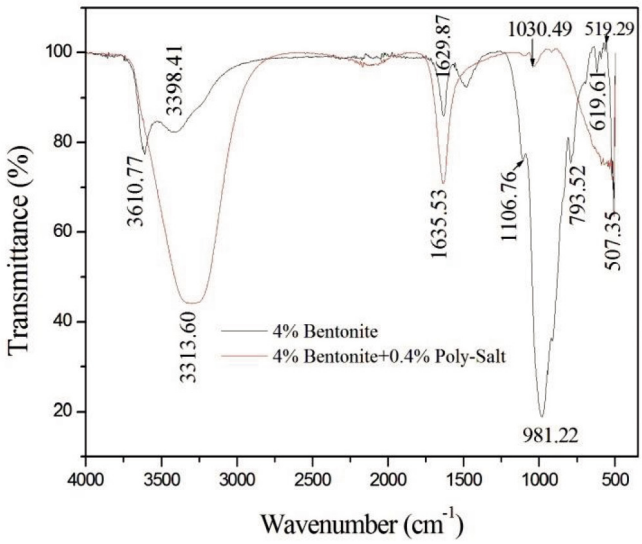

Fig. 11 IR spectrum of the bentonite and system poly-salt-water-bentonite
11. ábra A bentonit és a polimer só-víz-bentonit rendszer IR spektruma

4. Conclusions

The effect of new type of polymer the poly-salt on rheological proprieties of system poly-salt-water-bentonite was studied. The non-Newtonian stationary flow behavior of bentonite was successfully modeled by using the coupled Cross and Bingham models over the studied range poly-salt polymer.

The addition of poly-salt in a concentration ranging between 0 and 1% in system poly-salt-water-bentonite caused the increase in the yield stress, the zero shear rate viscosity, and the infinite shear rate viscosity with dose of poly-salt. The increase of these parameters was mainly related to the interaction between the solid particles and viscous effects. Then, the increase of the parameters of modified Cross model causes an increase in the friction and an increase in the viscosity of the system poly-salt-water-bentonitee.

The increase of quantity of poly-salt in system poly-salt-water-bentonite causes an increase in the degree of the flocculation. This increasing of degree of the flocculation improved the rheological properties of system poly-salt-water-bentonite. The effect of poly-salt on break-down behavior of bentonite suspension was also examined. The time dependent viscosity decreased rapidly with shearing time and reached a steady state. The structural kinetic model (SKM) was successfully applied to analyze the time-dependent behavior of system poly-salt-water-bentonite. The rate of structure breakdown (degree

of thixotropy) under shear rate is increased with increasing quantity of poly-salt added to system poly-salt-water-bentonite. Finally, from this study it noticed that this poly-salt as an effective additive in drilling mud has many advantages for a large range of applications. It is very economic, highly effective in high salinity and high hardness brines. In addition, it minimizes filtration damage to production zones and it was mainly used to control filtration and rheology stability in the drilling mud. However, the use of poly-salt this in drilling mud is limited due their rapid degradation in temperature of 135°C and it cannot be used with zinc.

References

[1] Hammadi L, Boudjenane N, Belhadri M (2014) Effect of polyethylene oxide (PEO) and shear rate on rheological properties of bentonite clay. Applied Clay Science 99: 306-311. https://doi.org/10.1016/j.clay.2014.07.016

[2] Xie G, Luo P, Deng M (2016) A novel method for determining the degree of clay swelling in clay–polymer–water systems. Chemistry and Technology of Fuels and Oils 52 (5): 542-549, https://doi.org/10.1007/s10553-016-0741-y

[3] Elkatatny S (2019) Enhancing the rheological properties of water-based drilling fluid using micronized starch. Arabian Journal for Science and Engineering 44(6): 5433-5442. https://doi.org/10.1007/s13369-019-03720-1

[4] Talalay P, Fan X, Xu H, Yu D, Han L, Han J, Sun Y (2014) Drilling fluid technology in ice sheets: hydrostatic pressure and borehole closure considerations. Cold regions science and technology 98: 47-54. https://doi.org/10.1016/j.coldregions.2013.10.012

[5] Mao H, Yang Y, Zhang H, Zhang J, Huang Y (2020) A critical review of the possible effects of physical and chemical properties of subcritical water on the performance of water-based drilling fluids designed for ultra-high temperature and ultra-high pressure drilling applications. Journal of Petroleum Science and Engineering 187: 106795. https://doi.org/10.1016/j.petrol.2019.106795

[6] Li M, Xie D, Shu Q, Ou H, Guo X (2018) Study on sodium fatty alcohol polyoxyethyleneether sulfate relieve the contamination of oil well cement with mineral oil-based drilling fluids. Construction and Building Materials 163: 450-459. https://doi.org/10.1016/j.conbuildmat.2017.12.109

[7] Kelessidis V.C, Tsamantaki C, Dalamarinis P (2007) Effect of pH and electrolyte on the rheology of aqueous Wyoming bentonite dispersions. Applied Clay Science 38: 86-96. https://doi.org/10.1016/j.clay.2007.01.011

[8] Benchaban A, Bekkour K (2006) Effects of anionic additives on the rheological behavior of aqueous calcium montmorillonite suspensions. Rheologica Acta 45: 425-434. https://doi.org/10.1007/s00397-005-0063-1

[9] Ben Azouz K.B, Bekkour K, Dupuis D (2016) Influence of the temperature on the rheological properties of bentonite suspensions in aqueous polymer solutions. Applied Clay Science 123: 92-98. https://doi.org/10.1016/j.clay.2016.01.016

[10] Salehnezhad L , Heydari A , Fattahi M (2019) Experimental investigation and rheological behaviors of water-based drilling mud contained starch-ZnO nanofluids through response surface methodology. Journal of Molecular Liquids 276: 417-430. https://doi.org/10.1016/j.molliq.2018.11.142

[11] Bayat A. E, Shams, R. (2019). Appraising the impacts of SiO_2, ZnO and TiO_2 nanoparticles on rheological properties and shale inhibition of water-based drilling muds. Colloids and Surfaces A: Physicochemical and Engineering Aspects 581: 123792. https://doi.org/10.1016/j.colsurfa.2019.123792

[12] Du M, Liu P, Clode P. L, Liu J, Haq B, Leong Y. K (2020). Impact of additives with opposing effects on the rheological properties of bentonite drilling mud: Flow, ageing, microstructure and preparation method. Journal of Petroleum Science and Engineering 192: 10728. https://doi.org/10.1016/j.petrol.2020.107282

[13] Mudaser Ahmad H, Shahzad Kamal M, Al-Harthi, M. A. (2018). Rheological and filtration properties of clay-polymer systems: impact of polymer structure. Applied Clay Science 160: 226-237. https://doi.org/10.1016/j.clay.2018.01.016

[14] Ahmed N, Alam M. S, Salam, M. A (2020) Experimental analysis of drilling fluid prepared by mixing iron (III) oxide nanoparticles with a KCl–Glycol–PHPA polymer-based mud used in drilling operation. Journal of Petroleum Exploration and Production Technology https://doi.org/10.1007/s13202-020-00933-1.

[15] Kuma M, Das B. M , Talukdar, P (2020) The effect of salts and haematite on carboxymethyl cellulose–bentonite and partially hydrolyzed polyacrylamide–bentonite muds for an effective drilling in shale formations. Journal of Petroleum Exploration and Production Technology 10:395–405. https://doi.org/10.1007/s13202-019-0722-x

[16] Benyounes K, Mellak A, Benchabane A (2010) The effect of carboxymethylcellulose and xanthan on the rheology of bentonite suspensions. Energy Sources, Part A: Recovery, Utilization, and Environmental Effects 32: 1634-1643. https://doi.org/10.1080/15567030902842244

[17] Benslimane A, Bahlouli I.M, Bekkour K, Hammiche D (2016) Thermal gelation properties of carboxymethyl cellulose and bentonite-carboxymethyl cellulose dispersions: Rheological considerations. Applied Clay Science 132: 702-710. https://doi.org/10.1016/j.clay.2016.08.026

[18] Shaikh S.M, Nasser M.S, Hussein I, Benamor A, Onaizi S.A, Qiblawey H (2017) Influence of Polyelectrolytes and Other Polymer Complexes on the Flocculation and Rheological Behaviors of Clay Minerals: A Comprehensive Review. Separation and Purification Technology 187: 137-161. https://doi.org/10.1016/j.seppur.2017.06.050

[19] Rinaldi V.A, Clariá J.J (2016) Time dependent stress–strain behavior of bentonite slurries; effect of thixotropy. Powder Technology 291: 311-321. https://doi.org/10.1016/j.powtec.2015.12.036

[20] Moghaddam A. K, Saadatabadi A. R (2020). Rheological modeling of water based drilling fluids containing polymer/bentonite using generalized bracket formalism. Journal of Petroleum Science and Engineering 189: 107028. https://doi.org/10.1016/j.petrol.2020.107028

[21] Besra L, Sengupta D.K, Roy S.K, P. Ay P (2004) Influence of polymer adsorption and conformation on flocculation and dewatering of kaolin suspension. Separation and Purification technology. 37: 231-246. https://doi.org/10.1016/j.seppur.2003.10.001

[22] Gregory J, Barany S (2011) Adsorption and flocculation by polymers and polymer mixtures. Advances in colloid and interface science 169: 1-12. https://doi.org/10.1016/j.cis.2011.06.004

[23] Dryabina S, Fotina K, Navrotskii A, Novakov I (2017) The flocculation of kaolin aqueous dispersion by two cationic polyelectrolytes. Colloids and Surfaces A: Physicochemical and Engineering Aspects 515: 12-21. https://doi.org/10.1016/j.colsurfa.2016.11.055

[24] Chen M, Liu B, Li L, Cao L, Huang Y, Wang S, Cheng X (2020) Rheological parameters, thixotropy and creep of 3D-printed calcium sulfoaluminate cement composites modified by bentonite. Composites Part B: Engineering 186: 107821. https://doi.org/10.1016/j.compositesb.2020.107821

[25] Grassi M, Lapasin R, Pricl S (1996) A study of the rheological behavior of scleroglucan weak gel systems. Carbohydrate Polymers 29:169-181. https://doi.org/10.1016/0144-8617(95)00120-4

[26] Guler E, Ozhan H.O, Karaoglu S (2018) Hydraulic performance of anionic polymer-treated bentonite-granular soil mixtures. Applied Clay Science 157 : 139-147. https://doi.org/10.1016/j.clay.2018.02.047

[27] Abu-Jdayil B (2011) Rheology of sodium and calcium bentonite–water dispersions: Effect of electrolytes and aging time. International journal of mineral processing. 98 (2011) 208-213. https://doi.org/10.1016/j.minpro.2011.01.001

[28] Nguyen Q.D, Jensen C.T, Kristensen P.G (1998) Experimental and modelling studies of the flow properties of maize and waxy maize starch pastes. Chemical Engineering Journal 70 : 165-171. https://doi.org/10.1016/S0923-0467(98)00081-5

[29] Abu-Jdayil B (2003) Modelling the time-dependent rheological behavior of semisolid foodstuffs. Journal of food engineering 57 : 97-102. https://doi.org/10.1016/S0260-8774(02)00277-7

[30] Roussel N (2006) A thixotropy model for fresh fluid concretes: theory, validation and applications. Cement and concrete research, 36:1797-1806. https://doi.org/10.1016/j.cemconres.2006.05.025

[31] Wang Q, Cui Y.J , Tang A.M , Barnichon J.D , Saba S, Ye W.M (2013) Hydraulic conductivity and microstructure changes of compacted bentonite/sand mixture during hydration. Engineering Geology, 164 : 67-76. https://doi.org/10.1016/j.enggeo.2013.06.013

[32] Ouaer H, Gareche M (2019) Hydroxyethyl cellulose as a rheology modifier for water-based drilling fluids formulated with Algerian bentonite. Journal of the Brazilian Society of Mechanical Sciences and Engineering 41: 123. https://doi.org/10.1007/s40430-019-1627-9

[33] Parab H, Mahadik P, Sengupta P , Vishwanadh B, Kumar S. D (2020) A comparative study on native and gamma irradiated bentonite for cesium ion uptake. Progress in Nuclear Energy 127: 103419. https://doi.org/10.1016/j.pnucene.2020.103419

[34] Stylianou M. A, Inglezakis V. J, Loizidou M. D, Agapiou A, Itskos G (2016) Equilibrium ion exchange studies of Zn2+, Cr3+, and Mn2+ on natural bentonite. Desalination and Water Treatment, 57: 27853-2786. https://doi.org/10.1080/19443994.2016.1235153

[35] El Bouraie M, Masoud A. A (2017). Adsorption of phosphate ions from aqueous solution by modified bentonite with magnesium hydroxide Mg (OH) 2. Applied Clay Science 140: 157-164. https://doi.org/10.1016/j.clay.2017.01.02

Ref.:
Hathout, Safaa – **Hammadi**, Larbi – **Boudjenane**, Nasr-Eddine: *Rheological properties of clay-polymer systems: application on water-based drilling mud*
Építőanyag – Journal of Silicate Based and Composite Materials, Vol. 74, No. 4 (2022), 136–143. p.
https://doi.org/10.14382/epitoanyag-jsbcm.2022.21

Effectiveness of cement kiln dust-silicate based mixtures on plasticity and compaction performance of an expansive soil

Imoh Christopher ATTAH ▪ Department of Civil Engineering, Akwa Ibom State University, Ikot Akpaden, Nigeria
Roland Kufre ETIM ▪ Department of Civil Engineering, Akwa Ibom State University, Ikot Akpaden, Nigeria
David Ufot EKPO ▪ Department of Civil Engineering, Akwa Ibom State University, Ikot Akpaden, Nigeria
Idorenyin Ndarake USANGA ▪ Department of Civil Engineering, Akwa Ibom State University, Ikot Akpaden, Nigeria

Érkezett: 2022. 03. 08. ▪ Received: 08. 03. 2022. ▪ https://doi.org/10.14382/epitoanyag-jsbcm.2022.22

Abstract
In an attempt to seek for cost-effective construction materials which is expected to stimulate sustainable road pavements, the use of waste industrial materials such as cement kiln dust (CKD) has become necessary. Metakaolin (MK) is a good silica-based pozzolanic material derived from calcined kaolin. The study entails understudying the effectiveness of these materials on plasticity and compaction response of an expansive soil. Laboratory examinations were initiated on both virgin and treated soils. The blending was achieved with the mixtures of 0 – 8% CKD and 0 to 10% MK, respectively. In the course of this study, the addition of additives into the virgin soil facilitated some alterations in the soil matrix. The consistency examinations of soil materials displayed a diminishing trend with the introduction of CKD-MK mixtures into the soil matrix which facilitated a considerable level of improvement in the plasticity tendency of the soil. For the compaction response, the increment in CKD and MK proportions occasioned the enhancement of maximum dry density (MDD) and a corresponding diminishment in optimum moisture content (OMC). The scan electron microscopy (SEM) of the virgin soil displayed series of cracks whereas the soil-CKD-MK mixtures did not show same which could be facilitated by the crystalline formation on adding the additives. The analysis of variance was employed for the testing of significant level of additives on the tested property. Thus, an optimal blend of 8% CKD/8% MK showed a drastic effect on the plasticity and compaction properties. It can be inferred that 8% CKD/8% MK blend in the soil could be useful as alternative to the conventional stabilizing materials.
Keywords: expansive soil, metakaolin, cement kiln dust, Atterberg limits, compaction, scanning electron microscope
Kulcsszavak: expanzív talaj, metakaolin, cementégető-kemence por, Atterberg-határérték, tömörítés, pásztázó elektronmikroszkóp

Imoh C. ATTAH
is a lecturer in the Department of Civil Engineering, Akwa Ibom State University, Ikot Akpaden, Nigeria. His research focus is in: optimization of civil engineering materials, soil re-engineering, sustainable infrastructures and construction engineering. He is a member of several professional societies.

Roland K. ETIM
is a lecturer in the Department of Civil Engineering, Akwa Ibom State University, Ikot Akpaden, Nigeria. His research interest is in the field of geotechnical and geo-environmental engineering as well as sustainable cleaner materials for civil engineering infrastructures. He is a member of several professional societies.

David U. EKPO
is a lecturer in Akwa Ibom State University. He is a registered Engineer with COREN and a corporate member of the Nigeria Society of Engineers. He has a Master's degree in Civil Engineering with specialization in Geotechnical and Geo-environmental Engineering. He has published scholarly articles in Geotechnical and Geo-environmental Engineering.

Idorenyin N. USANGA
is a lecturer in the Department of Civil Engineering, Akwa Ibom State University, Ikot Akpaden. He is a registered Engineer with COREN and a corporate member of the Nigeria Society of Engineers. He has a Master's degree in Highway and Transportation Engineering with several well-known scholarly articles. He is currently working as a consultant in Akwa Ibom Roads and Other Infrastructure Maintenance Agency (AKROIMA).

1. Introduction

The use of industrial waste in improving the engineering properties of soil for geotechnical applications has continued because of the need of protecting the environment from industrial waste pollution couple with the escalating cost of waste disposal [1]. The beneficial implication is the production of a sustainable highway construction materials cum protection of the environment via unnecessary waste disposal in the long run [2]. The two most utilized stabilizers (cement and lime) either when used singly or combined has proven effective in improving weak soil [3]. Soil stabilization with these traditional additives represents one of the most significant techniques of ground improvement in enhancing the engineering properties of expansive soils such as those of black cotton soil. The black cotton soil (BCS) belonging to the family of smectite, comprises of montmorillonite with its highly expansive nature are known to possess considerable swell-shrink properties as a result of adsorbed water between the combined sheets of gibbsite and silica. The BCS has caused a lot of construction problem most especially when it is wet thereby increasing compressibility with a corresponding decrease in shear strength [4, 5]. In as much as these expansive soils in their natural state are unfit for construction purposes, discarding them would be uneconomical, thereby necessitating the need to stabilize them with chemical additives as a viable alternative in enhancing their engineering properties. Stabilization techniques generally, has led to reduction in compressibility of the soil, increase in soil's bearing capacity, enhancement of the physical and chemical properties of the soil [6-8, 56]. The utilization of cement has been a potential source of CO_2 which in turn has led to the depletion of the ozone layer. In a bid to cushion this effect, geo-environmental engineers are saddled with the responsibilities of utilizing industrial waste materials which have pozzolanic properties in order to replace these traditional additives due to increased cost and environmental impact they cause during

production [9, 10] These industrial waste materials require a lot of resources to dispose them which are of utmost concern to the entire construction industry, and as such the utilization of these wastes both in soil reengineering and concrete works could be a good strategy of minimizing waste and this would be of great benefit both environmentally and economically. One of such wastes include: periwinkle shell ash [11-13], oyster shell ash [14-17], metakaolin [18], sawdust ash [19], concrete waste [20], rice husk ash [21], groundnut shell ash [55] and cement kiln dust [22-23]. In terms of environmental benefits, waste minimization reduces the occurrence of unnecessary waste disposal in the society and the economic benefit includes low cost sustainable construction materials. Also, the statistical reliability analysis of some these additives/wastes when used with deficient soils have been verified and far reaching results reported in a number studies [57-60].

Metakaolin (MK), produced when pure kaolinite is calcined at a temperature of 500-550°C, yields an amorphous aluminosilicate compounds which can be compared with other industrial by-products such as blast furnace slag, steel slag and fly ash possessing a higher purity, larger specific surface area and finer particle size, with a resultant higher activity. Previous application of MK as a mineral additive in the production of high-performance concrete has led to increase in unconfined compressive strength (UCS) and splitting tensile strength (STS) with a corresponding decrease in shrinkage, free shrinkage strain and cracking, respectively [24-28]. Recently, MK have also found applications in cemented soil [29-30] and in the treatment of lateritic and expansive soil, respectively [18, 31-33].

Cement kiln dust (CKD) on the other hand, is an industrial by-product obtained during the manufacturing processes of cement with a similar appearance as that of Portland cement, in recent past has proven to be a viable soil stabilizer in terms of strength increment, permeability reduction and can improve the durability and strength of weak soils admixed with a pozzolanic materials [33-36].

As a result of the above-mentioned applicability of MK and CKD for both concrete and stabilized soils, respectively, their combination became appealing, so that an authoritative data could be established. Moving forward, for a fine-grained soil whose engineering properties in its virgin state do not meet the criteria for use as a construction material, a single additive might not be adequate in ameliorating the engineering properties such soil [37-38]. In this paper, the use of MK-CKD blends to decrease the plasticity of high plasticity expansive soil is explored. The morphological properties of the soil were also studied using the scanning electron microscope.

2. Materials and methods

The expansive soil (ES) and CKD were sourced from different sources. The soil was from a deposit in Deba, Gombe State, while the CKD came from a factory in Calabar, Cross River State, Nigeria. Metakaolin is not derived naturally but it's a derivative of calcined kaolin obtained during the calcination of pure kaolin.

2.1 Method

Particle size fraction of the virgin soil was executed via guidelines of [39]. Also, the compaction and consistency tests which includes liquid limit (LL), plastic limit (PL) and plasticity index were carried on the virgin and CKD-MK ameliorated soil mixtures as stipulated in [40] and [41]. However, the soil additives combination was achievable by blending 0-8% of CKD and 0-10% of MK in increments of 2%, respectively, by dry weight of soil.

3. Results and discussion

3.1 General classification of the materials used

Presented in *Table 1* and *Fig. 1* are the basic geotechnical response and particle size fraction of the untreated soil in it virgin state. In the same vein, the elemental composition of the materials (expansive soil, cement kiln dust and metakaolin) used in the study are presented in *Table 2*. With the guidelines of [42] and [43], the virgin soil falls under the soil class of A-7-6 (20) group and CH, respectively.

Property	Quantity
NMC, %	20.20
Percentage Passing 75μm aperture	71.99
LL, %	56.30
PL, %	28.60
PI, %	27.70
Gs	2.40
USCS	CH
AASHTO Classification	A-7-6 (20)
MDD (Mg/m³)	1.61
OMC, (%)	22.9
CBR (%)	3
Dominant clay mineral	Montmorillonite
Colour	Greyish black

Table 1 Physical and mechanical response of virgin soil
1. táblázat A kezeletlen talaj fizikai és mechanikai reakciói

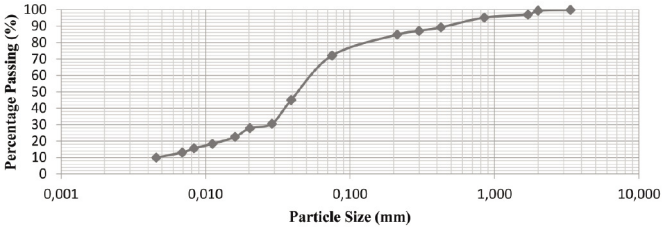

Fig. 1 Particle size distribution of the untreated soil
1. ábra A kezeletlen talaj szemcseméret-eloszlása

Oxides		SiO_2	CaO	SO_3	MgO	TiO_2	Fe_2O_3	Al_2O_3	Na_2O	K_2O	LOI
Mass fraction (%)	*BCS	48.50	0.90	-	2.22	-	2.20	18.60	1.55	0.70	10.10
	*CKD	18.82	66.82	2.01	0.01	0.40	2.05	6.34	0.20	1	1.03
	*MK	52.72	0.18	0.99	0.09	-	1.72	42.20	-	-	0.25

Table 2 Chemical analysis experiment of black cotton soil (BCS), cement kiln dust (CKD) and metakaolin (MK) [33]
2. táblázat A fekete talaj (BCS), cementégető-kemence por (CKD) és a metakaolin (MK) kémiai elemzése [33]

3.2 Specific gravity

The variation in the specific gravity of the soil was shown in the graph in *Fig. 2*. The higher the proportion of CKD-MK in the treated soil, the greater the specific gravity. The specific gravity of soil materials ranged between 2.40 and 2.56. It may interest you to know that the soil material in its virgin state had a specific gravity of 2.40 compared to the additives having 2.65 and 2.58 for CKD and MK, respectively. It is obvious the higher specific gravity of additive materials facilitated the increasing trend of soil treated with additives. Parallel upshots in specific gravity of fine-grained soil was documented by [5, 44].

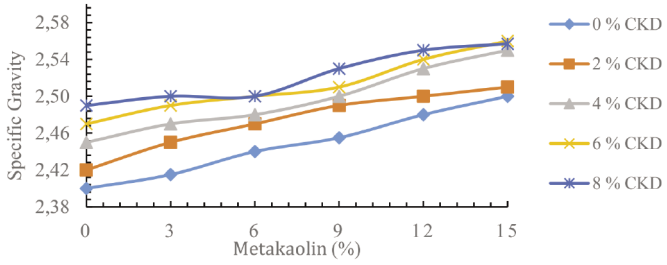

Fig. 2 Effect of metakaolin on soil-cement kiln dust (CKD) mixture
2. ábra A metakaolin hatása a talaj-cementégető-kemence por (CKD) keverékre

3.3 Consistency limits

3.3.1 Liquid limit

Fig. 3 presents the results of liquid limit (LL) test of an expansive soil blended with the mixtures of CKD-MK. The decrease in the soil's LL was significant. The LL of the natural soil decreased from 56.3% to 46% at 8% CKD-8% MK. The displayed outcome could be occasioned by the additives possessing pozzolanic tendencies and as such this altered the soil fabric. Also, the building up of flocs within the soil matrix could as well occasioned this outcome. However, this trend is comparable to the reports of [45-46].

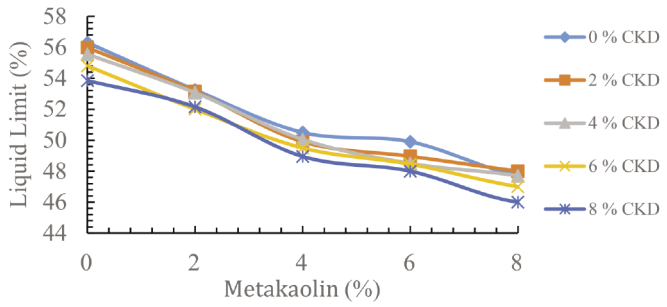

Fig. 3 Liquid limit results of expansive soil blended with cement kiln dust - metakaolin (CKD-MK) mixtures
3. ábra A cementégető-kemence por - metakaolin (CKD-MK) keverékkel készített expanzív talajok folyékonysági határértékének eredményei

3.3.2 Plastic limit

The graph of PL for various combinations of CKD-MK treated expansive soil is shown in *Fig. 4*. In a nut shell, the more the amount of additive material within the soil matrix, the lesser the PL. Metakaolin been one of the additive and a very reactive pozzolanic material in soil re-engineering, the trend of outcomes reflects it impact of non-plastic structure. Secondly, the existence of high chemical compositions of silica and alumina in the additives could as well occasioned the interplay amongst the clay particles and cations. The results of diminishing plastic limits of ameliorated soil materials had been documented by [16] and [35] who used waste materials in treating fine grain soils.

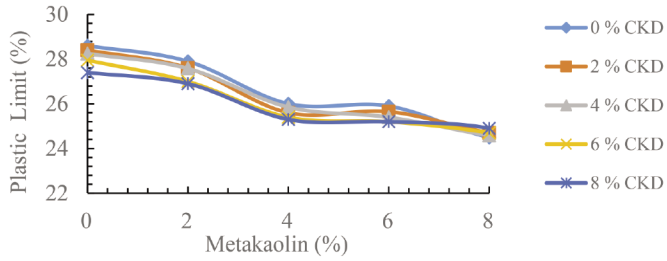

Fig. 4 Graph of PL of expansive soil - cement kiln dust (CKD) - metakaolin (MK) mixtures
4. ábra Az expanzív talaj - cementégető-kemence por (CKD) - metakaolin (MK) keverékek képlékenységi határ (PL) görbéje

3.3.3 Plasticity index

The graph of PI for various combinations of CKD-MK treated expansive soil is shown in *Fig. 5*. The no additive specimen displayed the highest PI of 27.70% while the specimen admixed 8% CKD - 8% MK displayed the lowest PI of 21.10%. Generally, the lessening of LL and PL of fine-grained soil due to the addition of additives facilitated the diminishing trend of PI. Thus, the reduction in PI is an indicator that the virgin soil has been improved upon the incorporation of the stabilizers. However, this behaviour could be facilitated by substituting the finer soil with additives [47-48, 51-54].

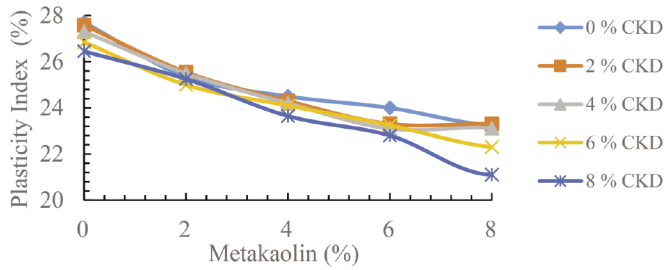

Fig. 5 Graph of PI of expansive soil - cement kiln dust (CKD) - metakaolin (MK) mixtures
5. ábra Az expanzív talaj - cementégető-kemence por (CKD) - metakaolin (MK) keverékek plaszticitási index (PI) görbéje

3.4 Compaction response

3.4.1 Maximum dry density

The graph of maximum dry density (MDD) for various combinations of CKD-MK treated expansive soil is shown in *Fig. 6*. The introduction of CKD-MK blend occasioned the increment in MDD of the studied soil from its lowest value of 1.63 to it topmost value of 1.731 Mg/m^3. The enhancement tendency in the soil material could be linked with some reasons, like (i) the specific gravity of the soil compared to that of the additives and (ii) probably the additives filling up the spores with the soil structure thereby increasing the weight of the soil. Equivalent results have been documented in literature by other researchers who worked on soil materials with high dominance of clay [5, 18, 36, 48].

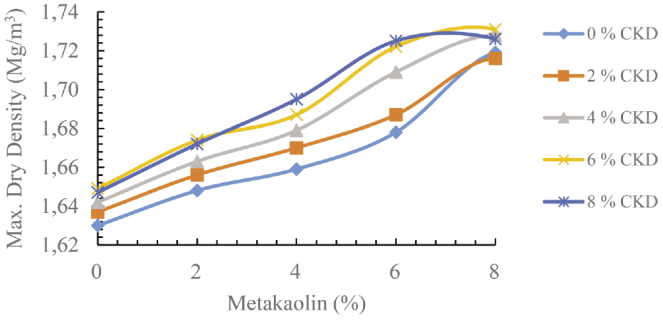

Fig. 6 Maximum dry density results of expansive soil blended with cement kiln dust (CKD) - metakaolin (MK) mixtures
6. ábra Az expanzív talaj - cementégető-kemence por (CKD) - metakaolin (MK) keverékek maximális száraz sűrűségének eredményei

3.4.2 Optimum moisture content

Fig. 7 demonstrates the results of optimum moisture content (OMC) exercise performed on an expansive soil blended with the mixtures of CKD-MK. For the OMCs of soil with CKD-MK, the results were contrary to the MDD outcomes. In a nutshell, the OMCs diminished in the course of introducing the additives into the soil matrix. This decrease in terms of OMCs could probably be occasioned by the ripple effect of increasing additive content which thereby lessens both silt and clay portion existing in the virgin soil. This trend of result is not new in soil re-engineering and others have reported similar trend [49, 15 -16].

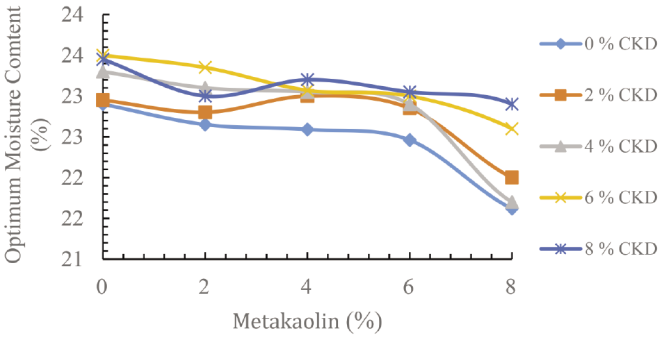

Fig. 7 Graph of OMC of expansive soil - cement kiln dust (CKD) - metakaolin (MK) mixtures
7. ábra Az expanzív talaj - cementégető-kemence por (CKD) - metakaolin (MK) keverékek optimális nedvességtartalom (OMC) görbéje

3.5 Scanning electron microscope

The result of the scanning electron microscope for the virgin and soil-CKD-MK is presented in *Fig. 8(a-b)*. The untreated soil consists of loosed packs of clay matrices with inter-assemblage pores within the soil grains. On *Fig 8(b)*, these pores appear to have been closed up on addition of the stabilizers which is not unconnected with the fact that there was an heterogenous exchangeable cation reaction between the additives and the soil which in turn resulted to formation of white lumps of calcium ions basically responsible for reduction in plasticity index thereby making the soil amenable. Previous researchers reported similar consistencies [5, 33, 36, 50-54].

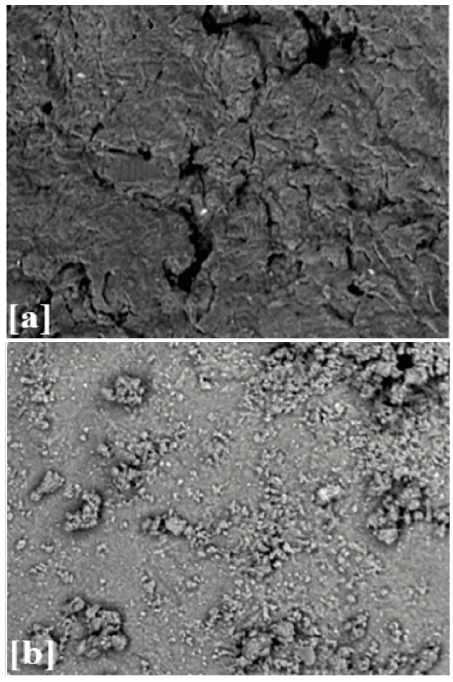

Fig. 8 SEM of (a) virgin soil (b) Soil - cement kiln dust (CKD) - metakaolin (MK)
8. ábra A kezeletlen talaj (a) és a talaj-cementégető-kemence por (CKD) - metakaolin (MK) (b) minták SEM felvétele

4. Conclusion

The utilization of waste materials in soil re-engineering can facilitate both economic and environmental benefits to the society. For this purpose, the plasticity and compaction properties of the expansive soil were investigated under laboratory studies in order to ascertain the effectiveness of the stabilizers. The result of the experimental investigations shows that the tested soil in its virgin state was classified as an A-7-6 (20) material and CH via AASHTO classification and USCS classification scheme, respectively. The LL, PL and PI of the expansive soil lessened with increased proportions of CKD and MK. The MDD value of the virgin soil enhanced from 1.63 Mg/m³ to its utmost value of 1.731 Mg/m³ at 6%CKD/8% MK with a corresponding decrease in OMC from 22.9% to 21.27%. The SEM result revealed the presence of cementitious compounds that contributed to in-filling of pores with a denser clay matrix. Based on this, an optimal blend of 8%CKD-8%MK could be a useful combination in stabilizing expansive soils for construction of highway. The environmental includes but not limited to reduction in disposals of CKD.

References

[1] Concrete Society (1987) Changes in the properties of ordinary Portland cement. Technical report 29: 1-30.
[2] Mehta PK (1998) Role of cementitious material in sustainable development of the concrete industry. In: Proceedings of 6th CANMET/ACI International Conference on Fly ash, silica fume, slag and natural pozzolans in concrete. 1: SP-178. Bangkok: V.M. Malhotra: 1-20.
[3] Ojuri OO, Adavi AA, Oluwatuyi OE (2017) Geotechnical and environmental evaluation of lime–cement stabilized soil–mine tailing mixtures for highway construction. Transportation Geotechnic. 10: 1–12. http://dx.doi.org/10.1016/j.trgeo.2016.10.001.
[4] Osinubi KJ, Sani EJ, Ijimdiya TS (2010) Lime and slag admixture improvement of tropical black clay road foundation". In: Transportation

Research Board (TRB) 89th Annual Meeting CD-ROM, Washington, D.C., U.S.A. January 10–14, 2010. Subject: Recycled Materials in Transportation Infrastructure, Session 243: AFP40 – Physico-chemical and Biological Processes in Soils Committee, Paper # 10–0585, 1–18.

[5] Etim RK, Eberemu AO, Osinubi KJ (2017) Stabilization of black cotton soil with lime and iron ore tailings admixture. Journal of Transportation Geotechnic, 10: 85-95. http://dx.doi.org/10.1016/j.trgeo.2017.01.002

[6] Sidek N, Mohamed K, Jais IM, Bakar IA (2016) Polyurethane foams in soil stabilization: A compressibility effect: In CIEC 2015, Springer, Singapore: pp. 369–377. http://dx.doi.org/10.1007/978-981-10-0155-033

[7] Du YJ, Jiang NJ, Liu SY, Horpibulsuk S, Arulrajah A (2016) Field evaluation of soft highway subgrade soil stabilized with calcium carbide residue. Soils Found. 56: 301 –314. http://dx.doi.org/10.1016/j.sandf.2016.02.012

[8] Oluwatuyi OE, Ojuri OO (2017) Environmental performance of lime–rice husk ash stabilized lateritic soil contaminated with lead or naphthalene. Geotech. Geol. Eng. 35: 2947–2964. http://dx.doi.org/10.1007/s10706-017-0294-9

[9] Al-homidy AA, Al-Amoudi O, Maslehuddin M, Saleh TA (2016) Stabilisation of dune sand using electric arc furnace dust. Int. J. Pavement Eng. 18: 513–520. http://dx.doi.org/10.1080/10298436.2015.1095904.

[10] Al-Amoudi OSB, Al-homidy AA, Maslehuddin M, Saleh TA (2017) Method and mechanisms of soil stabilization using electric arc furnace dust. Sci. Rep. 7: 1–10. http://dx.doi.org/10.1038/srep46676.

[11] Etim RK, Attah IC, Bassey OB (2017b) Assessment of periwinkle shell ash blended cement concrete in crude oil polluted environment. FUW Trends in Science and Technology Journal. 2 (2): 879 – 885.

[12] Etim RK, Attah IC, Eberemu AO, Yohanna P (2019) Compaction behaviour of periwinkle shell ash treated lateritic soil for use as road sub-base construction material. Journal of Geoengineering. 14 (3): 179 - 200. http://dx.doi.org/10.6310/jog.201909_14(3).6

[13] Attah IC, Etim RK, Ekpo DU (2018) Behaviour of periwinkle shell ash blended cement concrete in sulphuric acid environment. Nigerian Journal of Technology. 37 (2): 315 – 321. http://dx.doi.org/10.4314/njt.v37i2.5

[14] Etim RK, Attah IC, Ogarekpe NM, Robert EE (2018). Geotechnical behaviour of lateritic soil - oyster shell ash mixtures. Proceedings of 16th International Conference and Annual General Meeting 2018 of Nigerian Institution of Civil Engineers. Theme: Transforming National Economy through Sustainable Civil Engineering Infrastructure, Paradise 2018. Calabar International Convention Centre, Calabar, Cross River State. 24 – 26th Oct., 45 – 52

[15] Etim RK, Attah IC, Yohanna P (2020) Experimental study on potential of oyster shell ash in structural strength improvement of lateritic soil for road construction, International Journal of Pavement Research and Technology. 13 (4): 341-351. https://doi.org/10.1007/s42947-020-0290-y

[16] Attah IC, Etim RK, Sani JE (2019) Response of oyster shell ash blended cement concrete in sulphuric acid environment. Civil and Environmental Research. 11 (4): 62 – 74.

[17] Attah IC, Etim RK, Yohanna P, Usanga IN (2021b) Understanding the effect of compaction energies on the strength indices and durability of oyster shell ash-lateritic soil mixtures for use in road works. Engineering and Applied Science Research. 48 (2): 151-160. https://doi.org/10.14456/easr.2021.17.

[18] Attah IC, Agunwamba JC, Etim RK, Ogarekpe NM (2019) Modelling and predicting of CBR values of lateritic soil treated with metakaolin for road material. ARPN Journal of Engineering and Applied Science. 14 (20): 3609 – 3618.

[19] Alaneme GU, Mbadike ME, Attah IC, Udousoro IM (2022) Mechanical behavior optimization of sawdust ash and quarry dust concrete using adaptive neuro-fuzzy inference system. Innovative Infrastructure Solutions. https://doi.org/10.1007/s41062-021-00713-8

[20] Moses G, Etim RK, Sani JE, Nwude M (2018) Desiccation effect of compacted tropical black clay treated with concrete waste. Leonardo Electronic Journal of Practices and Technologies. 33: 69-88.

[21] Attah IC, Etim RK, Alaneme GU, Bassey OB (2020) Optimization of mechanical properties of rice husk ash concrete using Scheffe's theory.SN Applied Sciences, Springer Nature Switzerland AG. (2): 928. https://doi.org/10.1007/s42452-020-2727-y

[22] Alaneme GU, Attah IC, Etim RK, Dimonyeka MU (2021) Mechanical properties optimization of soil - cement kiln dust mixture using extreme vertex design. International Journal of Pavement Research and Technology. https://doi.org/10.1007/s42947-021-00048-8

[23] Alaneme, GU, Attah, IC, Mbadike ME, Dimonyeka MU, Usanga IN, Nwankwo HF (2022) Mechanical strength optimization and simulation of cement kiln dust concrete using extreme vertex design method. Nanotechnology for Environmental Engineering. 7(1) https://doi.org/10.1007/s41204-021-00175-4

[24] Batis G, Pantazopoulou P, Tsivilis S, Badogiannis E (2005) The effect of metakaolin on the corrosion behaviour of cement mortars. Cem. Concr. Compos. 27, 125–130

[25] Justice JM, Kurtis KE (2007) Influence of metakaolin surface area on properties of cement-based materials. J. Mater. Civ. Eng. 19 (9), 762–771.

[26] Khatib JM, Hibbert JJ (2005) Selected engineering properties of concrete incorporating slag and metakaolin. Constr. Build. Mater. 19, 460–472.

[27] Kim HS, Lee SH, Moon HY (2007) Strength properties and durability aspects of high strength concrete using Korean metakaolin. Constr. Build. Mater. 21, 1229–1237.

[28] Poon CS, Kou SC, Lam L (2006) Compressive strength, chloride diffusivity and pore structure of high performance metakaolin and silica fume concrete. Constr. Build. Mater. 20, 858–865

[29] Zhang TW, Yue XB, Deng YF, Zhang DW, Liu SY (2014) Mechanical behaviour and micro-structure of cement-stabilised marine clay with a metakaolin agent. Constr. Build. Mater. 73: 51–57

[30] Wu ZL, Deng YF, Liu SY, Liu QW, Chen YG, Zha FS (2016) Strength and microstructure evolution of compacted soils modified by admixtures of cement and metakaolin. Appl. Clay Sci. 127: 44–51.

[31] Yunzhi T, Yan H, Rui C, Wenjing S (2020). Shrinkage mechanism of laterite modified by lime and metakaolin. Hindawi, Advances in Civil Engineering. 20: 1-9. https://doi.org/10.1155/2020/6347597

[32] Ahmad M, Abdurrahman Y, Murtala U (2020). Assessment of lateritic soil stabilized using metakaolin. Journal of Geotechnical Studies. 5(1): 15-26. https://doi.org/10.5281/zenodo.3676443

[33] Attah IC, Okafor FO, Ugwu OO (2021a) Optimization of California bearing ratio of tropical black clay soil treated with cement kiln dust and metakaolin blend, International Journal of Pavement Research and Technology. 14 (6): 655-667 https://doi.org/10.1007/s42947-020-0003-6.

[34] Attah IC, Etim RK, Usanga IN (2021c) Potentials of cement kiln dust and rice husk ash blend on strength of tropical soil for sustainable road construction material. IOP Conference Series: Materials Science and Engineering. 1036: 012072. https://doi.org/10.1088/1757-899X/1036/1/012072

[35] Ekpo DU, Fajobi AB, Ayodele AL (2020) Response of two lateritic soils to cement kiln dust – periwinkle shell ash blends as road sub-base materials. International Journal of Pavement Research and Technology. https://doi.org/10.1007/s42947-020-0219-5

[36] Ekpo DU, Fajobi AB, Ayodele AL, Etim RK (2021) Potentials of cement kiln dust-periwinkle shell blends on plasticity properties of two selected tropical soils for use as sustainable construction materials. IOP Conf. Series: Materials Science and Engineering. 1036: 012033. http://doi.org/10.1088/1757-899X/1036/1/012033

[37] Alaneme GU, Onyelowe KC, Onyia ME, Bui Van D, Mbadike EM, Dimonyeka MU, Attah IC, Ogbonna C, Iro UI, Kumari S, Firoozi AA, Oyagbola I (2020a) Modelling of the swelling potential of soil treated with quicklime-activated rice husk ash using fuzzy logic. Umudike Journal of Engineering and Technology. 6 (1): 1 – 22. https://doi.org/10.33922/j.ujet_v6i1_1

[38] Alaneme GU, Onyelowe KC, Onyia ME, Bui Van D, Mbadike EM, Ezugwu CN, Dimonyeka MU, Attah IC, Ogbonna C, Abel C, Ikpa CC, Udousoro IM (2020b) Modelling volume change properties of hydrated-lime activated rice husk ash modified soft soil for construction purposes by artificial neural network. Umudike Journal of Engineering and Technology. 6 (1) 88 – 110. https://doi.org/10.33922/j.ujet_v6i1_9

[39] Head KH (1982) Manual of soil laboratory testing, soil classification and compaction tests, 2nd Ed., Pentech Press, London.

[40] BS 1377 (1990) Methods of testing soil for civil engineering purposes. British Standards Institution, London.

[41] BS 1924 (1990) Methods of tests for stabilized soils. British Standards Institute, London.
[42] American Association of State Highway and Transportation Official (1986) Standard Specifications for Transportation, Material and Method of Sampling and Testing, 14th Edition, AASHTO, Washington DC, USA.
[43] American Standard for Testing Material (1992) Annual Book of Standards Vol. 04.08. ASTM, West Conshohocken, PA, USA.
[44] Etim RK (2015) Stabilization of black cotton soil with lime-Iron Ore Tailing blends. Unpublished M.Sc. thesis, Department of Civil Engineering, Ahmadu Bello University, Zaria.
[45] Abood TT, Kasa AB, Chik ZB (2007) Stabilisation of silty clay soil using chloride compounds. Journal of Engineering Science Technology. 2(1):102–110.
[46] Sujatha ER, Dharinib K, Bharathia V (2015) Influence of groundnut shell ash on strength and durability properties of clay. Geomechanics and Geoengineering: An International Journal. pp. 1-8. http://dx.doi.org/10.1080/17486025.2015.1006265
[47] Baghdadi ZA, Fatani MN, Sabban NA (1995) Soil modification by cement kiln dust. J. Mater. Civ. Eng. 7 (4): 218–222.
[48] Okafor FO, Okonkwo UN (2009) Effect of rice husk ash on some geotechnical properties of lateritic soil. Leonardo Elec. J. Practices Technol. 15: 67-74.
[49] Attah IC, Okafor FO, Ugwu OO (2021d) Experimental and optimization study of unconfined compressive strength of ameliorated tropical black clay. Engineering and Applied Science Research. 48 (3): 238-248. https://doi.org/10.14456/easr.2021.26.
[50] Attah IC, Etim RK, Ekpo DU, Onyelowe KC (2021e) Understanding the impacts of binary additives on mechanical and morphological response of ameliorated soil for road infrastructures. Journal of King Saud University-Engineering Sciences. https://doi.org/10.1016/j.jksues.2021.12.001
[51] Etim RK, Ekpo DU, Ebong UB, Usanga IN (2021) Influence of periwinkle shell ash on the strength properties of cement-stabilized lateritic soil. International Journal of Pavement Research Technology, Chinese Society of Pavement Engineering, Springer Nature Singapore. https://doi.org/10.1007/s42947-021-00072-8
[52] Etim RK, Attah IC, Ekpo DU, Usanga IN (2021) Evaluation on Stabilization Role of Lime and Cement in Expansive Black Clay - Oyster Shell Ash Composite. Transportation Infrastructure Geotechnology. https://doi.org/10.1007/s40515-021-00196-1
[53] Etim RK, Ekpo DU, Etim GU, Attah IC (2021) Evaluation of lateritic soil stabilized with lime and periwinkle shell ash (PSA) admixture bound for sustainable road materials. Innovative Infrastructure Solutions. https://doi.org/10.1007/s41062-021-00665-z
[54] Etim RK, Ekpo DU, Attah IC, Onyelowe KC (2021) Effect of micro sized quarry dust particle on the compaction and strength properties of cement stabilized lateritic soil. Cleaner Materials, Elsevier. https://doi.org/10.1016/j.clema.2021.100023
[55] Moses G, Etim RK, Sani JE, Nwude M (2019) Desiccation-induced volumetric shrinkage characteristics of highly expansive tropical black clay treated with groundnut shell ash for barrier consideration. Civil and Environmental Research. 11(8):58–74. ISSN 2224-5790 (Paper) ISSN 2225-0514 (Online) https://doi.org/10.7176/CER/11-8-06
[56] Sani JE, Etim R, Joseph A (2019) Compaction Behaviour of Lateritic Soil–Calcium Chloride Mixtures. Geotechnical and Geological Engineering. Springer Nature Switzerland. 37:2343-2362. https://doi.org/10.1007/s10706-018-00760-6
[57] Yohanna P, Etim RK, Ijimdiya TS, Osinubi, KJ, Buki JM (2022) Reliability analysis of compaction characteristics of tropical black clay admixed with lime and iron ore-silica based dominant tailing. epitoanyag – Journal of Silicate Based and Composite Materials. 74(1). 13-20. http://doi.org/10.14382/epitoanyag-jsbcm.2022.3
[58] Sani, J. E., Yohanna, P., Etim K. R., Osinubi, J. K. and Eberemu, O. A. (2017). Reliability Evaluation of Optimum Moisture Content of Tropical Black Clay Treated with Locust Bean Waste Ash as Road Pavement Sub-base Material. Geotechnical and Geological Engineering Springer. http://link.springer.com/article/10.1007/sl0706-017-0256-2
[59] Osinubi KJ, Eberemu AO, Yohanna P, Etim RK (2016) Reliability estimate of compaction characteristics of iron ore tailings treated tropical black clay as road pavement sub-base material. GSP. 271, pp 855-864. http://dx.doi.org/10.1061/9780784480144.085
[60] Yohanna P, Kanyi MI, Etim RK, Eberemu OA, Osinubi KJ (2021) Experimental and statistical study on black cotton soil modified with cement–iron ore tailings. FUOYE Journal of Engineering and Technology. 6(1):2579-0617 http://dx.doi.org/10.46792/fuoyejet.vAiB.C

Ref.:
Attah, Imoh Christopher – **Etim**, Roland Kufre – **Ekpo**, David Ufot – **Usanga**, Idorenyin Ndarake: *Effectiveness of cement kiln dust-silicate based mixtures on plasticity and compaction performance of an expansive soil*
Építőanyag – Journal of Silicate Based and Composite Materials, Vol. 74, No. 4 (2022), 144–149. p.
https://doi.org/10.14382/epitoanyag-jsbcm.2022.22

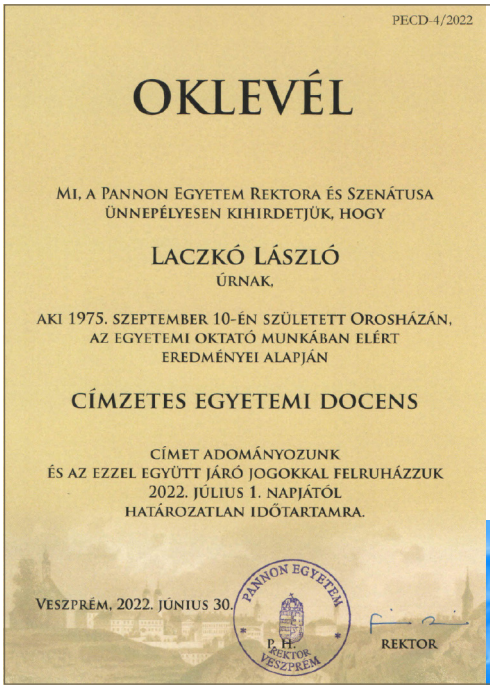
PECD-4/2022

OKLEVÉL

MI, A PANNON EGYETEM REKTORA ÉS SZENÁTUSA
ÜNNEPÉLYESEN KIHIRDETJÜK, HOGY

LACZKÓ LÁSZLÓ
ÚRNAK,

AKI 1975. SZEPTEMBER 10-ÉN SZÜLETETT OROSHÁZÁN,
AZ EGYETEMI OKTATÓ MUNKÁBAN ELÉRT
EREDMÉNYEI ALAPJÁN

CÍMZETES EGYETEMI DOCENS

CÍMET ADOMÁNYOZUNK
ÉS AZ EZZEL EGYÜTT JÁRÓ JOGOKKAL FELRUHÁZZUK
2022. JÚLIUS 1. NAPJÁTÓL
HATÁROZATLAN IDŐTARTAMRA.

VESZPRÉM, 2022. JÚNIUS 30.

PANNON EGYETEM
P. H.
REKTOR VESZPRÉM

REKTOR

A Veszprémi Pannon Egyetem Laczkó Lászlónak a SZIKKTI Labor Kft. laborvezetőjének, egyetemi oktató munkájának elismeréséül 2022. június 30-án CÍMZETES EGYETEMI DOCENS címet adományozott.

Az elismeréshez gratulálunk!

On 30th June 2022, the Pannonia University of Veszprém awarded László Laczkó, laboratory manager of SZIKKTI Labor Ltd. the title of HONORARY ASSOCIATE PROFESSOR in recognition of his work as an university lecturer.

Congratulations on his recognition.

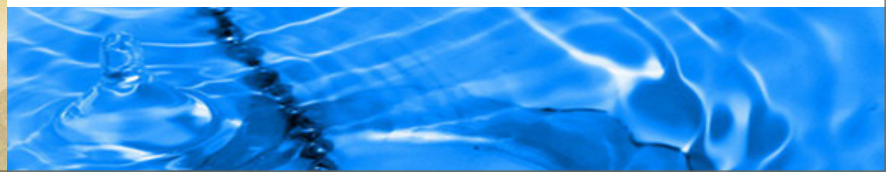

The single-stage steam gasification of magnetite heavy suspension separated coal samples from hungarian brown coal

Thuan Duc MAI ▪ Institute of Energy and Quality, University of Miskolc, Hungary ▪ tuzthuan@uni-miskolc.hu

Emese SEBE ▪ Institute of Energy and Quality, University of Miskolc, Hungary ▪ sebe.emese@uni-miskolc.hu

András Arnold KÁLLAY ▪ Institute of Energy and Quality, University of Miskolc, Hungary ▪ andras.kallay@uni-miskolc.hu

Érkezett: 2022. 08. 17. ▪ Received: 17. 08. 2022. ▪ https://doi.org/10.14382/epitoanyag-jsbcm.2022.23

Thuan D. MAI
is a PhD student at Institute of Energy and Quality, University of Miskolc, Hungary.

Emese SEBE
is a PhD student at Institute of Energy and Quality, University of Miskolc, Hungary.

András A. KÁLLAY PhD,
is a senior research fellow at the University of Miskolc, Faculty of Materials and Chemical Engineering, Institute of Energy and Quality Affairs, Chair Of The Board Of Trustees at the Engineers for Environmentally Friendly Energy Use, Higher Education Foundation and Secretary of Energy and Environment Working Committee, Hungarian Academy of Sciences Working Committee

Abstract

Currently, gasification of coal is considered the centre of the clean coal technology. In this study, there were two coal samples from the magnetite heavy suspension separated process used in the single stage fixed bed gasification within the non-moving of material. These two types of samples were marked as A1 and A2 sample, with the specific densities of ≤1.8 g/cm^3 and ≤1.6 g/cm^3, respectively and diameters 1-20 mm. The gasification experiments were conducted at steam flow rates of 5 and 10 g/min and gasification temperatures of 700, 800, and 900 °C. The main purpose of the experiments was to consider the effects of temperature and steam flow rate during the coal gasification from both, the energetic and chemical utilisation point of views. With higher temperature and steam flow rate, the experiments within A1 sample performed a better char yield and higher volume of produced syngas. In the case of A1 sample, the lowest char yield was 23.78 wt% at 900 °C gasification temperature and 10 g/min steam flow rate. At 900 °C of gasification temperature, the range of low heating value of synthesis gas were from 9.13 to 9.49 MJ/Nm^3 within 5 and 10 g/min of steam flow rate, indicating that the produced syngas is sufficient for energetic application. The range of H_2/CO ratio were from 1.96 to 2.52 at 900 °C of gasification temperature, which has a great potential for a further chemical application process.

Keywords: low rank coal, thermochemical process, coal gasification, synthesis gas
Kulcsszavak: gyenge minőségű szén, termokémiai folyamat, szénelgázosítás, szintézisgáz

1. Introduction

Coal is known to be the most abundant and widespread among fossil fuel resources. Today, coal is mainly used in the cement industry, iron and steel manufacturing, and electric power generation [1]. In 2018, the utilisation of coal accounted for the highest proportion in the electrical generation, approximately 37.93% [2]. Still now, the electricity generation from coal has been the most important resource and couldn't be directly replaced by the other energy primary sources.

The range of coal can be classified from peat to anthracite. In which, low-rank coals include lignite and sub-bituminous coals. These types of coal characterised by a lower heating value than high-rank coals (bituminous to anthracite) as a result of their lower carbon and higher moisture content. Lignite (brown coal) is a coal formed in the early stages of coalification, with the properties intermediate to those of bituminous coal and peat [3]. The major benefit of lignite combustion is the abundancy and low cost of mining. On the other hand, the use of lignite has a long list of disadvantages. Low calorific value, high moisture content that reduces the boiler efficiency, and ash properties that require specific combustion processes. Nevertheless, lignite has been successfully used as a raw material for gasification, liquefaction, and pyrolysis processes. The advantages of using lignite over higher rank coals in gasification and liquefaction relies on their high reactivity, non-caking properties, and catalytic property of alkali and alkaline-earth elements [4], [5].

Gasification is a thermochemical process, in which, using heat and gasifying agents to convert carbon-based materials (coal, biomass, municipal solid waste) into synthesis gas. In comparison with the conventional coal combustion in power generation, the gasification process exhibits several advantages [6]–[8]: (i) high ability to use a wide range of starting materials (coal, biomass, municipal solid waste), (ii) multi-production capacity (power generation, hydrogen fuel, or chemical products), (iii) lower emission of hazardous products (for example nitrogen, sulphur, mercury-based products, ash), (iv) reduced power and total budget for CO_2 capture. The major advantage of gasification is the high flexibility of synthesis gas utilisation. The quantity and quality of synthesis gas depend on different factors, such as the property of starting material, type of gasifiers, operational parameters, gasifying reactants, as well as catalyst [9]–[13].

Relative works regarding the gasification of Hungarian brown coal are quite rare. A. Pettinau et al. [14] studied in both bench-scale and pilot-scale fixed bed gasifier to investigate the potential industrial applications. The bench-scale gasification experiments carried out at 800 °C with steam and mixture of

steam and oxygen. While the experiments took place at a range of 900 to 950 °C with steam/air mixture in an up-draft pilot-scale gasifier. L. Bokányi and Á. Pintér-Móricz [15] investigated the plasma gasification of sub-bituminous Hungarian coal for the potential methanol-ethanol synthesis process. The experiments carried out within 30 kVA of plasma reactor with the temperature range of 1240-1588 °C. Oxygen was used as the gasifying agent in these experiments. There is a clear gap in the description of synergy effects of temperature and steam flow rate during the gasification of different Hungarian coal samples. In this study, there were two coal samples from the magnetite heavy suspension separated process used in the single stage fixed bed gasification. The main propose was to consider the effects of temperature and steam flow rate in both product distribution and gasification efficiency for these two coal samples and asses the significance of the separation method.

2. Materials and experiments

The main goal of this study is the investigation of gasification behaviour of two coal samples from the magnetite heavy suspension separated process. These two samples were marked as A1 and A2 sample, with the specific densities of ≤1.8 g/cm^3 and ≤1.6 g/cm^3, respectively and diameters 1-20 mm. The elemental analysis and heating values are presented in *Table 1*. In this scope, the elemental composition of coal samples was examined under the standard ISO 29541:2010 Solid mineral fuels - Determination of total carbon, hydrogen and nitrogen content - Instrumental method [16] within a Carlo Erba EA 1108 equipment analyser. The high heating value of coal samples were determined by a bomb calorimeter – Parr 6200 Isoperibol Calorimeter type analyser, using the ISO 1928:2009 - Solid mineral fuels - Determination of gross calorific value by the bomb calorimetric method and calculation of net calorific value standard [17]. The proximate analysis of coal samples was performed by thermal gravimetric analysis in a MOM Derivatograph-C type with the nitrogen and air ambient. The TG and DTG curves of coal samples are presented in *Fig. 1*.

Elemental analysis in air-dry samples, wt%					
	N-nitrogen	C-carbon	H-hydrogen	S-sulphur	O-oxygen (by difference)
A1	0.83	51.62	3.99	4.87	19.64
A2	0.82	48.38	3.92	5.18	16.65

Proximate analysis in air-dry samples, wt%					Heating value [MJkg-1]	
	M-moisture	V-volatile	FC-fixed carbon	A-ash	HHV	LHV
A1	9.37	36.75	34.84	19.05	20.029	18.966
A2	8.56	34.44	31.95	25.05	16.889	15.699

Table 1 Elemental analysis, proximate analysis, and heating value analysis of two different coal samples
1. táblázat Két különböző szénminta elemanalízise, nedvességtartalma és fűtőértéke

The experimental apparatus used in this study mainly consisted of heat resistant steel reactor (1200 mm long and 80 mm inner diameter), electrical heater (Carbolite 12/900), data logger, steam generator, manometer, venturi scrubber, cotton filter and gas meter, as illustrated in *Fig. 2*. The coal pyrolysis and steam gasification experiments were carried out at room pressure. The procedure of experiments is described as below:

In each experiment, there were 3 kg of brown coal loaded in the reactor. The electrical heater was then turned on to heat up the reactor. The starting point of the gasification with the introduction of steam into the reactor started when the pyrolysis process finished. The outlet of produced synthesis gas was in the bottom of the reactor, from where the gas was introduced into the venturi scrubber. In the venturi scrubber, the particles and tar removal process and cooling of the synthesis gas has taken place. The cooled synthesis gas was then filtered through a cotton wool filter before entering the gas meter and then combusted in a gas torch. After each experiment, the char was collected and weighted as the gasification char yield. During the gasification period, the temperature along reactor was displayed and recorded by a data logger in every minute. The gas volume was measured by a gas meter and gas flow rate calculated and also recorded by a data logger at every minute. The synthesis gas samples were analysed with an Agilent 490 micro-GC in every ~4 minutes using micro thermal conductivity detector (μ-TCD).

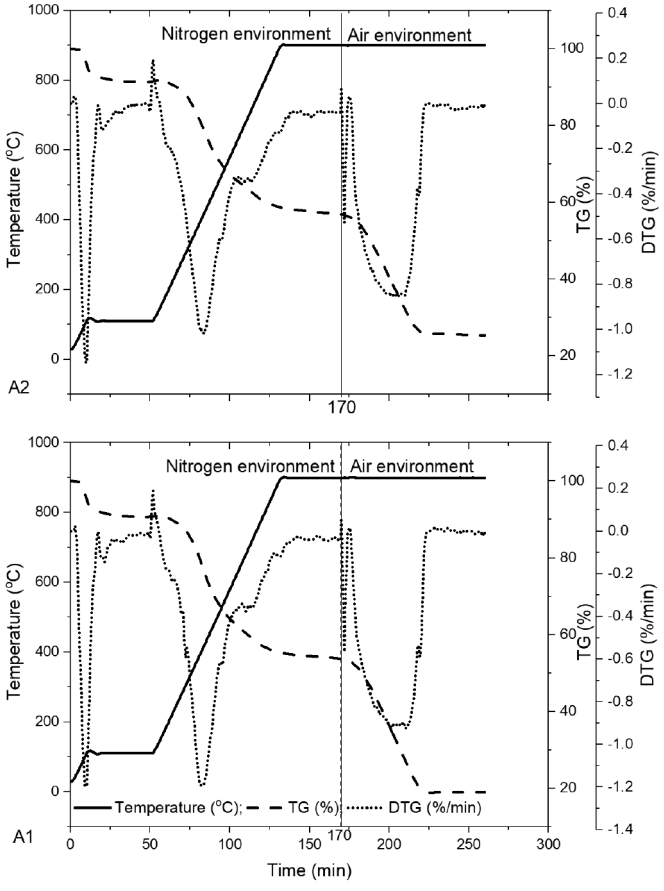

Fig. 1. Thermal analysis of coal samples (A2-top, A1-bottom)
1. ábra Szénminták termokémiai analízise

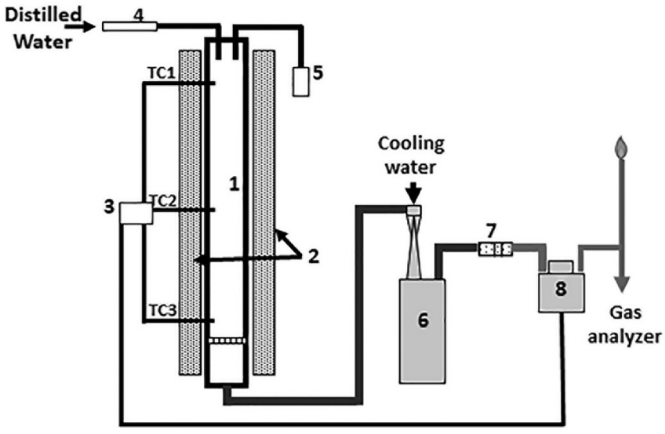

Fig. 2. The single stage lab-scale gasification system (1. Reactor, 2. Electrical heater, 3. Data logger, 4. Steam generator, 5. Manometer, 6. Venturi scrubber, 7. Cotton wool filter, 8. Gas meter, TC. thermocouple)

2. ábra Az egyfokozatú laboratóriumi elgázosítású rendszer (1. Reaktor, 2. Elektromos fűtőtest, 3. Adatgyűjtő, 4. Gőzfejlesztő, 5. Manométer, 6. Venturi mosó, 7. Vattaszűrő, 8. Gázmérő, TC. termoelem).

3. Results and discussions

The experiments focused on the gasification performance of coal char. Therefore, the analysis of pyrolysis gas was not included in this report. The gasification temperature was set to 700, 800, and 900 °C, with steam flow rate of 5 and 10 g/min for each temperature. The main chemical reactions within the steam gasification process that determines the syngas composition were the following:

Water-gas reaction (WGR):

$$C + H_2O \rightarrow CO + H_2 \ (\Delta H = 131 \text{ kJ/mol}) \quad (1)$$

Boudouard reaction:

$$C + CO_2 \rightarrow 2CO \ (\Delta H = 172 \text{ kJ/mol}) \quad (2)$$

Water-gas shift reaction (WGSR):

$$CO + H_2O \rightarrow CO_2 + H_2 \ (\Delta H = -41 \text{ kJ/mol}) \quad (3)$$

Methane reforming reaction:

$$CH_4 + H_2O \rightarrow CO + 3H_2 \ (\Delta H = 206 \text{ kJ/mol}) \quad (4)$$

3.1 Effect of temperature and steam flow rate on products distribution of gasification process

The effects of temperature and steam flow rate on gasification products are illustrated in *Fig. 3*. During the gasification experiments of A1 sample, the analysis of synthesis gas was absent in the experiment at 700 °C of gasification temperature and 5 g/min of steam flow rate due to technical problem. As consequently, further analysis for syngas composition and gasification performance (heating value, carbon conversion, and cold gas efficiency) are not include in the report. The char yields were calculated from the mass percentage of residual ash.

As the temperature increased, the char yields decreased, and the gas yields increased at all examined steam flow rate. In the case of A1 sample, the char yields declined sharply from 46.21 wt% and 40.39 wt% at 700 °C to 31.75 wt% and 23.78 wt% at 900 °C of gasification temperature, within the steam flow rate at 5 and 10 g/min, respectively. In the case of the A2 sample, from 40.44 wt% and 37.58 wt% at 700 °C decreased to 25.99 wt% and 25.68 wt% at 900 °C at the same steam flow rate conditions. Regarding to the synthesis gas yields, the increase in gasification temperature resulted in the increasing of synthesis gas production per kg of coal. With the gasification experiment of A1 sample at 10 g/min of steam flow rate, the synthesis gas yields rose drastically from 0.65 Nm^3/kg_{coal} at 700 °C to 1.29 Nm^3/kg_{coal} at 900 °C of gasification temperature. In the gasification process of A2 sample, the gas yields increased significantly from 0.37 Nm^3/kg_{coal} and 0.46 Nm^3/kg_{coal} at 700 °C to 0.96 Nm^3/kg_{coal} and 1.01 Nm^3/kg_{coal} at 900 °C, within the steam flow rate at 5 and 10 g/min. It can clearly be seen that the lowest char yield was at 900 °C and 10 g/min of steam flow rate. The trends shows that the endothermic reactions (Eq. (1), (2), (4)) were strongly promoted with the higher gasification temperature [18]–[20].

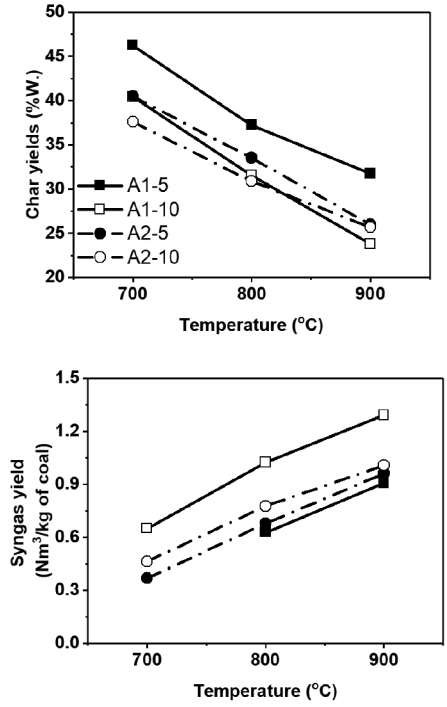

3. ábra Az elgázosítási folyamat termékeinek eloszlása a hőmérséklet és a gőz áramlási sebessége szerint (5 g/perc - szilárd szimbólum és 10 g/perc - nyitott szimbólum; A1 - szilárd vonal és négyzet szimbólum és A2- szaggatott pontvonal és kör szimbólum).

Fig. 3 Products distribution of gasification process by temperature and steam flow rate (5 g/min-solid symbol and 10 g/min – open symbol; A1-solid line and square symbol and A2- dash-dot line and circle symbol)

At each gasification temperature, the higher steam flow rate resulted in the lower char yields and the higher gas yields. It was illustrated that the more addition of steam increased the rate of reactions of Eq. (1), Eq. (3), and Eq. (4) [21]. However, the effects of steam flow rate were different in the gasification process of sample A1 and A2. At 900 °C of gasification temperature, the effect of steam flow rate on char yields showed clearly for A1 sample, 31.75 wt% at 5 g/min and 23.78 wt% at 10 g/min. While that for A2 sample was relatively similar, 25.99 wt% at 5 g/min and 25.68 wt% at 10 g/min of steam flow rate and gasification temperature at 900 °C. The comparison trends were also presented in the change of synthesis gas flow rate. With higher temperature and steam flow rate the gasification process of A1 sample had a better char yield and higher volume of syngas production.

Syngas composition (V/V%)			H_2		CO		CH_4		CO_2	
Steam flow rate (g/min)			5	10	5	10	5	10	5	10
Samples	A1	Gasification temperature (°C) 700		60.88		5.34		2.25		23.12
		800	57.6	58.96	14.29	11.83	2.11	1.36	18.42	19.84
		900	53.91	55.83	23.78	22.17	1.43	0.85	13.14	14.42
	A2	700	60.22	61.09	5.84	5.19	2.75	2.14	22.63	23.4
		800	58.02	58.49	13.28	12.61	1.81	1.49	18.71	19.48
		900	53.06	55.46	27.05	22.74	0.97	0.93	11.45	14.25

Table 2 Total synthesis gas composition by temperature and steam flow rate
2. táblázat A teljes szintézisgáz összetétele hőmérséklet és gőzáramlás szerint.

3.2. Effect of temperature and steam flow rate on synthesis gas composition

Table 2 illustrates the effects of gasification temperature and steam flow rate on the syngas composition of total syngas volume. The main components of synthesis gas were H_2, CO, CO_2, and CH_4 with over 92 V/V% under all experiments.

As the gasification temperature increased from 700 to 900 °C, the total composition of H_2, CO_2, and CH_4 showed a decreasing trend in the experiments for both sample type. While CO concentration increased with the increase of gasification temperature. The trends could be results of the improved rate of endothermic reactions (water gas reaction- Eq. (1), Boudouard reaction-Eq. (2), and methane reforming reaction-Eq. (4)) [18], [19] therefore the more CO produced and the more CO_2 and CH_4 were consumed. The water-gas shift reaction- Eq. (3) is a light exothermic reaction consequently, it was reversed when the temperature was higher than the equilibrium temperature [20]. Therefore, it led to a slight drop in H_2 concentration.

The synthesis gas composition changed at different rates with the increase of temperature. In case of the gasification experiment of A1 sample at a steam flow rate of 10 g/min, the H_2 concentration decreased by 1.92 V/V% when temperature increased from 700 to 800 °C. While that was 3.13 V/V% when temperature increased from 800 to 900 °C. In case of the A2 sample at the same gasification conditions, these numbers were 2.6% and 3.03%, respectively. The trend was even more emphasised in the changing of CO and CO_2 concentrations.

As steam flow rate increased from 5 to 10 g/min in the gasification process, the H_2 and CO_2 concentration increased in both samples. While that of CO and CH_4 showed a decreasing trend at all temperature conditions. The higher steam flow rate increased the reaction rate of water gas reaction- Eq. (1), water gas shift reaction- Eq. (3) and methane reforming reaction- Eq. (4) [22]–[24].

The composition of the synthesis gas at higher gasification temperature presented a higher differentiation with the increased steam flow rate. At lower gasification temperatures (700 and 800 °C) the difference in the changing of H_2, CO and CO_2 composition were not as significant when the steam flow rate was changed from 5 to 10 g/min. However, the difference was significant at a gasification temperature of 900 °C. In the case of the A2 sample, the H_2 concentration increased only by 0.87 V/V% at 700 °C and 0.47 V/V% at 800 °C when steam flow rate from was increased from 5 to 10 g/min. While that change was 2.4 V/V% at 900 °C. Similar trends were observed in the variation of CO and CO_2 concentrations. This could be the consequence of the change in the reaction rate of water gas shift reaction- Eq. (3). In the one hand, the higher concentration of steam enhanced the water gas shift reaction to produce a higher concentration of CO_2 and H_2. In the other hand, the higher gasification temperature led to the reverse direction of the water gas shift reaction. Therefore, the temperature had a significant effect on water-gas shift reaction when the gasification temperature was over the equilibrium temperature.

3.3. Effect of temperature and steam flow rate on gasification performance

The total of H_2/CO ratio, the low heating value of synthesis gas, carbon conversion and cold gas efficiency by gasification temperature and steam flow rate are shown in *Fig. 4*.

The low heating value of synthesis gas is defined as follow:

$$LHV_{synthesis\ gas} = \begin{pmatrix} H_2\% * 10.783 + CO\% * 12.633 \\ +CH_4\% * 35.883 \end{pmatrix} /100 \quad (5)$$

The carbon conversion efficiency of the gasification process is calculated by:

$$\eta_{carbon\ conversion} = \left(\frac{12 * Y * (CO\% + CO_2\% + CH_4\%)}{22.4 * C\%}\right) * 100 \quad (6)$$

The cold gas efficiency is calculated by:

$$\eta_{cold\ gas} = \left(\frac{LHV_{synthesis\ gas} * Y}{LHV}\right) * 100 \quad (7)$$

in which, H_2%, CO%, CO_2% and CH_4% are volume concentration of H_2, CO, CO_2 and CH_4 in synthesis gas V/V%. Y is the yield of synthesis gas Nm^3kg_{coal}. C% is carbon content of raw material in weight percentage wt%.

The H_2/CO ratio, heating value of synthesis gas, carbon conversion and cold gas efficiency were obviously driven by the components in synthesis gas (H_2, CO, CO_2 and CH_4). The results showed that the CO concentration increased drastically with the increased gasification temperature. It led to a decline in the H_2/CO ratio and an increasing trend in the low heating value of synthesis gas, carbon conversion and cold gas efficiency. Furthermore, the increase in gasification temperature improved the synthesis gas yield in the gasification process. It likewise enhanced carbon conversion and cold gas efficiency.

As an increase in gasification temperature, the H_2/CO ratio showed a converging trend in both samples. In the case of A1 sample at 900 °C of gasification temperature, the H_2/CO ratio was 2.27 at 5 g/min and 2.52 at 10 g/min of steam flow rate. In the case of A2 sample that was 1.96 and 2.44, respectively. However, this trend was only in the case of the A2 sample for the carbon conversion and cold gas efficiency.

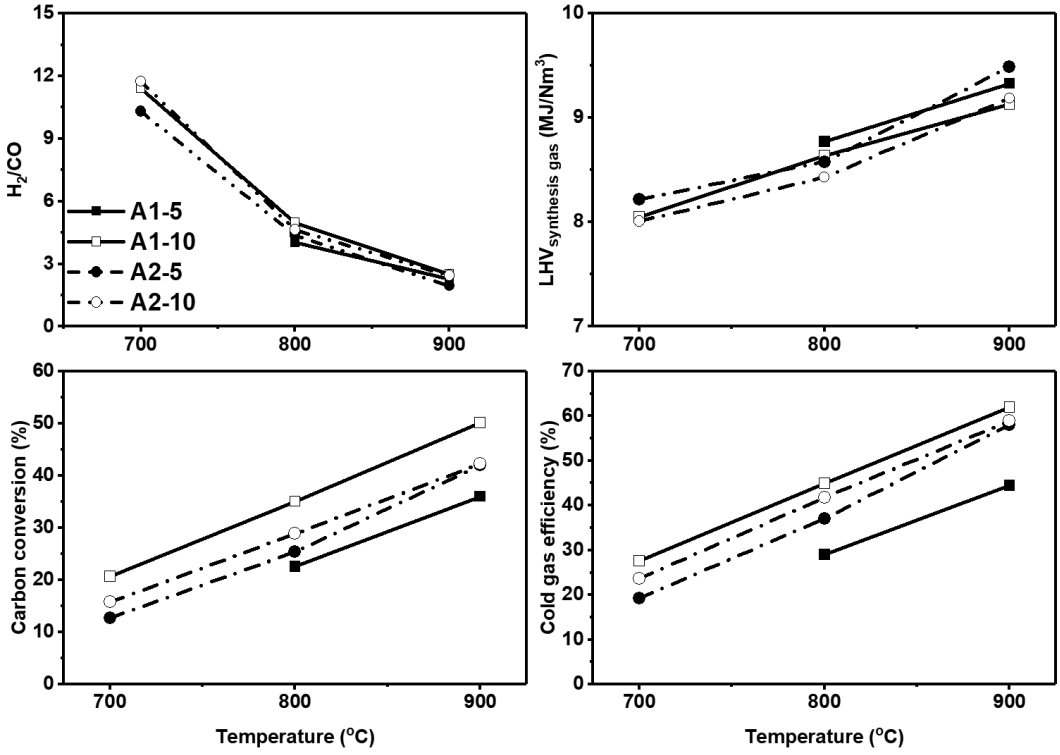

Fig. 4 Gasification performance by temperature and steam flow rate (5 g/min-solid symbol and 10 g/min – open symbol; A1-solid line + square symbol and A2- dash-dot line + circle symbol)

4. ábra Elgázosítás hőmérséklet és gőzáramlás szerint (5 g/min - szilárd szimbólum és 10 g/min - nyitott szimbólum; A1 - szilárd vonal + négyzet szimbólum és A2- szaggatott pontvonal + kör szimbólum).

As an increase in steam flow rate from 5 g/min to 10 g/min, the CO concentration decreased at all temperature conditions. As a result, the H_2/CO ratio at 5 g/min was lower than that at 10 g/min of steam flow rate. While the low heating value of synthesis gas at 5 g/min was higher than that at 10 g/min of steam flow rate. The highest low heating value of synthesis gas reached at 5 g/min of steam flow rate and 900 °C of gasification temperature for both samples, 9.33 MJ/Nm^3 for A1 sample and 9.49 MJ/Nm^{-3} for A2 sample. In the other hand, the higher steam flow rate led to an increase in CO_2 and synthesis gas yield. Therefore, the carbon conversion and cold gas efficiency were increased with the increase of steam flow rate at all temperature conditions.

Regarding to the effect of samples in gasification performance, the A1 sample was shown a more promising starting material for gasification than the A2 sample in term of carbon conversion and cold gas efficiency, especially at 900 °C of gasification temperature. In case of A2 sample, the carbon conversion efficiency was 41.98% at 5 g/min and 42.28% at 10 g/min of steam flow rate. While that was 36.01% and 50.12%, respectively, for A1 sample. The highest cold gas efficiency was 61.97% in the case of A1 sample at 900 °C of gasification temperature and 10 g/min of steam flow rate.

4. Conclusions

The two different coal samples were gasified at steam flow rates of 5 and 10 g/min and gasification temperatures of 700, 800, and 900 °C in a single stage fixed bed gasifier within the non-moving of material. The highest synthesis gas yields of samples were achieved at 900 °C of gasification temperature and 10 g/min of steam flow rate. The synthesis gas yields from the gasification process of A1 sample were higher than that of A2 sample at all experiment temperature conditions within 10 g/min of steam flow rate. The gasification temperature had a significant effect on the concentration of CO and CO_2. The higher gasification temperature led to a decrease trend in the H_2/CO ratio due to the increasing CO concentration. The range of H_2/CO ratio were from 1.96 to 2.52 at 900 °C of gasification temperature, which has a great potential for chemical application process. Furthermore, the A1 sample showed the better results in the carbon conversion and cold gas efficiency within 10 g/min of steam flow rate at all gasification temperature case. Based on the experiment results, the gasification process is a viable method to utilization the Hungarian low rank coals for the higher value application and the magnetite heavy suspension separation could further increase the carbon conversion rate and the cold gas efficiency.

Acknowledgements

The cross-cutting research was conducted at the University of Miskolc as part of the „More efficient exploitation and use of subsurface resources" project implemented in the framework of the Thematic Excellence Program funded by the Ministry of Innovation and Technology of Hungary (Grant Contract reg. nr.: NKFIH-846-8/2019), and within the subsequent „Developments aimed at increasing social benefits deriving from more efficient exploitation and utilization of domestic subsurface natural resources" project supported by the

Ministry of Innovation and Technology from the National Research, Development and Innovation Fund according to the Grant Contract issued by the National Research, Development and Innovation Office (Grant Contract reg. nr.: TKP-17-1/PALY-2020).

References

[1] M. Melikoglu, "Clean coal technologies: A global to local review for Turkey," *Energy Strateg. Rev.*, vol. 22, no. October, pp. 313–319, 2018, https://dx.doi.org/10.1016/j.esr.2018.10.011.

[2] IEA, "Global energy and CO2 status report - 2018," 2018.

[3] O. of A. Q. P. and S. Environmental Protection Agency, Research Triangle Park, "Compilation of air pollutant emission factors. Volume 1. Stationary point and area sources. Fifth edition," 1995. [Online]. Available: https://www.osti.gov/biblio/104236-compilation-air-pollutant-emission-factors-volume-stationary-point-area-sources-fifth-edition

[4] L. Závodská and J. Lesný, "Recent development in lignite investigation," *Hungrian Eletronic J. Sci.*, pp. 1–15, 2006, [Online]. Available: http://heja.szif.hu/ENV/ENV-061026-A/env061026a.pdf

[5] L. Ren, R. Wei, and Y. Gao, "Co-gasification reactivity of petcoke and coal at high temperature," *Fuel*, vol. 190, pp. 245–252, 2017, https://dx.doi.org/10.1016/j.fuel.2016.11.020.

[6] A.-M. Cormos and C.-C. Cormos, "Techno-economic assessment of combined hydrogen & power co-generation with carbon capture: The case of coal gasification," *Appl. Therm. Eng.*, vol. 147, pp. 29–39, Jan. 2019, https://dx.doi.org/10.1016/j.applthermaleng.2018.10.064.

[7] K. S. Weil, "Coal gasification and IGCC technology: a brief primer," *Proc. Inst. Civ. Eng. - Energy*, vol. 163, no. 1, pp. 7–16, Feb. 2010, https://dx.doi.org/10.1680/ener.2010.163.1.7.

[8] A. Arnold, K. Vivien, G. Nagy, and T. Koós, "The analysis of the solid and liquid phase products of two-stage pyrolysis," *Mater. Sci. Eng.*, vol. 42, no. 1, pp. 46–58, 2017.

[9] A. Mishra, S. Gautam, and T. Sharma, "Effect of operating parameters on coal gasification," *Int. J. Coal Sci. Technol.*, vol. 5, no. 2, pp. 113–125, 2018, https://dx.doi.org/10.1007/s40789-018-0196-3.

[10] A. A. P. Susastriawan, H. Saptoadi, and Purnomo, "Small-scale downdraft gasifiers for biomass gasification: A review," *Renew. Sustain. Energy Rev.*, vol. 76, no. March, pp. 989–1003, 2017, https://dx.doi.org/10.1016/j.rser.2017.03.112.

[11] L. Emami Taba, M. F. Irfan, W. A. M. Wan Daud, and M. H. Chakrabarti, "The effect of temperature on various parameters in coal, biomass and CO-gasification: A review," *Renew. Sustain. Energy Rev.*, vol. 16, no. 8, pp. 5584–5596, Oct. 2012, https://dx.doi.org/10.1016/J.RSER.2012.06.015.

[12] V. Kirsanovs, A. Žandeckis, D. Blumberga, and I. Veidenbergs, "The influence of process temperature , equivalence ratio and fuel moisture content on gasification process : A review," *27st Int. Conf. Effic. Cost, Optim. Simul. Environ. Impact Energy Syst. ECOS 2014, Turku, Finl.*, vol. 2, no. JUNE, 2014, [Online]. Available: http://ecos2014.abo.fi/ocs/index.php/2014/ECOS2014

[13] M. Inayat, S. A. Sulaiman, J. C. Kurnia, and M. Shahbaz, "Effect of various blended fuels on syngas quality and performance in catalytic co-gasification: A review," *Renew. Sustain. Energy Rev.*, vol. 105, pp. 252–267, May 2019, https://dx.doi.org/10.1016/j.rser.2019.01.059.

[14] A. Pettinau, Z. Dobó, Z. Köntös, and A. Zsemberi, "Experimental characterization of a high sulfur Hungarian brown coal for its potential industrial applications," *Fuel Process. Technol.*, vol. 122, pp. 1–11, 2014, https://dx.doi.org/10.1016/j.fuproc.2014.01.018.

[15] L. Bokányi and Á. Pintér-Móricz, "Potential methanol-ethanol synthesis from Hungarian sub-bituminous coal via plasma gasification and Fischer-Tropsch synthesis," *Int. J. Oil, Gas Coal Technol.*, vol. 18, pp. 55–73, 2018.

[16] BSI, *BSI Standards Publication Solid biofuels — Determination of total content of carbon , hydrogen and nitrogen — Instrumental methods*. 2011.

[17] BSI, *Solid mineral fuels — Determination of gross calorific value by the bomb calorimetric method and calculation of net calorific value*. 2009, pp. 1–59.

[18] Y. Xiao, S. Xu, Y. Liu, and C. Qiao, "Catalytic steam co-gasification of biomass and coal in a dual loop gasification system with olivine catalysts," *J. Energy Inst.*, vol. 93, no. 3, pp. 1074–1082, Jun. 2020, https://dx.doi.org/10.1016/j.joei.2019.10.002.

[19] S. Chang, Z. Zhang, L. Cao, L. Ma, S. You, and W. Li, "Co-gasification of digestate and lignite in a downdraft fixed bed gasifier: Effect of temperature," *Energy Convers. Manag.*, vol. 213, p. 112798, Jun. 2020, https://dx.doi.org/10.1016/j.enconman.2020.112798.

[20] Z. Chen *et al.*, "High quality syngas production from catalytic coal gasification using disposable Ca(OH) 2 catalyst," *Chem. Eng. J.*, vol. 316, pp. 842–849, May 2017, https://dx.doi.org/10.1016/j.cej.2017.02.025.

[21] D. S. Upadhyay, K. R. Panchal, A. Kumar V Sakhiya, and R. N. Patel, "Air-Steam gasification of lignite in a fixed bed gasifier: Influence of steam to lignite ratio on performance of downdraft gasifier," *Energy*, p. 118187, Jul. 2020, https://dx.doi.org/10.1016/j.energy.2020.118187.

[22] C.-L. Lin and W.-C. Weng, "Effects of different operating parameters on the syngas composition in a two-stage gasification process," *Renew. Energy*, vol. 109, pp. 135–143, Aug. 2017, https://dx.doi.org/10.1016/j.renene.2017.03.019.

[23] N. Cerone, F. Zimbardi, L. Contuzzi, J. Baleta, D. Cerinski, and R. Skvorčinskienė, "Experimental investigation of syngas composition variation along updraft fixed bed gasifier," *Energy Convers. Manag.*, vol. 221, p. 113116, Oct. 2020, https://dx.doi.org/10.1016/j.enconman.2020.113116.

[24] K. Mondal, K. Piotrowski, D. Dasgupta, E. Hippo, and T. Wiltowski, "Hydrogen from Coal in a Single Step," *Ind. Eng. Chem. Res.*, vol. 44, no. 15, pp. 5508–5517, Jul. 2005, https://dx.doi.org/10.1021/ie048974d.

Ref.:
Mai, Thuan Duc – **Sebe**, Emese – **Kállay**, András Arnold: *The Single-Stage Steam Gasification of Magnetite Heavy Suspension Separated Coal Samples from Hungarian Brown Coal*
Építőanyag – Journal of Silicate Based and Composite Materials, Vol. 74, No. 4 (2022), 150–155. p.
https://doi.org/10.14382/epitoanyag-jsbcm.2022.23

A víz-cement tényező hatása a cementek hidratációjára

LACZKÓ László ▪ SZIKKTI Labor Kft. ▪ szikktilaborkft@t-online.hu
WOJNÁROVITSNÉ HRAPKA Ilona ▪ SZIKKTI Labor Kft. ▪ szikktilaborkft@t-online.hu
SPRÁNITZ Ferenc ▪ Dolomit Kft. ▪ sprafer.dolomit@gmail.com

Érkezett: 2022. 04. 12. ▪ Received: 12. 04. 2022. ▪ https://doi.org/10.14382/epitoanyag-jsbcm.2022.24

Kivonat

Különböző típusú cementek (CEM I 52,5 R; CEM I 42,5 R; CEM I 42,5 N-SR0 és CEM II/A-S 42,5N) esetén vizsgáltuk a víz-cement tényező (0,3; 0,4; 05; 0,6) hidratációra gyakorolt hatását röntgendiffrakciós, pásztázó elektronmikroszkópos (SEM) és higanyporozimetriás módszerekkel.

A hidratáció mértékére a fázisösszetételből számított hidratációs fok (azaz a hidrátfázisban kötött CaO-tartalom összes CaO-tartalomhoz viszonyított aránya) alapján következtettünk.

90 nap után (v/c=0,6 mellett) a portlandcementek közül legnagyobb a CEM I 52,5 R (~68%), ezt követően CEM I 42,5 R (~65%), legkisebb a szulfátálló CEM I 42,5N-SR0 (~56%) hidratációs foka. A CEM II/A-S 42,5 N kohósalak-portlandcementből készített mintáknál a hidratációs fok ~61%.

A különböző cementkövek porozitás vizsgálata alapján megállapítható, hogy a kumulatív pórustérfogatot a hidratáció ideje mellett nagymértékben befolyásolja a v/c értéke, mely a pórusokat benövő, a hidratáció során keletkező reakciótermékek, illetve kristályfázisok milyenségével, mennyiségével függ össze. A különböző cementkövek egymáshoz viszonyított porozitása eltérően változhat a hidratációs idő és a v/c függvényében, mely a hidratáció eltérő sebességével függhet össze.

90 nap után, a különböző v/c értékeknél általában a CEM I 42,5N-SR0 minta porozitása a legnagyobb, vagyis itt a leglassúbb a hidratáció. míg legkisebb porozitás (azaz leggyorsabb hidratáció) a CEM I 52,5 R, illetve a CEM I 42,5 R anyagokra jellemző.

A cementkő porozitását a kumulatív pórustérfogat mellett a pórusméret-eloszlás jellemzi. A finompórusok (D<30 nm) legnagyobb részaránya a CEM I 52,5 R cementkőre jellemző.

Kulcsszavak: cementhidratáció, fázisösszetétel, morfológia, porozitás
Keywords: Cement hydration, phase composition, morphology, porosity

LACZKÓ László
Okl. vegyész, okl. kémia szakos tanár (Veszprémi Egyetem Szilikátkémia szakirány 2001, 2004); (2004), Veszprémi Egyetem szilikátkémia szakirány. 2001–2004 Doktori (Ph.D) ösztöndíj Veszprémi Egyetem Anyagtudományok és –Technológiák Doktori Iskola; Szilikát- és Anyagmérnöki Tanszék), címzetes egyetemi docens (Pannon Egyetem, 2022). Oktatási terület: Veszprémi Pannon Egyetem Anyagmérnöki Intézet: Szilikátkémia laboratóriumi gyakorlatok, szilikátipari nyersanyagok és késztermékek analitikai vizsgálata. Kutatási terület: Cementek és kiegészítőanyagaik. Közéleti tevékenység: MTA Anyagtudományi és Szilikátkémiai Munkabizottság, 2000-től a Szilikátipari Tudományos Egyesület tagja, SZTE Minősítő Bizottság elnöke.

WOJNÁROVITSNÉ HRAPKA Ilona
Okl. vegyészmérnök (1967), mérnök-közgazdász (1974); KŐSZIG vállalatnál kutató vegyész (1967-73), Szilikátipari Központi Kutató és Tervező Intézet (SZIKKTI) tudományos tanácsadó (1974-1994). SZIKKTI Labor Kft. ügyvezető igazgatója (1994 -). A kémiai tudományok kandidátusa (1980), MTA doktora (1993), címzetes egyetemi docens (Veszprémi Egyetem, 1989). Érdeklődési terület: szilikátszálak jellemzői és korrózió; szilikátok műszaki jellemzői közötti összefüggések tanulmányozása; szilikátkémiai anyagvizsgálatok. Közéleti tevékenység: MTA Szilikátkémiai és Műszaki Kémiai Bizottságának tagja; SZTE Szilikátkémiai Bizottságának vezetője (1981-1990); az Építőanyag folyóirat felelős szerkesztője (1991-2005)

SPRÁNITZ Ferenc
Okkl. építőmérnök (1985), okl. betontechnológus szakmérnök (2000). Építésügyi szakértő, a Dolomit Kft. betonüzemének vezetője. Érdeklődési területe: levegőn szilárduló, valamint hidraulikus kötőanyaggal készülő termékek, gyártástechnológiák fejlesztése; vibropréselt, öntömörödő, megnövelt savállóságú, szálerősített és felkeményedő viselkedésű betonok, továbbá padozati szerkezetek (esztrich, ipari padló) tervezése, készítése, szakértése. Hazai és nemzetközi szakmai szervezetek tagja (*fib*, MMK, SzTE, ÉTE, BTE), az Esztrich és Ipari Padló Egyesület tiszteletbeli elnöke.

1. Bevezetés

A CEM I 52,5 R; CEM I 42,5 R; CEM I 42,5 N-SR0 és CEM II/A-S 42,5 N cementekből 0,3; 0,4; 0,5 és 0,6 víz/cement tényező mellett készített 7, 28, 56 és 90 napos próbatestek esetén tanulmányoztuk a hidratáció során végbemenő fázisösszetételi, morfológiai, valamint a porozitásban bekövetkező változást.

Munkánk célját a további kutatások szempontjából optimális víz-cement tényező kiválasztása képezte, mely technológiai szempontból is érdekes.

A portlandcementben lévő klinkerásványok hidratációja során vízben oldhatatlan hidráttermékek képződnek [1, 2].

Az alit (C_3S) viszonylag gyorsan reagál a vízzel (*1. egyenlet*).

$$2\,(3CaO{\cdot}SiO_2) + 5\,H_2O \rightarrow 3\,Ca(OH)_2 + 3CaO{\cdot}2SiO_2{\cdot}2H_2O$$
$$\mathbf{2\,C_3S + 5\,H \rightarrow 3\,CH + C_3S_2H_2} \quad (1)$$

A $C_3S_2H_2$ összetételű tobermoritban a $CaO:SiO_2$ arány 0,8 … 1,5 között változhat.

A belit (C_2S) hidratációja az alitéhoz hasonló, de lényegesen lassabban megy végbe.

A trikalcium-aluminát (C_3A) hidratációja (*2. egyenlet*).

$$2\,(3\,CaO{\cdot}Al_2O_3) + 21\,H_2O \rightarrow 4\,CaO{\cdot}Al_2O_3{\cdot}13H_2O + 2\,CaO{\cdot}Al_2O_3{\cdot}8H_2O$$
$$\mathbf{2\,C_3A + 21\,H \rightarrow C_4AH_{13} + C_2AH_8} \quad (2)$$

Az instabil hidrátvegyületek időben stabil hidráttermékekké alakulnak (*3. egyenlet*).

$$4\,CaO{\cdot}Al_2O_3{\cdot}13H_2O + 2\,CaO{\cdot}Al_2O_3{\cdot}8H_2O \rightarrow 2\,(3CaO{\cdot}Al_2O_3{\cdot}6H_2O) + 9\,H_2O$$
$$\mathbf{C_4AH_{13} + C_2AH_8 \rightarrow 2\,C_3AH_6 + 9\,H} \quad (3)$$

A brownmillerit (C_4AF) hidratációjakor kolloid $Fe(OH)_3$ és $Al(OH)_3$ is képződik (*4; 5. egyenletek*).

$$3\,(4CaO{\cdot}Al_2O_3{\cdot}Fe_2O_3) + 30\,H_2O \rightarrow 3\,(3CaO{\cdot}Al_2O_3{\cdot}6H_2O) + 3CaO{\cdot}Fe_2O_3{\cdot}6H_2O + 2Fe(OH)_3$$
$$\mathbf{3\,C_4AF + 30\,H \rightarrow 3\,C_3AH_6 + C_3FH_6 + 2\,FH_3} \quad (4)$$

$$3\,(4CaO{\cdot}Al_2O_3{\cdot}Fe_2O_3) + 30\,H_2O \rightarrow 3\,(3CaO{\cdot}Fe_2O_3{\cdot}6H_2O) + 3CaO{\cdot}Al_2O_3{\cdot}6H_2O + 2Al(OH)_3$$
$$\mathbf{3\,C_4AF + 30\,H \rightarrow 3\,C_3FH_6 + C_3AH_6 + 2\,AH_3} \quad (5)$$

A hidratáció során kialakuló cementkő pórusai szilárd anyaggal ki nem töltött terek, amelyekben többnyire levegő, ill. folyadék található. A pórusok általában nyitottak, méretük alapján történő besorolást az *1. táblázat* tartalmazza [3]. A cementkő porozitását a kumulatív pórustérfogat mellett a pórusméret-eloszlás jellemzi.

A légpórusok a szilárduló cementkőben a gondos tömörítés mellett is visszamaradó, viszonylag nagyobb méretű pórusok.

A légbuborékok a beton fagyállóságának, olvasztósó-állóságának javítására légbuborékképző adalékszerrel a cementkőben tudatosan létrehozott, közel gömb alakú, egymástól független pórusok. A légbuborék-eloszlásra követelmény, hogy az ún. távolsági tényező, azaz a cementkő

bármely pontjától a hozzá legközelebb eső légbuborék felszínének távolsága, mely nem lehet több, mint 0,2 mm. [4,5]

Megnevezés	Pórusátmérő
mikropórusok	≤ 2 nm
mezopórusok	2 ... 50 nm
makropórusok:	> 50 nm
– mikrokapilláris	50 ... 2000 nm
– kapilláris	... 50 µm
– makrokapilláris	> 50 µm

1. táblázat A cementkőben lévő pórusok hozzávetőleges átmérője
Table 1 Approximate diameter of the pores presented in the cement paste

A cementkőben kialakuló fázisok térfogati arányait nagymértékben befolyásolja a v/c arány.

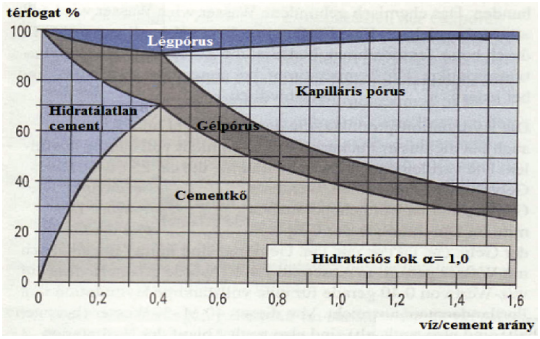

1.ábra A cementkőben kialakuló fázisok térfogataránya a v/c függvényében [3]
Fig. 1 Volume fraction of phases formed in cement paste as a function of v/c [3]

A cementkőben lévő kapilláris pórusok a keverővíz mennyiségétől függően keletkeznek. A cement hidratációja során a cementkőbe legfeljebb a 30-35 m/m% vízmennyiség épülhet be, ami 0,30 - 0,35 víz-cement tényezőnek felel meg. Ha a beton ennél több vízzel készül, akkor az elpárolgó vízfelesleg finom, hajszálcsöves, gyakran összefüggő pórusrendszert hoz létre. Ezek alkotói a beton felületére is kivezető kapilláris pórusok, melyek mennyiségének növekedésével a cementkő és a beton minősége romlik.

A gélpórusok: a cement klinkerásványainak hidratációja során képződő gélalkotók közötti pórusok. A gélpórusok a folyadékokat és a gázokat gyakorlatilag nem eresztik át. A cement hidratáció előrehaladtával a hidratációs termékek mennyisége növekszik és a gélpórusok mennyisége csökken.

2. Vizsgálati módszer

A cementekből különböző víz/cement tényezőjű pépeket készítettünk, melyeket szilikon sablonban 20 °C–on telített páratérben (klímakamrában) tároltunk. A megszilárdult mintákat, 24 óra után a sablonból kivéve 20 ± 1 °C–os desztillált vízbe helyeztük és a vizsgálatokig tároltuk.

A röntgendiffrakciós mérésekhez PW 1729/1820 típusú készüléket, a SEM leképezéshez JEOL JSM 5200 típusú berendezést alkalmaztunk. A porozitás méréseket QuantaChrome Poremaster 60 GT típusú higanypenetrációs poroziméterrel végeztük, mely 950 µm – 3,6 nm pórusátmérő tartományban tesz lehetővé méréseket.

A higany a legtöbb közegben, így a cementkőben is nem nedvesítő folyadékként viselkedik, ezért az anyag pórusaiba, repedéseibe, hézagaiba nem hatol be spontán, hanem ehhez nyomás szükséges. Ha feltételezzük, hogy a pórusok kör keresztmetszetűek, a sugaruk r, és p a külső nyomás, akkor a nem nedvesítő folyadékot $r^2\pi p$ nyomóerő préseli a pórusokba. A nyomóerővel szemben ható erő a higany nedvesítési szögétől (α) és felületi feszültségtől (σ) függ. Az alkalmazott higanynyomás és a pórusméret közötti összefüggést a Washburn egyenlet (*6. egyenlet*) írja le [6,7]:

$$r = \frac{-2 \cdot \sigma \cdot Cos\ \alpha}{p} \qquad (6)$$

ahol: σ a higany felületi feszültsége (az adott esetben 0,4855 N/m)
α a higany nedvesítési szöge (az adott esetben 140°)
p az adott higanynyomás (Pa)
r a pórus sugara (nm)

Az alkalmazott módszerrel a mérés során a nyomás 400 MPa fölé történő fokozatos növelésével a nagyobb pórusoktól a kisebbek felé haladva 250 µm-től 3,6 nm tartományban határoztuk meg a kumulatív porozitást. Munkánkban az eredmények jobb értelmezése céljából az abszcisszán a kisebb értékektől a nagyobbak felé logaritmikus skálán ábrázoltuk a pórusátmérőt.

3. Kísérleti eredmények

A *2-3. táblázatok* adatai alapján legkisebb szemcseméretű és legnagyobb fajlagos felületű a CEM I 52,5 R, míg legnagyobb szemcseméret és legkisebb fajlagos felület a CEM II/A-S 42,5 cementre jellemző. Legnagyobb alit tartalommal a CEM I 42,5 N cement rendelkezik.

Fázisok	CEM I 52,5 R	CEM I 42,5 R	CEM I 42,5 N -SR0	CEM I I/A-S 42,5 N
	Fázisösszetétel, m/m%			
C_3S	53,5	56,5	58,5	45,0
C_2S	21,5	17,5	14,0	15,0
C_3A	9,0	8,5	-	9,0
$C_{12}A_7$	-	-	3,5	-
C_4AF	9,0	9,5	12,0	9,0
C_2F	-	-	-	-
$CaSO_4 \cdot 2H_2O$	6,0	-	1,0	-
$CaSO_4 \cdot 0{,}5H_2O$	-	7	5,5	6,0
CaO	1,0	0,5	1,0	0,5
Kvarc	-	-	1,0	-
MgO (periklász)	-	-	1,0	-
$CaCO_3$ (kalcit)	-	-	-	6,0
$CaCO_3 \cdot MgCO_3$ (dolomit)	-	-	-	-
Röntgenamorf (üveges)	-	-	-	8,0

2. táblázat Cementek röntgendiffrakcióval meghatározott fázisösszetétele
Table 2 Phase composition of cements determined by X-ray diffraction

	Fajlagos felület (Blaine); cm^2/g	Szemcsefrakció-összetétel, m/m%		
		0-3 μm	3-32 μm	32-200 μm
CEM I 52,5 R	4870	31,17	68,15	0,67
CEM I 42,5 R	4210	28,42	69,97	1,61
CEM I 42,5 N – SR0	4150	28,62	70,01	1,37
CEM II/A-S 42,5 N	3600	23,86	68,95	7,19

3. táblázat Cementek fajlagos felülete és szemcseméret-összetétele
Table 3 Specific surface area and particle size distribution of the cements

3.1 Fázisösszetételi és morfológiai változások

A különböző portlandcementek hidratációja során végbemenő változásokat terjedelmi okok miatt részletesebben csak a CEM I 52,5 R esetén ismertetjük:

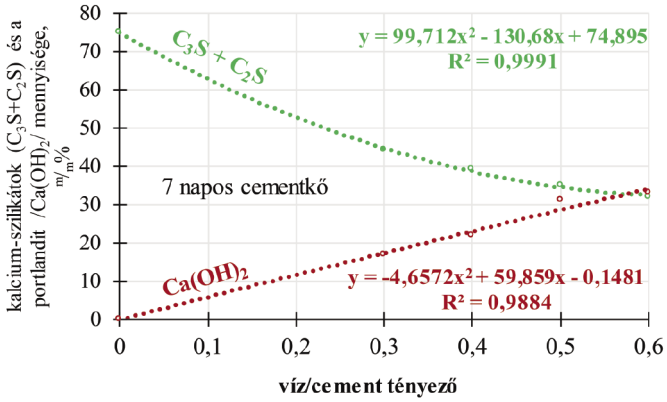

2.a ábra CEM I 52,5 R cementből különböző v/c mellett készített 7 napos minták kalcium-szilikát (C3S+C2S) és Ca(OH)2 (portlandit) tartalmának változása
Fig. 2a Variation in calcium silicate (C3S+C2S) and Ca(OH)2 (portlandite) content of 7-day samples of CEM I 52.5 R cement at different v/c

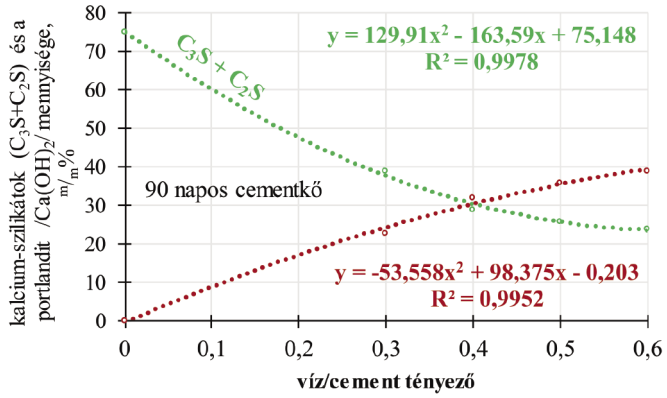

2.b ábra CEM I 52,5 R cementből különböző v/c mellett készített 90 napos minták kalcium-szilikát (C3S+C2S) és Ca(OH)2 (portlandit) tartalmának változása
Fig. 2.b Variation in calcium silicate (C3S+C2S) and Ca(OH)2 (portlandite) content of 90-day samples of CEM I 52.5 R cement at different v/c

Az *2 a-b. ábrák* alapján megállapítható, hogy adott hidratációs időnél (7 és 90 nap után) a v/c tényező növekedésével a klinkerben lévő kalcium-szilikátok (C_3S+C_2S) mennyisége egyre nagyobb mértékben csökken, míg a portlandité $Ca(OH)_2$ nő. A hidratáció nem teljes mértékű, mivel a klinkerben lévő alit és belit jelentős része kb. 25-27% visszamarad. A hidratáció mértékére a fázisösszetételből számított hidratációs fok (azaz a hidrátfázisban kötött CaO-tartalom összes CaO-tartalomhoz viszonyított aránya) alapján következtettünk (*3. ábra*). Megállapítható, hogy a CEM I 52,5 R esetén adott hidratációs időnél minél nagyobb a v/c értéke, annál nagyobb a hidratációs fok. Az is kitűnik, hogy adott v/c aránynál (0,3; 0,4; 0,5; 0,6) a hidratáció előrehaladtával (7-90 nap) szintén nő a hidratációs fok.

CEM I 42,5 R és CEM I 42,5 N-SR0 cementkövekre is jellemző (*4-5. ábrák*), hogy adott idejű hidratációnál a v/c arány növelésével (0,3-0,4) kezdetben nő a hidratációs fok, de a CEM I 52,5 R mintától eltérően ennek mértéke a nagyobb v/c értékeknél (0,5-0,6) kisebb, illetve stagnál. A 7-90 nap során, kis v/c aránynál (0,3-0,4) a CEM I 42,5 R és CEM I 42,5 N-SR0 minták hidratációja a CEM I 52,5 R a mintához képest kisebb mértékű.

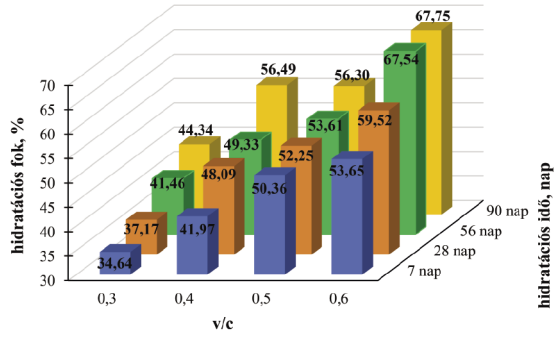

3. ábra a CEM I 52,5 R cementkő minták hidratációs foka
Fig. 3 Degree of hydration of CEM I 52.5 R cement paste samples

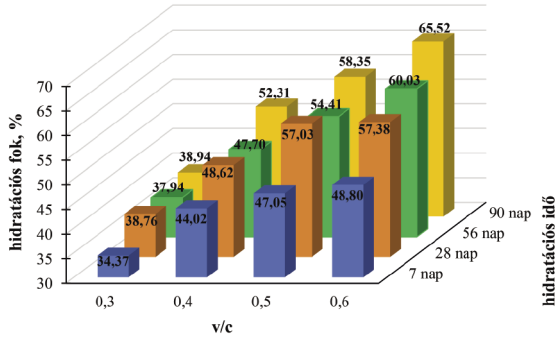

4. ábra A CEM I 42,5 R cementkő minták hidratációs foka
Fig. 4 Degree of hydration of CEM I 42.5 R cement paste samples

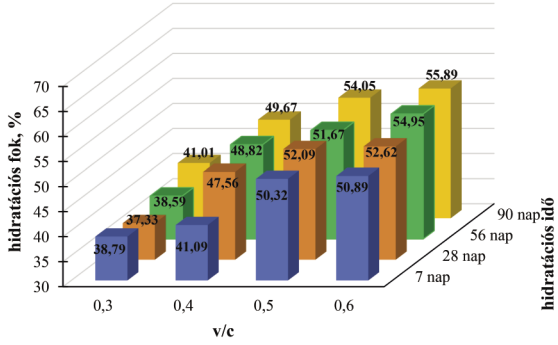

5. ábra A CEM I 42,5 N – SR0 cementkő minták hidratációs foka
Fig. 5 Degree of hydration of CEM I 42.5 N – SR0 cement paste samples

A kohósalak-portlandcement (CEM II/A-S 42,5 N) esetén hasonló körülmények között a hidratációs fok változása CEM I 52,5 R mintához viszonyítva kisebb mértékű (*6. ábra*).

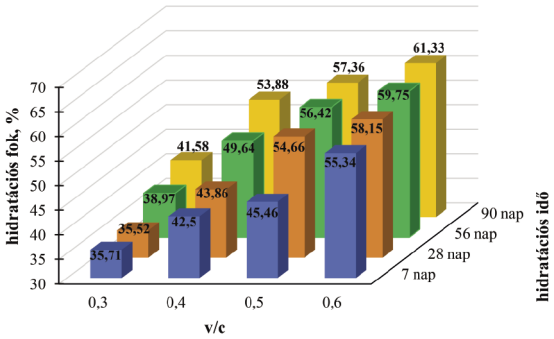

6. ábra a CEM II/A-S 42,5 N cementkő minták hidratációs foka
Fig. 6 Degree of hydration of CEM II/A-S 42.5 N cement paste samples

90 nap hidratáció után (v/c=0,6 mellett) a portlandcementek közül legnagyobb a CEM I 52,5 R (~68%), ezt követően CEM I 42,5 R (~65%), legkisebb a szulfátálló CEM I 42,5N-SR0 (~56%) hidratációs foka**.** A CEM II/A-S 42,5 N kohósalak-portlandcementből készített próbatesteknél ennek értéke (~61%). A v/c=0,3 mellett a különböző cementek hidratációs fokának eltérése lényegesen kisebb.

A SEM vizsgálatok alapján jól követhető a hidratáció során bekövetkező morfológiai változás, amit példaként a CEM I 52,5 R cementkövek esetén mutatunk be. Az XRD vizsgálatok eredménye arra utalt, hogy 90 nap elteltével sem játszódik le a klinkerben lévő alit és belit teljes hidratációja. A végig amorf fázisban jelenlévő C-S-H mellett, csak monoszulfát ($C_3A{\cdot}CaSO_4{\cdot}12H_2O$), esetlegesen C-A-H, valamint monokarboaluminát ($C_3A{\cdot}CaCO_3{\cdot}11H_2O$) és portlandit kristályfázisok azonosíthatók. Az 56 nap hidratáció után v/c=0,6 mellett, a próbatestek felületén már megindul a karbonátosodás vagyis $CaCO_3$ kimutatható.

7 nap után v/c=0,3 tényezőnél a klinkerszemcsék felületén megindul a hidratáció, azaz tized mikron nagyságrendű „szőrösödés", mely a gélszerű röntgenamorf kalcium-szilikát-hidrát fázis, továbbiakban C-S-H képződéssel függ össze, mely csomószerűen is rendeződhet (*7.a ábra*). Ezzel egyidejűen a pórusokban kialakulnak a kb. 0,5 µm vastag, 10-20 µm lapméretű hexaéderes portlandit kristályok (*7.a ábra*).

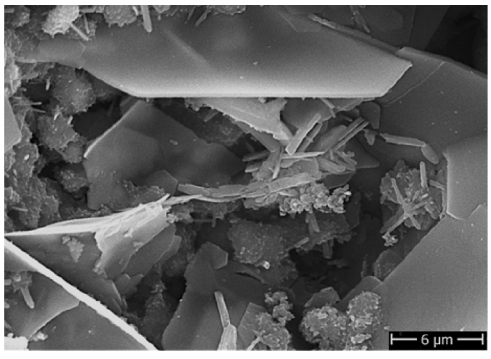

7.a ábra CEM I 52,5 R cementkő (v/c=0,3; 7 nap) SEM felvétele
Fig. 7.a SEM image of CEM I 52.5 R cement stone (w/c=0.3; 7 days)

A v/c arány növekedésével egyre nagyobb mértékű a hidratáció. A v/c=0,6 értéknél a gélszerű C-S-H fázis mellett, már megfigyelhetők a pórusokat is benövő monoszulfátra ($C_3A{\cdot}CaSO_4{\cdot}12H_2O$) jellemző vastagabb szálszerű alakzatok is (*7.b ábra*).

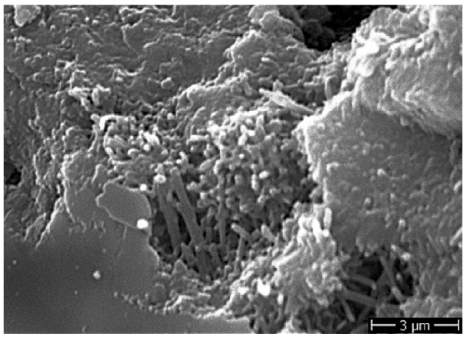

7.b ábra CEM I 52,5 R cementkő (v/c=0,6; 7 nap) SEM felvétele
Fig. 7.b SEM image of CEM I 52.5 R cement stone (w/c=0.6; 7 days)

28 nap után a v/c=0,3 tényezővel készült mintában a C-S-H szálszerű képződményei megfigyelhetők a klinkerszemcsék felületén (*7.c ábra*). A nagyméretű portlandit alakzatok egyre jobban benövik a pórusokat (*7.d ábra*). A *7.e ábrán* megfigyelhetők az eseténként 6 µm hosszúságú botszerű monoszulfát kristályok.

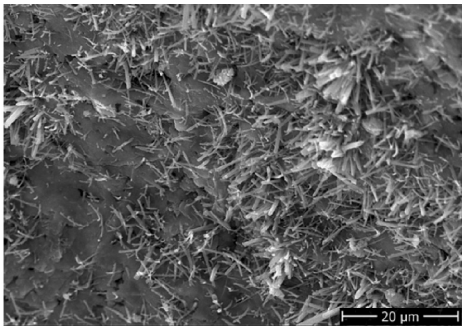

7.c ábra CEM I 52,5 R cementkő (v/c=0,3; 28 nap) SEM felvétele
Fig. 7.c SEM image of CEM I 52.5 R cement stone (w/c=0.3; 28 days)

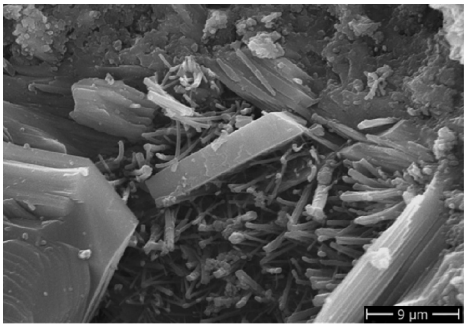

7.d ábra CEM I 52,5 R cementkő (v/c=0,3; 28 nap) SEM felvétele
Fig. 7.d SEM image of CEM I 52.5 R cement stone (w/c=0.3; 28 days)

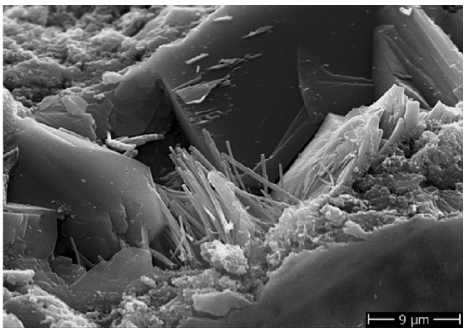

7.e ábra CEM I 52,5 R cementkő (v/c=0,3; 28 nap) SEM felvétele
Fig. 7.e SEM image of CEM I 52.5 R cement stone (w/c=0.3; 28 days)

A v/c tényező növekedésével a hidrátvegyületek képződése erőteljesebb. A v/c=0,5-0,6 értéknél jellemzőek a megnövekedett hosszúságú (5-10 μm) és vastagságú (0,5 μm) pórusokban is előforduló C-S-H tűkristályok mellett, a botszerű monoszulfát jelenléte (*7.f ábra*). A monokarbo-aluminát ($3CaO{\cdot}Al_2O_3{\cdot}CaCO_3{\cdot}11H_2O$) hasábos tömbszerű alakzata a 7.f ábra jobb oldalán látható.

56-90 nap után a v/c arány növekedésével a pórusokat egyre jobban benövik a portlandit kristályok, melyek a táblás morfológia mellett, egyre nagyobb gyakorisággal tömör lépcsőzetes (8-12 μm méretű) alakzatban állnak össze (*7.g ábra*).

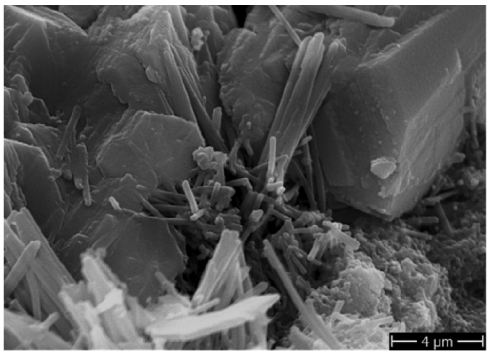

7.f ábra CEM I 52,5 R cementkő (v/c=0,5; 28 nap) SEM felvétele
Fig. 7.f SEM image of CEM I 52.5 R cement stone (w/c=0.5; 28 days)

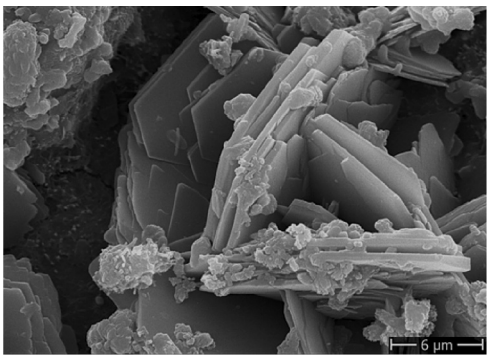

7.g ábra CEM I 52,5 R cementkő (v/c=0,5; 56 nap) SEM felvétele
Fig. 7.g SEM image of CEM I 52.5 R cement stone (w/c=0.5; 56 days)

3.2 Porozitásvizsgálat

A porozitás méréseket négy különböző típusú, négy különböző víz/cement tényezőjű és négy különböző korú, összesen 64 db cementkő mintán végeztük.

A következőkben részletesebben csak a CEM I 52,5 R típusú cementkövek porozitás vizsgálatát ismertetjük. Mind a négy kor (7, 28, 56, 90 nap) esetén jellemző, hogy a v/c tényező növekedésével a cementkő porozitása nő (*8. ábra*). Kis v/c (0,3-0,4) esetén, a hidratáció előrehaladtával a porozitás fokozatosan csökken; de v/c=0,5 értéknél ez csak 7-28 nap között tapasztalható; míg v/c=0,6 mellett 28 nap után a kumulatív pórustérfogat gyakorlatilag változatlan.

Mind a négyfajta cementkő esetén a hidratációs idő növekedésével azonos v/c (0,3 és 0,6) mellett porozitásuk csökken, illetve bizonyos idő (56-90 nap) után stagnál (*9-10. ábrák*). Ez általában annál rövidebb idő után következik be, minél nagyobb a v/c tényező.

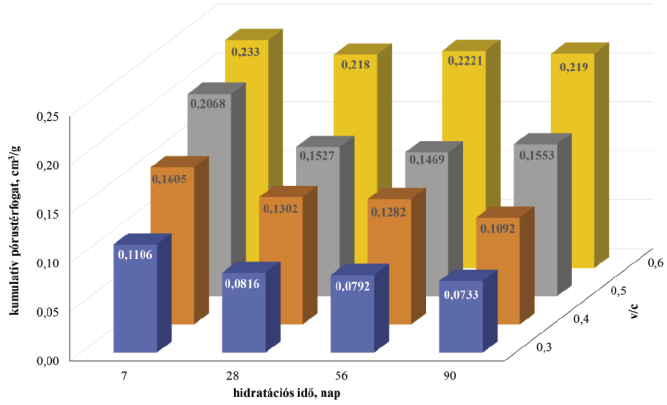

8. ábra CEM I 52,5 R cementkő minták kumulatív pórustérfogatának változása a hidratációs idő és a v/c függvényében
Fig. 8 Variation of cumulative pore volume of CEM I 52.5 R cement paste samples with hydration time and v/c

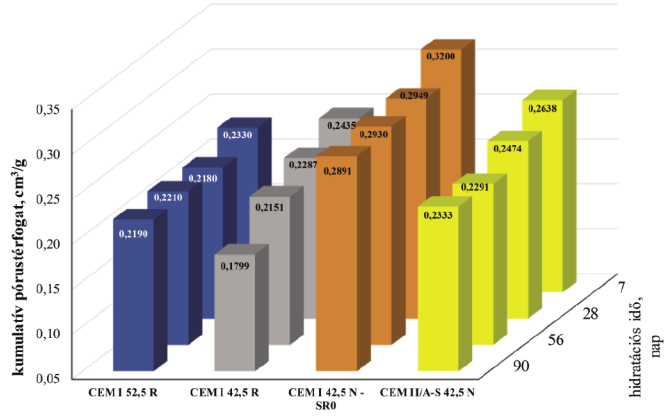

9. ábra CEM I 52,5 R; CEM I 42,5 R, CEM I 42,5 N - SR0 és CEM II/A-S 42,5 N cementkő minták porozitása a hidratációs idő függvényében (v/c = 0,6)
Fig. 9 Porosity of CEM I 52.5 R; CEM I 42.5 R, CEM I 42.5 N - SR0 and CEM II/A-S 42.5 N cement paste samples as a function of hydration time (v/c = 0.6)

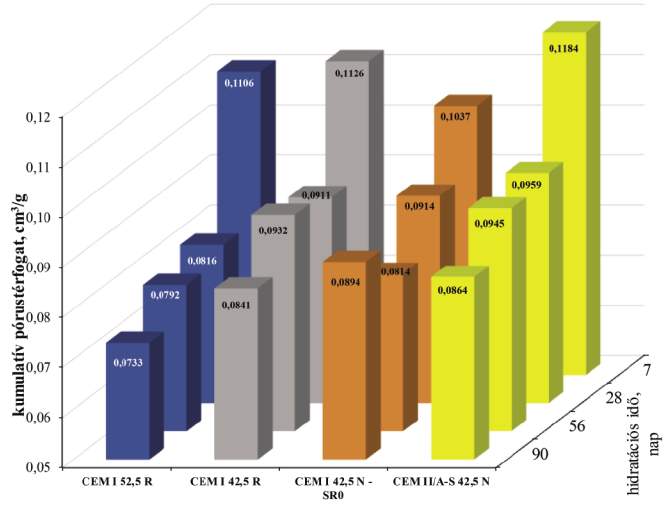

10. ábra CEM I 52,5 R; CEM I 42,5 R, CEM I 42,5 N - SR0 és CEM II/A-S 42,5 N cementkő minták porozitása a hidratációs idő függvényében (v/c = 0,3)
Fig. 10 Porosity of CEM I 52.5 R; CEM I 42.5 R, CEM I 42.5 N - SR0 and CEM II/A-S 42.5 N cement paste samples as a function of hydration time (v/c = 0.3)

A 7-90 nap hidratáció során legnagyobb porozitás a v/c=0,6 mellett a 7 napos cementkövekre jellemző (*9. ábra*). Legnagyobb kumulatív pórustérfogat a CEM I 42,5 N-SR0, míg

legkisebb a CEM I 52,5 R mintánál állapítható meg. A 90 nap hidratáció után továbbra is legnagyobb a CEM I 42,5N-SR0, legkisebb viszont a CEM I 42,5 R, ezt követően CEM I 52,5 R minta porozitása.

7-90 nap hidratáció során kis v/c=0,3 mellett 7 nap után a különböző cementkövek porozitását összehasonlítva (*10. ábra*) legnagyobb a CEM II/A-S 42,5 N, míg legkisebb a CEM I 42,5 N-SR0 mintára mért érték. 90 nap hidratáció után legnagyobb CEM I 42,5 N-SR0 és legkisebb a CEM I 52,5 R minta porozitása.

Az előzőek alapján megállapítható, hogy a kumulatív pórustérfogatot a hidratáció ideje mellett nagymértékben befolyásolja v/c értéke, mely a pórusokat benövő, a hidratáció során keletkező reakciótermékek, illetve kristályfázisok milyenségével, mennyiségével függ össze. A különböző cementkövek egymáshoz viszonyított porozitása eltérően változhat a hidratációs idő és v/c függvényében, mely a hidratáció eltérő sebességével függhet össze.

90 nap hidratáció után, a különböző v/c értékeknél általában a CEM I 42,5N-SR0 minta porozitása a legnagyobb, vagyis itt a leglassúbb a hidratáció. míg legkisebb porozitás (azaz leggyorsabb hidratáció) a CEM I 52,5 R, illetve a CEM I 42,5 R anyagokra jellemző (*11. a* és *12. a ábrák*).

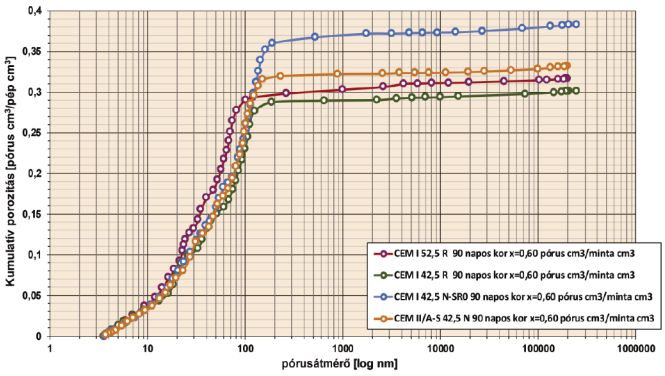

11.a ábra *Különböző típusú cementkő minták porozitása 90 napos korban v/c=0.6 mellett*

Fig. 11.a *Porosity of different types of cement paste samples at 90 days with v/c=0.6*

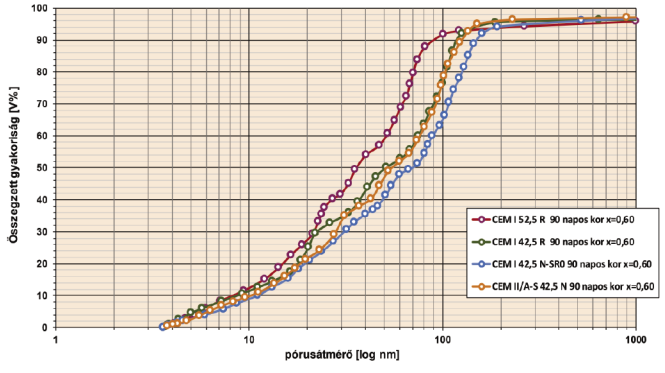

11.b ábra *Különböző típusú cementkő minták pórusméret-eloszlása 90 napos korban v/c=0.6 mellett*

Fig. 11.b *Pore size distribution of different types of cement paste samples at 90 days of age with v/c=0.6*

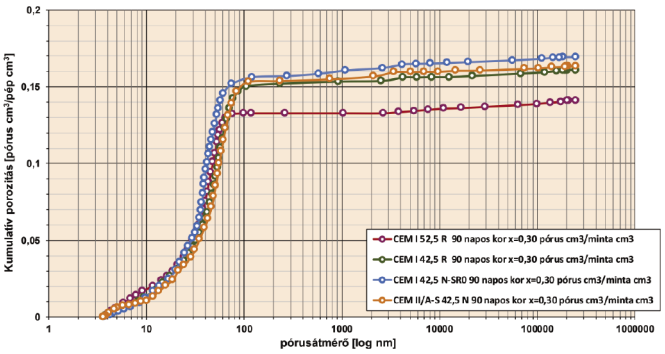

12.a ábra *Különböző típusú cementkő minták porozitása 90 napos korban v/c=0.3 mellett*

Fig. 12.a *Porosity of different types of cement paste samples at 90 days with v/c=0.3*

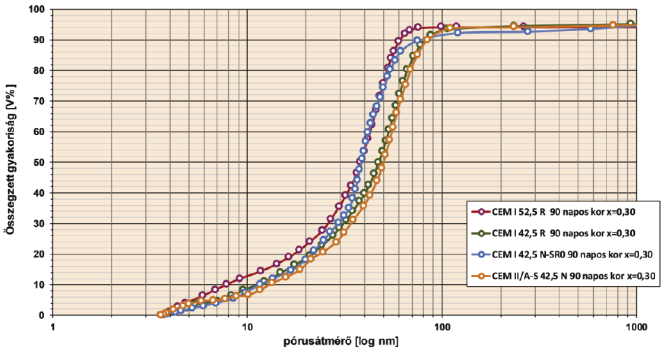

12.b ábra *Különböző típusú cementkő minták pórusméret-eloszlása 90 napos korban v/c=0.3 mellett*

Fig. 12.b *Pore size distribution of cement paste samples of different types at 90 days of age with v/c=0.3*

A különböző 90 napos minták pórusméret-eloszlását összehasonlítva v/c=0,6 esetén a legnagyobb méretű pórusok (10-200 nm) a CEM I 42,5 N-SR0, míg legkisebb méretűek a CEM I 52,5 R mintára jellemzőek (*11.b ábra*). A v/c=0,3 értéknél a különböző cementkövek pórusméret-eloszlása (30-100 nm tartományban) hasonló (*12.b ábra*), de a 30 nm alatti finompórusok részaránya a CEM I 52,5 R minta esetén a legnagyobb.

4. Összefoglaló

Megállapítottuk, hogy a négy vizsgált cementtípus közül 0,3 víz-cement tényezőnél 90 napos korban a CEM I 52,5 R típus mutatta a legkedvezőbb térfogati porozitást. Ez összefügghet az adott cementtípus kedvező szemcseméret- eloszlásával, illetve az ebből számított kedvezően nagy egyenletességi tényezővel. Munkánk során kitűnt, hogy 28 nap után (v/c=0,3) a további hidratáció porozitásra gyakorolt hatása általában jelentősebb a lassú hidratációjú kohósalak-portlandcementnél, mint a gyors hidratációjú portlandcementek esetében, melyek porozitás változása is kisebb. Különösen kedvezőtlen a CEM I 42,5N-SR0 jelű cementkő porozitása a nagy víz-cement tényezőnél (0,6) mert 28 napos korban nemcsak a legnagyobb értéket, hanem 90 napos korra a legkisebb javulást mutatja.

A vasbetonszerkezetek tartóssága szempontjából a finompórusok tekinthetők a legkedvezőbbnek, mert ezekben a leglassúbb a betont vagy betonacélt károsító ionok, molekulák vándorlási sebessége. A finompórusok (30 nm

alatti pórusok) részarányának kitüntetett szerepe van mind az áteresztőképesség, mind az oldódásos korrózió szempontjából. A végzett vizsgálatok alapján a legnagyobb finompórus részarány a CEM I 52,5 R cementkőre jellemző.

A pórusszerkezet és más anyagtulajdonságok további vizsgálata elősegítheti a betonösszetételek tervezését, az élettartamuk biztonságosabb becslését.

Köszönetnyilvánítás: A Danucem (korábbi CRH) Magyarország Kft. támogatásával az NVKP-16-1-2016-0019 pályázat keretében végzett munka. A munkánkat segítő kollégáknak ezúton is szeretnénk köszönetet mondani.

Irodalom

[1] MSZ 4702-2:1997 szabvány: Cementek. Követelmények és megfelelőségi feltételek

[2] Riesz L.: Cement és mészgyártási kézikönyv, Építésügyi Tájékoztatási Központ, Budapest (1989) 210-217. oldal

[3] http://www.betonopus.hu/notesz/fogalomtar/54-cement-hidratacio.pdf (megtekintés időpontja: 2019. 01.31.)

[4] MSZ EN 480-11:2006 szabvány: Adalékszerek betonhoz, habarcshoz és injektálóhabarcshoz. Vizsgálati módszerek. 11. rész: A megszilárdult beton légbuborék-jellemzőinek meghatározása

[5] ASTM C 457:1998 szabvány: Standard Test Method for Microscopical Determination of Parameters of the Air-Void System in Hardened Concrete

[6] S. Diamond: Mercury porosimetry: An inappropriate method for the measurement of pore size distributions in cement-based materials; Cement and Concrete Research Vol. 30 (2000) p.1517-1525, https://doi.org/10.1016/S0008-8846(00)00370-7

[7] Qiang Zeng; Kefei Li; Teddy Fen-Chong; Patrick Dangla: Analysis of pore structure, contact angle and pore entrapment of blended cement pastes from mercury porosimetry data; Cement and Concrete Composites, Vol. 34. (2012) p. 1053-1060, https://doi.org/10.1016/j.cemconcomp.2012.06.005

Ref.:
Laczkó, László – **Wojnárovitsné Hrapka**, Ilona – **Spránitz**, Ferenc: *Effect of water/cement ratio on cement hydration*
Építőanyag – Journal of Silicate Based and Composite Materials, Vol. 74, No. 4 (2022), 156–162. p.
https://doi.org/10.14382/epitoanyag-jsbcm.2022.24

Fenntartható Cement- és Betonipari Technológiák VI. című szakmai nap a Miskolci Egyetemen

2022. május 26-án került megrendezésre a „Fenntartható Cement- és Betonipari Technológiák" c. szakmai nap a Miskolci Egyetem Műszaki Földtudományi Karán. A rendezvényen kilenc előadást mutattak be az egyetemek és ipari cégek szakemberei.
A szakmai ülés apropóját egyrészt az adja, hogy az elmúlt időszakban több területen jelentkező nyersanyaghiányt hogyan lehetne kielégíteni másodnyersanyagokból. Továbbá világviszonylatban nagy mennyiségű ipari melléktermék, hulladék keletkezik évente, amely hasznosítása a megfelelő technológiák alkalmazásával, továbbfejlesztésével megoldható. Ez környezetbarát anyagok fejlesztésére ad lehetőséget a CO_2 kibocsájtás és energiaigény csökkentése mellett, így megvalósítható a körforgásos gazdálkodás és fenntartható nyersanyag-gazdálkodás. Mindemellett a hazai építőipar fejlődése jelentős mennyiségű és jó minőségű nyersanyagot igényel a következő időszakban, amely további kihívásokat jelent a hazai ipar és K+F+I szektor számára.

A rendezvény programja a következő volt:

10:00-10:10 **Megnyitó**
PROF. DR. HORVÁTH ZITA rektor, Miskolci Egyetem

10:10-12:35 **Szekcióülés**
Levezető elnök: PROF. DR. MUCSI GÁBOR dékán, Miskolci Egyetem Műszaki Földtudományi Kar, SZTE Cement Szakosztály elnök

10:10-10:30 URBÁN FERENC ügyvezető, Cemkut Kft.
A beton szerepe a körforgásos gazdaságban

10:30-10:45 DR. NEHME SALEM GEORGES egyetemi docens, ANNA SZIJÁRTÓ PhD hallgató, Budapesti Műszaki és Gazdaságtudományi Egyetem
Nagy és ultranagy szilárdságú öntömörödő beton

10:45-11:00 LACZKÓ LÁSZLÓ laboratórium vezető, SZIKKTI Labor Szilikátkémiai Anyagvizsgáló-Kutató Kft.
Kiegészítőanyagok hatása a cementek hidratációjára

11:00-11:20 DR. SZABÓ ROLAND tudományos munkatárs, DOLGOS FANNI tanszéki mérnök, NAGY GÁBORNÉ AMBRUS MÁRIA tudományos segédmunkatárs, PROF. DR. MUCSI GÁBOR egyetemi tanár, DR. KRISTÁLY FERENC tudományos főmunkatárs, Miskolci Egyetem
Alacsony feldolgozottságú ásványi nyersanyagok, melléktermékek reakcióképességének fokozása különböző eljárástechnikai műveletekkel

11:20-11:35 ŐZE CSILLA PhD hallgató, KRISTÓFNÉ DR. MAKÓ ÉVA egyetemi docens, Pannon Egyetem
Kaolin mechanokémiai aktiválása puccolános anyagokkal és alkalmazásuk cement kiegészítőanyagként

11:35-11:50 DR. KRISTÁLY FERENC tudományos főmunkatárs, Miskolci Egyetem
Cementkiegészítő anyagok ásványi nyersanyag szemszögből - források, reakciók, termékek

11:50-12:05 DR. KOCSERHA ISTVÁN egyetemi docens, HAMZA ALEXANDRA tanszéki mérnök, ASZTALOS FLÓRA, Miskolci Egyetem
Cementhab alapú építőelemek fejlesztése

12:05-12:20 PROF. DR. MUCSI GÁBOR egyetemi tanár, PAPNÉ HALYAG NÓRA, Miskolci Egyetem, PROF CARINA ULSEN., PAULA OLIVEIRA FIGUEIREDO, University of Sao Paulo
Betonhulladék finom frakciójának hasznosítása cementkiegészítő anyagként

12:20-12:35 SZAKÁCS-SIMON SÁNDOR, RÁCZ ÁRPÁD, Austrolab Kft
A cementgyártás során szükséges analitikai eljárások

A szakmai nap jó lehetőséget biztosított a területen működő cégek (cementgyárak, betonüzemek, minősítő szervezetek) valamint a kutatás – fejlesztés és felsőoktatás szakembereinek az eszmecseréjére, amelyre több mint 60 fő vett részt.
A Szervezők bíznak a kutatóhelyek és a cégek által megkezdett együttműködések folytatásában mind a kutatás-fejlesztés-innováció, mind pedig a felsőfokú oktatás vonatkozásában.
A rendezvény szervezői: Szilikátipari Tudományos Egyesület, Cement Szakosztálya, Beton Szakosztálya, a MTA Földtudományok Osztály, Bányászati Tudományos Bizottság, Bányászati, Geotechnikai és Nyersanyagelőkészítési Albizottsága, az MTA MAB Nyersanyagelőkészítési és Környezeti Eljárástechnikai Munkabizottsága, valamint a Miskolci Egyetem, Műszaki Földtudományi Kar továbbá az Országos Magyar Bányászati és Kohászati Egyesület Miskolci Egyetemi Szakosztálya.

További információk és fényképek a rendezvényről: https://www.uni-miskolc.hu/hirek?news_id=3610

GUIDELINE FOR AUTHORS

The manuscript must contain the followings: title; author's name, workplace, e-mail address; abstract, keywords; main text; acknowledgement (optional)**; references; figures, photos with notes; tables with notes; short biography** (information on the scientific works of the authors).

The full manuscript should not be more than 6 pages including figures, photos and tables. Settings of the word document are: 3 cm margin up and down, 2,5 cm margin left and right. Paper size: A4. Letter size 10 pt, type: Times New Roman. Lines: simple, justified.

TITLE, AUTHOR

The title of the article should be short and objective.

Under the title the name of the author(s), workplace, e-mail address.

If the text originally was a presentation or poster at a conference, it should be marked.

ABSTRACT, KEYWORDS

The abstract is a short summary of the manuscript, about a half page size. The author should give keywords to the text, which are the most important elements of the article.

MAIN TEXT

Contains: materials and experimental procedure (or something similar), results and discussion (or something similar), conclusions.

REFERENCES

References are marked with numbers, e.g. [6], and a bibliography is made by the reference's order. References should be provided together with the DOI if available.

Examples:

Journals:

[6] Mohamed, K. R. – El-Rashidy, Z. M. – Salama, A. A.: In vitro properties of nano-hydroxyapatite/chitosan biocomposites. *Ceramics International.* 37(8), December 2011, pp. 3265–3271, http://doi.org/10.1016/j.ceramint.2011.05.121

Books:

[6] Mehta, P. K. – Monteiro, P. J. M.: Concrete. Microstructure, properties, and materials. *McGraw-Hill*, 2006, 659 p.

FIGURES, TABLES

All drawings, diagrams and photos are figures. The **text should contain references to all figures and tables**. This shows the place of the figure in the text. Please send all the figures in attached files, and not as a part of the text. **All figures and tables should have a title**.

Authors are asked to submit color figures by submission. Black and white figures are suggested to be avoided, however, acceptable.

The figures should be: tiff, jpg or eps files, 300 dpi at least, photos are 600 dpi at least.

BIOGRAPHY

Max. 500 character size professional biography of the author(s).

CHECKING

The editing board checks the articles and informs the authors about suggested modifications. Since the author is responsible for the content of the article, the author is not liable to accept them.

CONTACT

Please send the manuscript in electronic format to the following e-mail address: femgomze@uni-miskolc.hu and epitoanyag@szte.org.hu or by post: Scientific Society of the Silicate Industry, Budapest, Bécsi út 122–124., H-1034, HUNGARY

We kindly ask the authors to give their e-mail address and phone number on behalf of the quick conciliation.

Építőanyag – *Journal of Silicate Based and Composite Materials*, Quarterly peer-reviewed periodical of the Hungarian Scientific Society of the Silicate Industry, SZTE.
http://epitoanyag.org.hu